

Solar-Terrestrial Centre of Excellence

Annual Report 2018



STCE

Solar-Terrestrial Centre of Excellence

<http://stce.be/>

Ringlaan 3

B-1180 Brussels

Tel.: +32 2 373 0211

Fax: + 32 2 374 9822

Front page: The planeterrella is a tool to study the solar atmosphere, the earth environment and the polar lights (aurora). It was on display during the Open Doors 2018 at the Space Pole and attracted a lot of visitors. The planeterrella is a glass jar, which is vacuumed by a pump that sucks out almost all air. An electrical tension is put over the electrodes (the two metal objects in the planeterrella), high enough to move the negatively charged electrons away from the negative electrode towards the positive electrode. Accelerated by this high tension, they collide with the few remaining air molecules still present in the planeterrella, making these molecules emit light. In the planeterrella is normal air (nitrogen and oxygen) which leads to the typical pinkish-purple colour.

Table of Contents

A word from the STCE coordinator.....	4
Structure of the STCE	5
Monitoring space weather: solar-terrestrial highlights in 2018	8
Public outreach meets Science.....	10
Open Doors at the Space Pole.....	10
ASGARD: balloons for Science	11
COSPAR award to Dr Tobias Verhulst.....	12
Fundamental research.....	14
First detection of solar flare emission in mid-ultraviolet Balmer continuum.....	14
Exploring the middle corona	15
ALF radio bursts: new signature of plasma waves in solar flares.....	19
Size distributions of solar proton events and their associated SXR flares.....	20
Shocking research: near Earth, from supernova remnants, and close to comets.....	22
Cross-validation of GPS tomography models and methodological improvements.....	24
STCE researchers study the inner magnetosphere	25
Instrumentation and experiments	27
Studying the plasmasphere from the ground with the AWDA VLF antennas	27
The joint use of ALC measurements with eddy-covariance measurements	27
Measurement of polarization of auroral emission lines.....	28
On meteors: new facilities, BRAMS, and ionospheric observations	29
Characterization of the VIS-NIR detectors for MAJIS/JUICE.....	32
Applications, modeling and services.....	35
PECASUS – Pan-European Consortium for Aviation Space weather User Services	35
DigiSun : a tool to extract scientific data from sunspot drawings.....	36
Next generation of JHelioviewer: browsing the Sun.....	38
Inter-hemispheric comparison of the ionosphere-plasmasphere.....	40
Publications	43
Peer reviewed articles.....	43
Presentations and posters at conference	47
Public Outreach: Talks and publications for the general public	60
List of abbreviations	64

A word from the STCE coordinator



At this very moment, you are looking into the 2018 STCE annual report.

Once again it shows that we, the STCE, are doing an excellent job. We can put forward a very long list of peer-reviewed articles, of talks and posters at conferences, and of public outreach activities. We have also contributed in many different ways to meetings and workshops. We have set up public outreach events with tons of enthusiasm.

I want to highlight three achievements. We have reached an ideal balance between research and services which fits perfectly the tasks and goals of a federal scientific institute and the STCE. PECASUS, an international project that offers services to civil aviation on a worldwide level, is our current crown jewel. The

expertise of different STCE partners has been brought together and forms now a strong and essential pillar in PECASUS. Also, we are and remain true to our original promise that the STCE is only "seed money", i.e. from a modest input, we are able to establish a firm base on which many other projects can mature and thrive.

All these strengthen my confidence in the future. You will certainly hear more good things about us.

We wish you an enjoyable reading experience!

Ronald Van der Linden
General Coordinator of the Solar-Terrestrial Centre of Excellence
Director General of the Royal Observatory of Belgium

Structure of the STCE

The Solar-Terrestrial Centre of Excellence is a project of scientific collaboration that focuses on the Sun, through interplanetary space, up to the Earth and its atmosphere.

The solid base of the STCE is the expertise that exists in the 3 Federal Scientific Institutes of the Brussels Space Pole: the Royal Observatory of Belgium, the Royal Meteorological Institute and the Royal Belgian Institute for Space Aeronomy. The STCE supports fundamental solar, terrestrial and atmospheric physics research, is involved in earth-based observations and space missions, offers a broad variety of services (mainly linked to space weather and space climate) and operates a fully established space weather application centre. The scientists act at different levels within the frame of local, national and international collaborations of scientific and industrial partners.

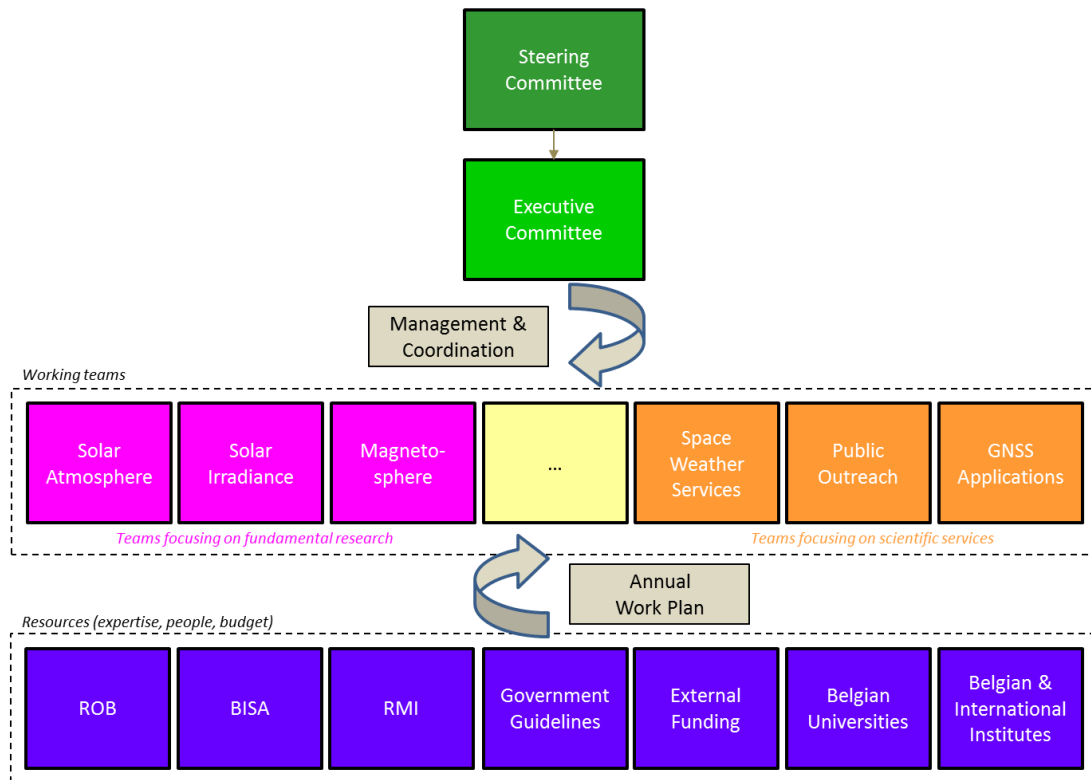


Figure 1: The STCE management structure

The STCE's strengths are based on sharing know-how, manpower, and infrastructure.

In order to optimize the coordination between the various working groups and institutions, as well as the available resources such as ICT, personnel and budget, a management structure for the STCE was put into place, consisting of a steering committee and an executive committee.

The **steering committee** takes all the final decisions on critical matters with regard to the STCE. It assures the integration of the STCE into the 3 institutions and the execution of the strategic plans. It is composed of:

- BELSPO Director General “Research Programmes and Applications”

Dr. Frank Monteny (BELSPO)

- Director General of each of the 3 institutions at the Space Pole

Dr. Ronald Van der Linden (ROB)

Dr. Daniel Gellens (RMI)

Dr. Martine De Mazière (BISA)

The **executive committee** assures the global coordination between the working groups and the correct use of the budgetary means for the various projects. It also identifies new opportunities and is the advisory body to the Steering Committee. It is composed of:

- STCE Coordinator

Dr. Ronald Van der Linden

- Representatives of the research teams in the 3 institutes

Dr. David Berghmans (ROB)

Dr. Carine Bruyninx (ROB)

Dr. Johan De Keyser (BISA)

Dr. Norma Crosby (BISA)

Dr. Stanimir Stankov (RMI)

Dr. Steven Dewitte (RMI)

Dr. Hugo De Backer (RMI)

A promotional movie giving a flavor of the STCE’s tasks, interactions and various research programs can be found via the [STCE](#) website (in [English](#), and subtitled in [French](#) and [Dutch](#)).



Life at the STCE - The tradition continues: A PROBA2 guest investigator gets a warm and happy welcome by the other team members. Clearly, the poor researcher (front right) has no idea yet about all the hard work that is coming at her. Notice the grin on the other faces. (Picture by Matt West)

Monitoring space weather: solar-terrestrial highlights in 2018

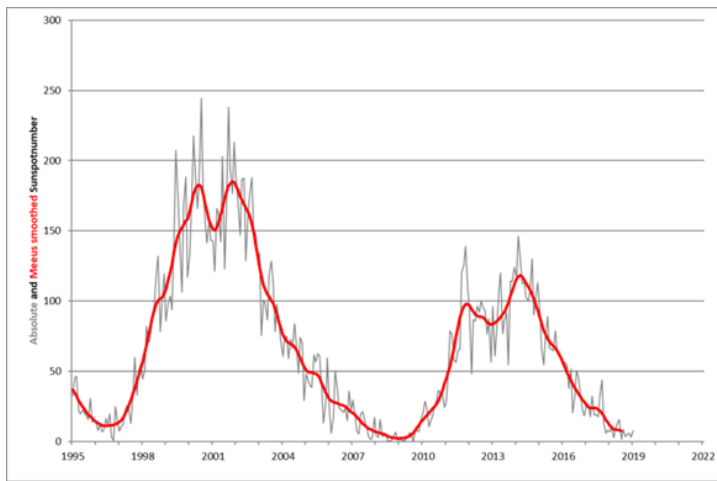


Figure 2: The evolution of the monthly and monthly smoothed SN (1995-2018). Pending the smoothing formula used, Solar Cycle 24 (SC24) reached its maximum of 116.4 in April 2014 (SILSO formula), or 118.2 in March 2014 (Meeus formula).

The official annual sunspot number (SN) for 2018, as determined by the [WDC-SILSO](#) (World Data Center - Sunspot Index and Long-term Solar Observations), was 7.0. This is a further decrease compared to 2017, when it was 21.7. The highest daily sunspot number (56) was recorded on 20 June. However, there were also 208 spotless days (see SILSO's [Spotless Days page](#)). The longest spotless stretches so far this solar cycle transit occurred on 22 October - 07 November 2018 and on 16-31 December 2018, totaling respectively 17 and 16 spotless days.

In 2018, the Sun produced a total of 0 (zero) M- and X-class flares. The strongest event was a C8.1 flare generated by NOAA 2699 on 7 February. This region would eventually become the source of 6 of the only 11 C-class flares recorded in 2018. There were also no proton events or Ground Level Enhancements reported.

Of note was small sunspot group NOAA 2694 that appeared on 8 and 9 January at a latitude of -32 degrees. That's a perfect latitude for a region of the new solar cycle, but... the region had the *same* magnetic polarity as sunspot groups on the southern hemisphere of the *old* solar cycle (SC24). It currently looks like this region is indeed a genuine SC25 group which happens to have a reversed polarity (3 to 5 % of the groups in a solar cycle have a reversed polarity). Later in the year, groups at high latitudes with the correct (SC25) magnetic polarity appeared on both solar hemispheres, but they were too small or too short-lived to get a NOAA-number. Hence, NOAA 2694 together with NOAA 2620 (visible in December 2016) are currently the only two numbered regions that can claim SC25-membership, despite both having their oddities (see the STCE Newsitems from [9 January](#) and [13 November](#)).

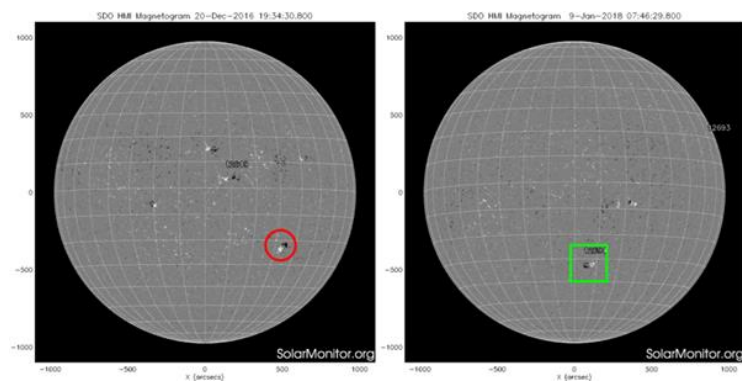


Figure 3: NOAA 2620 (left) and NOAA 2694 (right) are currently the only two numbered sunspot regions that may belong to the new solar cycle 25 (SC25).

So far this solar cycle, no extremely severe geomagnetic storm has been observed ($K_p = 9$). In 2018, also no severe geomagnetic storm was recorded, and only 1 strong storm ($K_p = 7$). The latter occurred on 26 August and was the result of a coronal mass ejection (CME) associated with a modest filament eruption on 20 August. The CME was barely visible in [SOHO](#)'s coronagraphs, and in fact, the feature was so weak that [CACTus](#), a tool to automatically detect CMEs in these coronagraphic images, did not even capture the CME. With the help of [STEREO-A](#) imagery, it was determined that this CME had an earth-directed component which arrived, as predicted, at Earth on 26 August. The ensuing geomagnetic storm was surprisingly intense, with K_p reaching strong levels ($K_p = 7$). The (Quicklook) Dst index ([WDC Kyoto](#)) reached -174 nT, making this the [3rd strongest storm of SC24](#) after the two famous storms in March and June 2015. Geomagnetically induced currents were observed in Norway with voltages about 10 times stronger than usual.



Figure 4: NOAA 2699 was the largest sunspot group in 2018, having a size of about 1.5 times the total surface area of the Earth. It produced 6 of the 11 recorded C-class flares in the year, with a C8.1 flare on 7 February being the strongest event. On 12 February, while the region was near disk-centre, it produced also a [C1 long duration event](#) (LDE) lasting more than 3 hours. The associated halo coronal mass ejection (CME) was weak and had a speed of about 500 km/s. Only active geomagnetic conditions were observed when it hit the earth environment 3 days later.

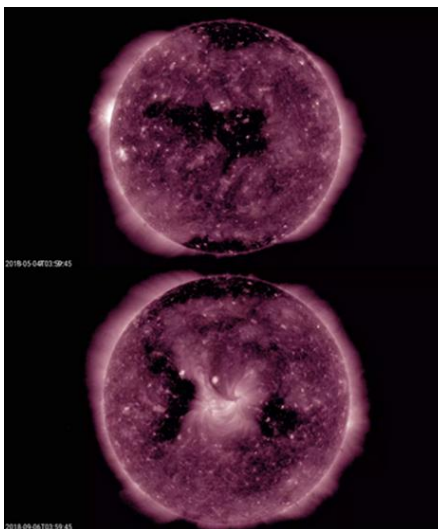


Figure 5: Some of the more significant coronal holes in 2018 were visible in May and June (top) and in September (bottom).

Most of the geomagnetic activity in 2018 was a result of wind streams related to [coronal holes](#) (CHs). These CHs were significantly smaller and patchier than in previous years. Only early May and early June solar wind speeds above 700 km/s were recorded by the [DSCOVR](#) spacecraft. As a result, K_p and Dst were mostly restricted to resp. 5 or 6 and around -50 - -60 nT. Often, geostationary satellites recorded high fluxes of energetic electrons (energies ≥ 2 MeV), which are an important source of electrostatic charging effects inside satellites. Some of the more significant coronal holes in 2018 can be seen in Figure 5. The high speed stream of a large elongated CH resulted in wind speeds up to 710 km/s in May and around 785 km/s one solar rotation later (early June). The CH itself developed from an extension of the southern polar CH in November 2017, and lasted 9 solar rotations. From February till May, it had a remarkable elongated structure. A small equatorial hole and an extension from the northern polar CH transited the Sun early September. These CHs developed in July and remained visible till the end of the year. Minor to moderate geomagnetic storming levels were recorded and Dst reached -60 nT, the most intense of all co-rotating interaction region/high-speed stream pairs from coronal holes in [2018](#).

Public outreach meets Science

Open Doors at the Space Pole

The Open Doors, taking place during the weekend of 29-30 September, was without a doubt the main event on the Space Pole in 2018. Also, and for the first time, a visit for the schools was organized during the afternoon of 28 September, as well as a VIP event on Saturday morning. With all three institutes participating, the range of topics offered to the visitors was broad and various. The STCE participated in a long series of events.



Figure 6: Explaining the size of the planets in our solar system to a primary class on Friday afternoon.

Guided 10-12 minutes tours were organized in the Solar Dome, handling approximately 2000 visitors in groups of 10-15 persons.

In the waiting hall, there was the ringing sunspot set-up which had been used previously during the European Space Weather Week (ESWW), as well as a movie on the most spectacular solar eruptions of solar cycle 24, lasting about 20 minutes.

As during the previous Open Doors, the Proba2 Science Center, with a full-scale model of the PROBA2 solar satellite on display, was co-located with the SSCC in the room of the [SSCC](#) (SSA Space weather Coordination Centre). The main corridor also hosted a space weather (SWx) stand (SIDC/RWC), which

was located next to the seismology room. Obviously, the researchers got a lot of questions on any link between earthquakes and solar activity.



Figure 7: Explaining the art of solar drawing and sunspot classification. Visitors could also try to draw these blemishes themselves on a projected solar image.

projected solar image. These two set-ups were also operated during the visit of the schools on Friday afternoon.

In the "Experiments tent", numerous hands-on activities were presented by the three institutes. The STCE manned 2 stands: A set-up on solar spectroscopy, with a run-of-the-mill spectroscope, as well as a stand on sunspot drawing where visitors could draw sunspots from a

The Planeterrella experiment (BISA/ROB) focused on the research on polar lights and was located in the BISA building to allow for better (dark) viewing. BISA also hosted a "Lecture room" in which presentations of about 20 minutes were given to the general public, in Dutch or French. These talks not only concerned space weather, but also earthquakes, the planets, and the ionosphere; as well as a series of talks on aeronomy. Especially during the afternoon these presentations attracted large crowds!



Figure 8: At the spectroscopy stand, visitors could look into a small spectroscope at the different spectra generated by different types of lamps.

Other highlights for the public were the climate centre, the virtual weather office, and numerous displays and hands-on stands on the study of the Earth, planets, moons and comets from our own solar system to far beyond in the universe. There were also plenty of activities for children. A picnic area and food trucks were also available on site.

With 9000 visitors, the Open Door 2018 was a big success. This would not have been possible without the efforts of all the speakers, guides, and other experts patiently explaining and answering all the

questions from the audience. But also the IT-specialists, the helpdesks, and all -and there were many- involved in the logistics and practical organization of the event played a very important role. No wonder the visitors were very pleased with the event, suggesting not to wait another 4 years to organize the next Open Doors.

ASGARD: balloons for Science

For several years now, the Planetarium (Heysel) and the Space Pole (Uccle) host the ASGARD project from ESERO Belgium and St-Pieterscollege Jette. Student teams think of their own scientific experiment



Figure 9: Explaining the secrets of space weather forecasting to a class participating in the ASGARD project.

to send into near-space with a stratospheric balloon from the Royal Meteorological Institute (RMI). Teams, whose proposals are selected by the jury, can then build their experiment for real, presenting it to the other selected participants, and launch it from the Space Pole plateau in Brussels.

This educationally all-inclusive project is open to all students from European secondary schools. In 2018, no less than

20 projects got a green light, with participating schools from Belgium, Spain, Portugal, Poland, and the UK. and this time even one from the United States. Because of all the experiments, 2 balloons had to be used. As with all good scientific projects, some last-minute problems popped up and the launch got delayed by 45 minutes.



Figure 10: The ASgard participants also visited the Weather bureau at the RMI.

Traditionally, during launch day, the students also had the opportunity to participate in several workshops and visit some of the facilities of the 3 institutes at the Space Pole. A few highlights were the spectroscopy stand at BISA, a visit of the big telescope at the ROB, explanations on the weather balloon and in the weather bureau at RMI, and the solar walk along PROBA2, the Space Weather Forecasting Centre, the solar telescopes and on the sunspot number. These young future scientists

certainly had an interesting and exciting field day!

COSPAR award to Dr Tobias Verhulst

The COSPAR Bureau has awarded an “Outstanding Paper Award for Young Scientists” to Dr. T. Verhulst for the following paper:

Verhulst, T.G.W., Sapundjiev, D., and Stankov, S.M. (2016): High-resolution ionospheric observations and modeling over Belgium during the solar eclipse of 20 March 2015 including first results of ionospheric tilt and plasma drift measurements. *Advances in Space Research*, 57, 11, 2407-2419, DOI: [10.1016/j.asr.2016.03.009](https://doi.org/10.1016/j.asr.2016.03.009).



Figure 11: Our colleague Dr Tobias Verhulst was awarded a prestigious prize by the Committee on Space Research ((COSPAR).

“Advances in Space Research” is the official scientific journal of the Committee on Space Research (COSPAR), a Scientific Committee of the International Science Council (ISC). *Advances in Space Research* covers all areas of space research including: space studies of the Earth’s surface, meteorology, climate, planets and small bodies of the solar system, upper atmospheres, ionospheres and magnetospheres of the

Earth and planets including reference atmospheres, space plasmas in the solar system, astrophysics from space, life sciences as related to space, fundamental physics in space, space weather, earth observations of space phenomena,... The award was conferred at the COSPAR General Assembly in Pasadena, California, and published in the COSPAR information bulletin, Space Research Today, 203, 19-21, 2018.



Life at the STCE - The ROB team-building day 2018 consisted of visits to the research laboratories at Rochefort-Lorette and at Humain. Here we see the participants readying themselves for the descent into the Lorette caves. Everybody survived the memorable trip.

Fundamental research

First detection of solar flare emission in mid-ultraviolet Balmer continuum

Solar flares and associated coronal mass ejections are the most powerful energy release events in the solar system. Surprisingly little is known about the distribution of the flare energy over the full solar spectrum. Routine measurements of the x-ray and extreme ultraviolet (EUV) emissions probe only a small part of the total energy radiated during a flare. The parts of the solar spectrum between 1000 and 3000 Å, i.e., far-ultraviolet (FUV), mid-ultraviolet (MUV), and near-ultraviolet (NUV), make a probably important but still poorly known contribution to the total energy emitted during flares.

In September 2017, after several months of relative quiet, a sudden increase of solar activity was observed on the Sun, when an active region started to grow quickly. This active region produced multiple strong flares before disappearing behind the western solar limb on 10 September. Among them were the two strongest flares observed during the current solar cycle: the X9.3 flare on 6 September and the limb X8.2 flare on 10 September.

LYRA is a radiometer from the Royal Observatory of Belgium, which flies aboard the satellite PROBA2 and observes the Sun in four broadband channels covering the soft X-rays (SXR) to MUV spectral range. At the time of these events, the instrument was performing a special flare observation campaign, involving one of its spare units. So, it delivered clear observations of the X9.3 flare (see Figure 12), unaffected by the aging effects that otherwise affect the observations (LYRA was launched in 2009).

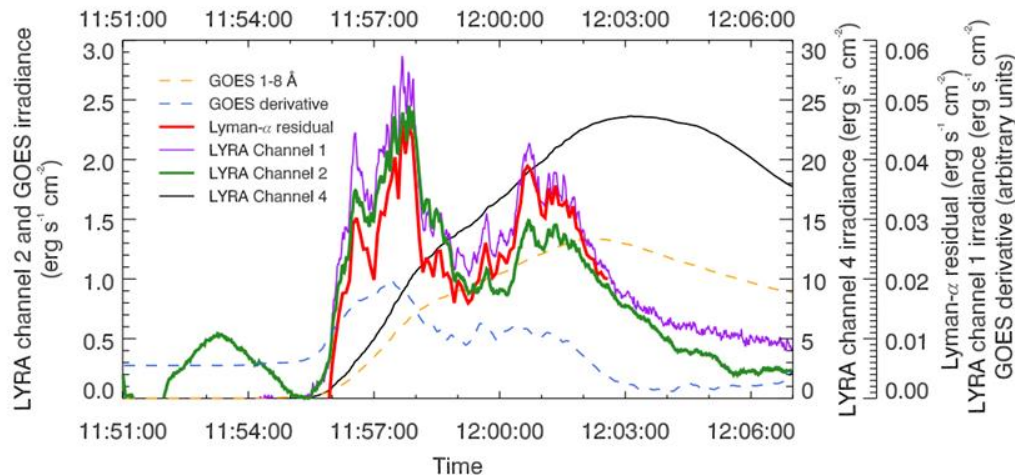


Figure 12: Observations of the strongest flare of the solar cycle by the LYRA and GOES instruments. The four channels of LYRA captured a signature of the flare. LYRA channel 3 was cleaned to remove the contribution from unwanted wavelengths and is therefore called "Lyman-alpha residual".

The LYRA data set for the X9.3 flare is rather unique. The two SXR/EUV channels of LYRA (named channels 3 and 4) are specifically used for monitoring solar flares and have captured hundreds of them, but flare observations are relatively rare in the channel 1 (observing the Lyman-alpha range around 1216 Å), and no flare had ever been observed with the channel 2 (which observes the MUV wavelengths around 2000 Å) until then. This time, the instrument observed signatures of the flare in all its channels.

The origin of the emission in the channel 2 has been modeled (see Figure 13). Comparing the model to the observations, we demonstrated that the emission detected at these wavelengths by LYRA is consistent with hydrogen emission by a chromospheric slab heated up to 10,000 K. We determined the densities in the slab, and found it to be around $6.7 \times 10^{13} \text{ cm}^{-3}$, which is consistent with previous works.

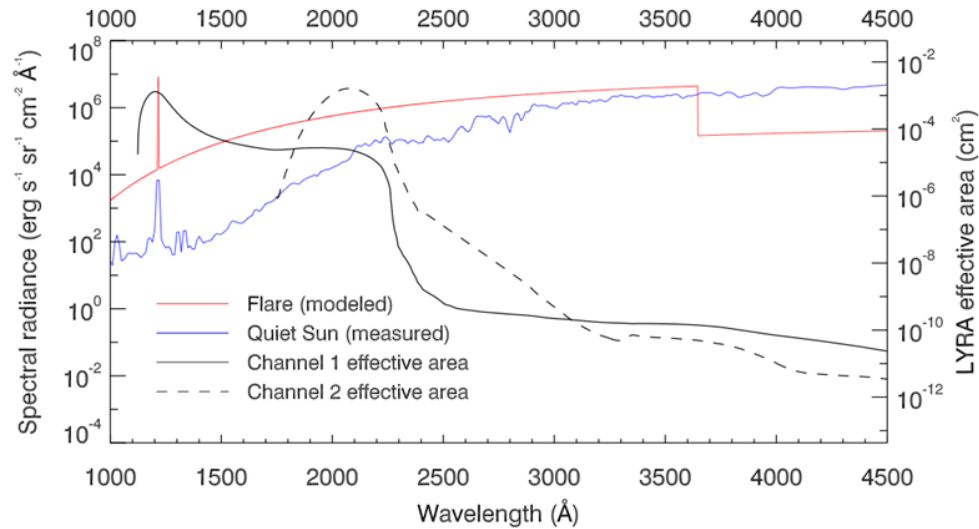


Figure 13: Model of the flare emission (red line) compared to observations in quiet-Sun conditions (blue line). The two black lines represent the spectral zones in which LYRA channels 1 and 2 are sensitive.

Interestingly, the X8.2 flare on 10 September, despite being the second strongest flare of the solar cycle, only produced a signature in the usual SXR channels. This may be due to the fact that the flare was located at the limb of the Sun and that at least one of the footpoints was hidden behind the limb.

Exploring the middle corona

Two primary instruments used for observing the morphology of the solar atmosphere are EUV imagers and coronagraphs. The middle panel of Figure 14 shows an image of the solar atmosphere in the EUV portion of the electromagnetic spectrum, effectively observing the Sun at a temperature around 600,000 degrees Celsius. The image was made using data from the SWAP EUV imager on the ESA PROBA2 satellite operated from the Royal Observatory of Belgium. The instrument is able to do this by filtering out (blocking) all the other wavelengths, allowing us to observe just a small section of the electromagnetic spectrum.

The temperatures SWAP sees make it ideal for observing the solar atmosphere, in particular the solar corona. The solar atmosphere is seen as a central solar disk, which is very bright in the centre of the image, and the off-limb solar atmosphere surrounding it. The emission diminishes with distance from the disk, due to the density dropping with height.

If we look more closely at the solar disk, we see the solar atmosphere is not uniform in appearance, but is composed of bright structures known as active regions (AR), dark regions known as coronal holes (CH ; not real holes, just regions of lower or cooler emission) and the remainder is known as the “Quiet Sun”.

All of these structures are created by magnetic fields generated deep within the Sun in the convection zone, extending out through the surface and permeating the atmosphere, they are made visible by the hot plasmas trapped upon them. The active regions are formed of tight bundles of magnetic field and can cause violent eruptions when the fields become unstable. The coronal holes are created by magnetic fields extending far out into the heliosphere, allowing plasma to flow away from the lower solar atmosphere, creating regions that are cooler and appear darker.

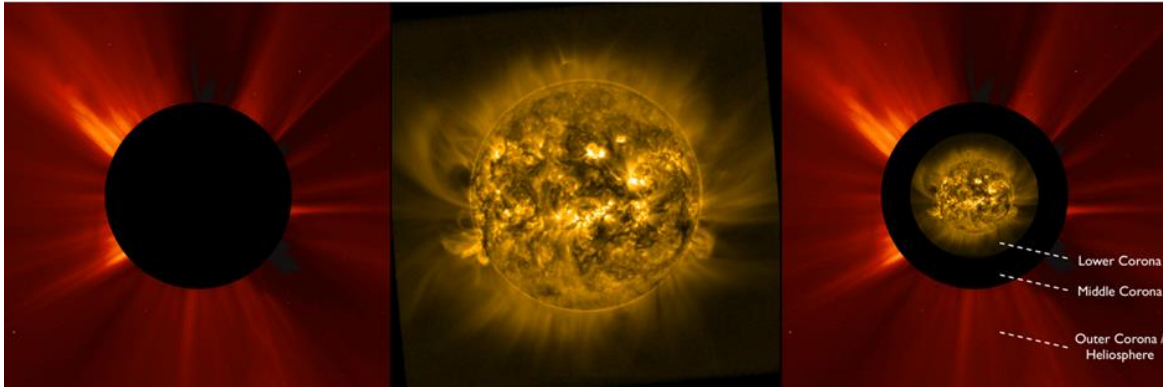


Figure 14: Two common methods used for imaging the solar atmosphere. The left panel shows a LASCO coronagraph image, where the bright solar disk has been blocked out. The middle image shows an image from the PROBA2 SWAP instrument in the EUV section of the electromagnetic spectrum. The right panel shows the two previous images superimposed on each other allowing us to see the true extent of the atmosphere.

The Sun undergoes an 11-year activity cycle which sees the number of active regions wax and wane. The images in Figure 14 were taken on 18 April 2014 when the Sun was near the maximum of its activity cycle, hence why we see more bright structures. Looking at the features surrounding the solar disk we see the solar atmosphere in profile, where structures can be seen to extend to the edge of the field of view.

The left panel in Figure 14 shows an observation made by the LASCO coronagraph on the NASA/ESA SOHO satellite (operating since 1995). Coronagraphs create artificial eclipses by effectively blocking the bright solar disk using an occulter, allowing us to see the extended solar atmosphere. Due to complications with the optics and the brightness of the Sun it's very difficult to make observations close to the body of the Sun, and therefore a gap has to be left between the inner edge of the coronagraph and the observed solar disk.

Coronagraph images reveal bright extensions known as "streamers" stretching radially outwards from the lower solar atmosphere. These structures are also formed by the Sun's magnetic field and vary over a solar activity cycle. Sometimes the magnetic fields near the solar surface can become unstable and erupt as huge magnetic bubbles, known as coronal mass ejections (CMEs), these can be tracked through coronagraphic images. These volatile structures form an important aspect of space weather that can affect the Earth and other parts in the solar system.

The right panel on Figure 14 shows the EUV image superimposed on the coronagraphic image (adjusted for size) where we see the lower coronal features extending out from the solar disk into the outer corona. With closer inspection one can see small inconsistencies between the structures seen in the EUV

image and those seen in the coronagraph. These are due to the images being created with different filters, showing different wavelengths, and effectively showing the Sun at different temperatures.

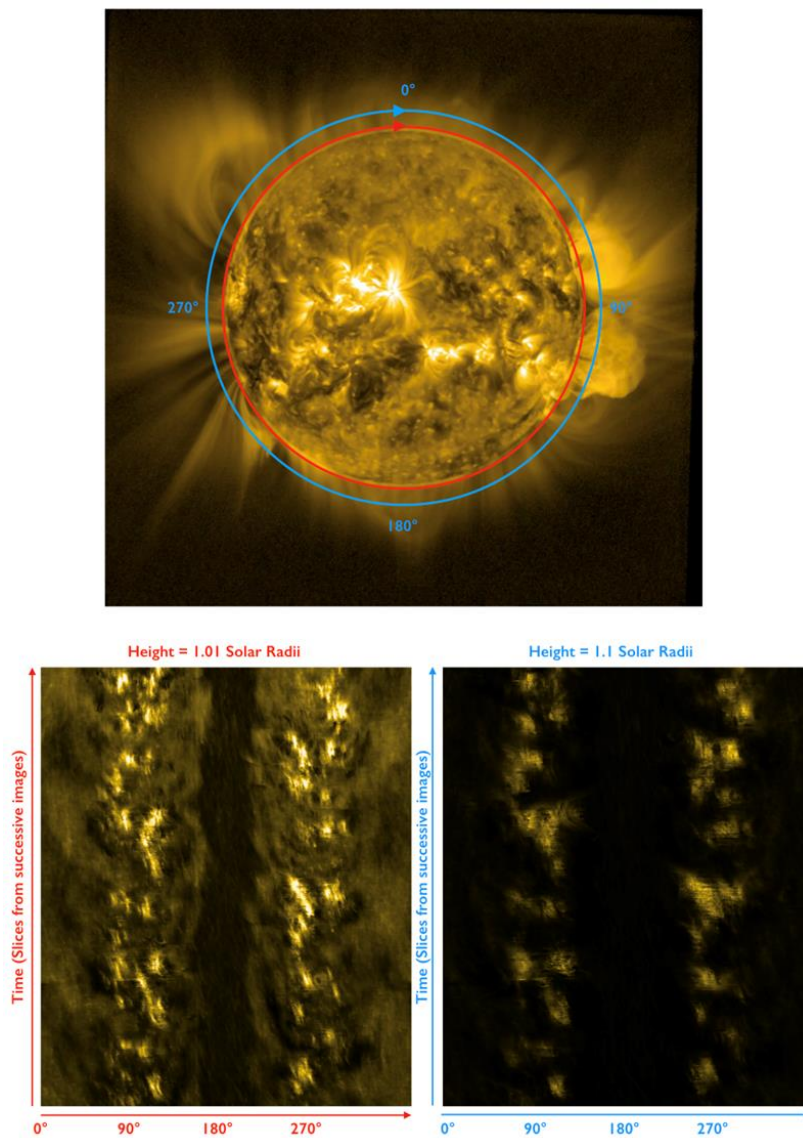


Figure 15: A solar image made by the PROBA2 SWAP EUV imager. Two circles have been drawn around the Sun at different heights in the solar atmosphere; 1.01 Solar Radii (Red) and 1.1 Solar Radii (Blue). These circles are straightened out, and successive circles stacked to form the images seen in the bottom two panels. Each of these images is composed of slices taken over 3 solar rotations.

atmosphere, processed data is freely available at the [PROBA2 website](http://proba2.oma.be).

One recently developed method to explore this region is through synoptic maps of the solar atmosphere. These involve taking a slice at different heights through the atmosphere on successive images, and then stacking the slices up. An example can be seen in Figure 15, which shows the changing atmosphere at different heights over a period of three solar rotations (nearly 3 months). It can be seen

Most EUV observations of the Sun do not extend far above the solar disk, as the drop in emission with distance is extremely high. We had to wait until 2009 for the launch of the SWAP instrument before we could make continuous high cadence observations of this region, which is often referred to as the Middle Corona. This region is currently under considerable study as it is relatively unexplored, and only newly created image processing techniques have enabled to tease out structures here. The region is of fundamental importance for space weather studies and how the Sun's atmosphere can affect the Earth. It is in this region that CMEs are accelerated and the solar atmosphere transitions from a predominantly magnetically dominated environment into a thermal pressure dominated region.

The PROBA2 team at the Royal Observatory of Belgium has been investigating and developing new techniques to explore the observations of the extended solar

from these images how different structures vary over time. The PROBA2 team has automated the techniques used to make these images, and the latest synoptic map can be found [here](#).

Future missions that will explore the solar atmosphere

The SWAP instrument has gone a long way towards helping us understand the middle corona, however there is an inescapable gap in our observations between the EUV and coronagraph images seen in Figure 14, i.e. the region where the middle corona is located. Scientists and engineers at the Royal Observatory of Belgium are at the forefront of middle corona research and are currently members of several international consortiums developing future instrumentation that will help explore this region. These include the ESA Solar Orbiter, PROBA3 and Lagrange missions (Figure 16).



Figure 16: Three artist renditions of the three solar missions currently being developed by ESA to explore the Sun and its atmosphere. The left image represents the PROBA3 mission, the middle image represents the Lagrange mission and the right image represents the Solar Orbiter mission. The images are all courtesy of the ESA webpage.

Solar Orbiter is a planned Sun-observing satellite, under development by the European Space Agency. The mission will make some of the closest approaches to the Sun and is host to several instruments dedicated to observing the Sun and the solar atmosphere. Amongst the instruments there will be a coronagraph and two EUV imagers that will provide some of the highest resolution images of the Sun and its atmosphere. The mission will be unique in that it will orbit the Sun with an orbit that will take it out of the ecliptic, allowing imaging of the solar polar regions. The Royal Observatory of Belgium is co-leading the development of the EUV imager that will provide wide field-of-view images of the Sun, and therefore be able to monitor the middle corona. Solar Orbiter is scheduled to be launched in 2020.

PROBA-3 is the fourth mission in the European Space Agency's series of PROBA low-cost satellites that are being used to validate new spacecraft technologies while also carrying scientific instruments. PROBA-3 will be composed of two independent spacecraft that will orbit the Earth and perform formation flying at 150 meters separation. The two satellites will form a coronagraph with the camera on one satellite and the occulter on the second. The design will allow the inner edge of the coronagraph to be much closer to the solar disk, providing a greater view of the middle corona. PROBA-3 development is being led by the Royal Observatory of Belgium and is scheduled to launch in 2020.

Lagrange is a 2018 concept study for a solar weather mission by the European Space Agency. The mission concept is designed to monitor space weather from a position known as the L5 Lagrange point. This position is to the side of the Sun-Earth line, allowing instruments to monitor space weather between the Sun and the Earth. On-board, amongst others, there will be an EUV instrument and a coronagraph. The development of the EUV instrument is being led by the Royal Observatory of Belgium and the Centre Spatial de Liège (CSL).

ALF radio bursts: new signature of plasma waves in solar flares

Solar radio observations provide valuable information on the energetic phenomena in the solar atmosphere and are used for their early diagnostics. In particular, solar flares and coronal mass ejections manifest solar type III and II radio bursts, respectively. These energetic events affect the radiation conditions in interplanetary space and can cause severe geomagnetic storms. Using the large Ukrainian radio telescope URAN-2, we -i.e. STCE scientists in collaboration with Ukrainian colleagues- have studied ALF radio bursts – faint solar radio bursts in the frequency range 20-30 MHz. These bursts were not visible before because of the lower sensitivity and resolution of previous radio telescopes. Similarly to type III bursts, the ALF bursts occur in close association with solar flares. In Figure 17 we show the radio spectrogram of a flare-related event recorded on 18 April 2014, in which several ALF bursts have been identified (they are encircled by dashed lines). Measuring the polarization of the radio emission (bottom panel of Figure 17), URAN-2 allows to identify very weak ALF bursts not clearly visible in the emission power (upper panel of Figure 17). The measured ALF parameters (frequency drift rates of about -0.1 MHz/s, relative frequency bandwidths of 0.01, and burst durations around 3 s) clearly set ALF bursts apart from the previously known burst types.

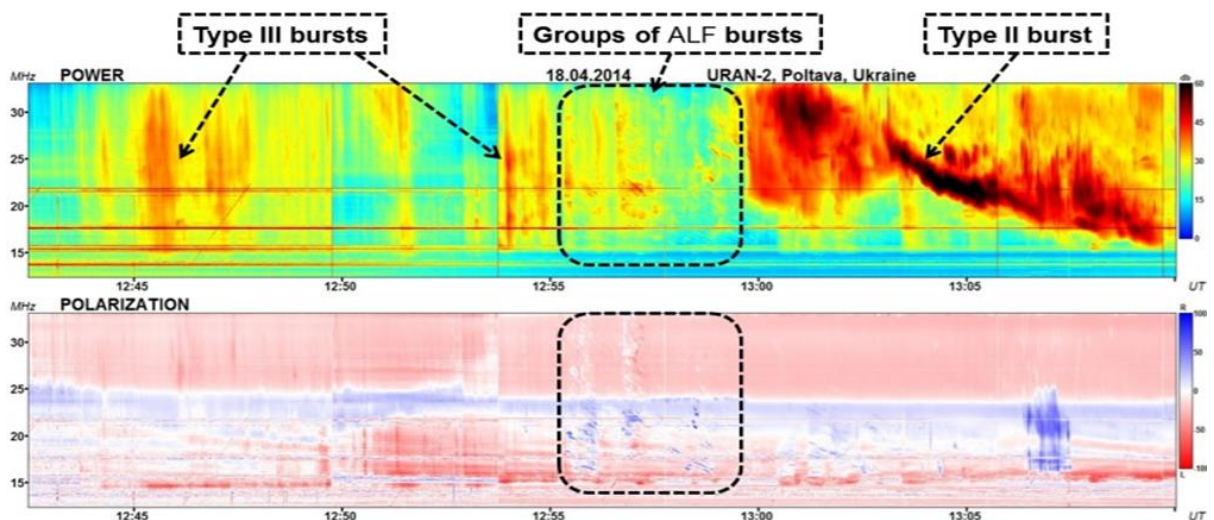


Figure 17: Flare-related event with multiple ALF bursts (group of ALF bursts is encircled by the dashed lines). Top panel: power of radio emission. Bottom panel: polarization of radio emission. Some ALFs are better visible in the polarization spectrogram.

But where are they coming from? The fact that the emission sources of ALF bursts propagate with near-Alfvén velocities suggests a generation mechanism for them involving Alfvén waves. To make the ALF bursts clearly visible, the Alfvén waves responsible for the phenomenon have to perturb the plasma density, which implies kinetic effects. These and other properties of ALF bursts deduced from radio spectrograms can be naturally explained by a model incorporating intermittent kinetic Alfvén waves (KAWs) propagating upward in the solar corona at heliocentric distances of about 2 solar radii. Such KAWs can be generated by magnetic reconnection in solar flares. The key element of the proposed generation mechanism is that the KAWs can sweep and accumulate Langmuir waves (these Langmuir waves were excited earlier by the electron beams that are faster than KAWs). The main steps of the proposed generation scenario are presented and explained schematically in Figure 18.

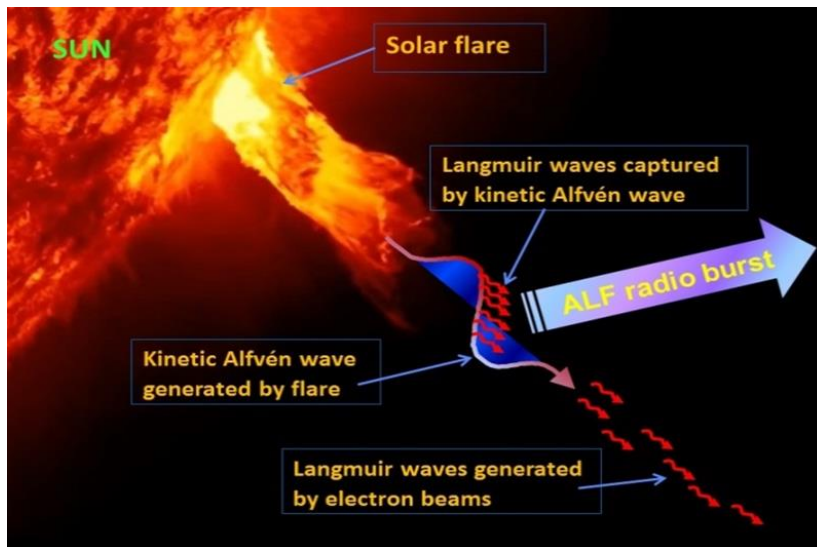


Figure 18: Generation scenario for ALF bursts: (i) magnetic reconnection in flares accelerates electron beams and generates KAWs; (ii) electron beams excite Langmuir waves; (iii) KAWs capture and amplify Langmuir waves; (iv) clusters of amplified Langmuir waves generate ALF radio bursts by the plasma emission mechanism.

Our theory explains not only the frequency drift rates of ALF bursts, but also their instantaneous frequency bandwidths, durations, and life times. Moreover, it also predicts the properties of KAWs in the flaring solar atmosphere. All the theoretically predicted KAW parameters, i.e. magnetic amplitudes, angular frequencies, and perpendicular wavenumbers are compatible with observations. These KAWs are not merely sources for ALF radio bursts, but also contribute to the processes of energy release and transport in the solar atmosphere. The theoretically constrained wave

and plasma parameters in the solar corona above active regions can be used in modeling coronal mass ejections and the production of solar energetic particles.

Size distributions of solar proton events and their associated SXR flares

It has been known for some time that the size distributions of solar radio bursts and soft x-ray (SXR) flares have steeper power-law slopes (α ; about 1.8) than those of solar energetic proton (SEP) events (α of about 1.2). Hudson (1978) suggested three possibilities for this difference:

- (1) proton flares are fundamentally different from ordinary flares;
- (2) proton flares represent the large end of the total energy distribution of ordinary flares;
- (3) proton flare characteristics have a threshold behaviour.

In some sense, each of these conjectures applies, although (1) and (3) are paramount.

Cliver et al. (2012) argued that proton flares are fundamentally different from ordinary flares (hypothesis (1)) because they are eruptive (Kahler et al. 1978). Because of their associated coronal mass ejections (CMEs), proton flares are intrinsically more energetic, satisfying hypothesis (2). Cliver et al. presented evidence for these statements by constructing power-law size distributions for (relatively small) samples of large ("gradual") >10 MeV proton events (58 events), their associated $\geq M1$ SXR flares (52 events), $\geq M1$ SXR flares associated with fast (≥ 1000 km/s) CMEs (59 events), and $\geq M1$ soft X-ray flares (540 events). They found that the power-law slopes of distributions of SEP intensity (α about 1.2) and the peak SXR fluxes of SEP-associated flares (α about 1.3) were closer to that of the peak SXR fluxes of flares associated with fast CMEs (α about 1.4) than they were to that of all $\geq M1$ SXR flares (α about 2.1). Subsequently, D'Huys et al. (2016) noted that size distribution studies of solar phenomena which use graphical methods, i.e. where the power-law exponent is estimated by a linear fit on a log-

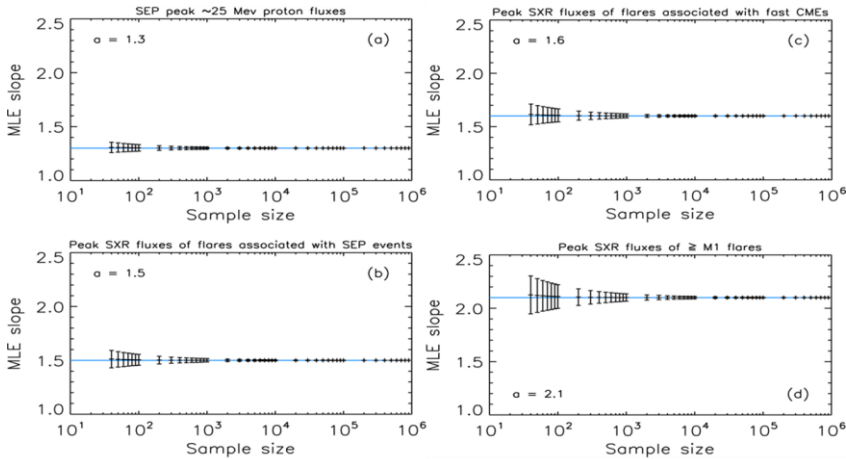


Figure 19: MLE-scaling parameter estimates as a function of sample size for (a) 25 MeV SEP events, (b) and (c) SXR flares associated with SEP events and ≥ 1000 km/s CMEs, respectively, and (d) $\geq M1$ SXR flares.

transformed histogram of the data (as was the case for Cliver et al. (2012)), require very large data samples (about $10^3 - 10^4$ events) to provide statistically reliable results. In lieu of such methods, D'Huys et al. advocated the use of the more robust maximum likelihood estimator (MLE). Following their suggestion, we (Cliver and D'Huys 2018) revisited the Cliver et al. analysis using the MLE approach.

The MLE method determines a value for the power-law slope (α) of a distribution by maximizing the likelihood of the data, which is the probability that the data were drawn from that model. The results of the MLE application to samples of 136 25 MeV SEP events, 113 $\geq M1$ SEP-associated flares, 159 ≥ 1000 km/s CMEs, and 716 $\geq M1$ SXR flares, show that the pattern for α is similar to that found by Cliver et al. (2012), with the α -values for the SXR flares associated with SEP events (α about 1.5) and fast CMEs (α about 1.6) being closer to that for SEP events (α about 1.3) than to the α -value for all $\geq M1$ SXR flares (α about 2.1). As shown by D'Huys et al. (2016), and illustrated in Figure 19 by generating random samples of different size with a given scaling parameter, a sample size of at least 100 events is required to obtain a reliable result with the MLE method, and this minimum value increases as the slope of the distribution increases. These results for SEP-events and SEP-associated SXR flares are consistent with those obtained graphically by Belov et al. (2007) for a large data sample.

Figure 20 shows that the large SEP events considered here are associated with CMEs with speeds ≥ 400 km/s, corresponding to the nominal Alfvén speed in the low corona. Thus large SEP events are characteristically accompanied by shock waves manifested by type II radio bursts in the metric and/or decametric-hectometric (nominally 14 - 1 MHz for the Waves experiment on the Wind spacecraft) wavelength range.

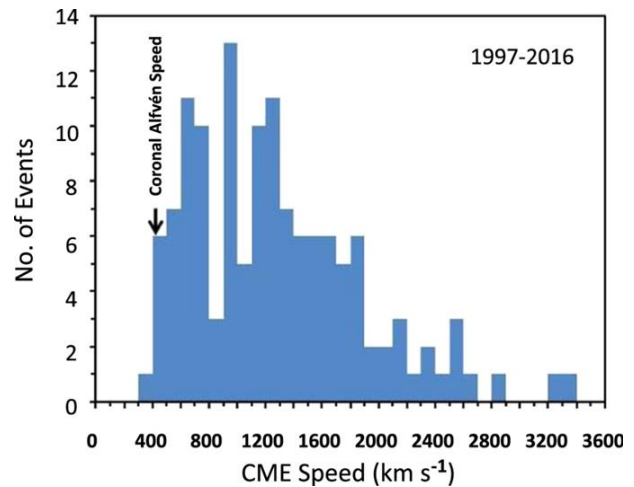


Figure 20: Histogram of speeds of CME associated with large 25 MeV SEP events.

Figure 20 shows that Hudson's (1978) third possible explanation - a threshold effect - for the difference between the α -values of size distributions of flare electromagnetic emissions and SEP events is also at play. CMEs with speeds > 400 km/s are required to drive the shocks that accelerate protons in large

gradual SEP events. Smaller ("impulsive") SEP events are also commonly associated with CMEs, many with speeds in excess of 400 km/s, but for such events the ejected mass is moving along field lines in an x-ray jet magnetic topology (Shimojo and Shibata 2000), whereas movement of magnetoplasma perpendicular to the ambient magnetic field (as in standard loop-like CMEs) is required for shock formation (Vršnak and Cliver 2008).

The key inference or application of the power-law size distributions of flare electromagnetic emissions is the avalanche model of Lu and Hamilton (1991). In that model, based on the self-organized criticality concept, solar flares are viewed as avalanches of small-scale reconnection events. The smaller value of α for SEP size distributions argues for a different physical mechanism for acceleration of the protons that escape into space, one based on fast CMEs and coronal/interplanetary shock waves.

Shocking research: near Earth, from supernova remnants, and close to comets

Terrestrial foreshock research and the physics of supernova remnants

It is well documented by satellite data, and supported by theory and modeling, that the solar-wind ions reflected from the terrestrial bow shock form hot ion beams in the terrestrial foreshock region. The currents carried by these beams, together with the background return currents, establish a compensated-current system in the foreshock. Similar compensated-current systems are expected to be present in the interstellar medium in front of the shocks of expanding supernova remnants, generated by the interstellar ions reflected from the supernova shocks. A supernova usually is the explosion of a

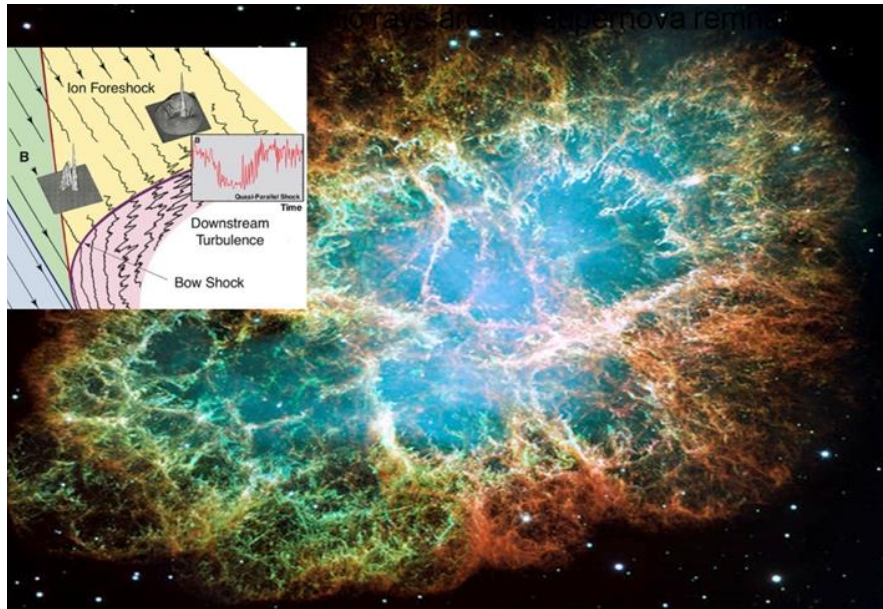


Figure 21: Similarly to the terrestrial magnetosphere interacting with the solar wind, as is schematically shown in the embedded picture, an expanding supernova remnant interacts with the interstellar plasma.

massive star at the end of its life. The analogy between the terrestrial magnetosphere interacting with solar wind and the expanding supernova remnants interacting with the interstellar medium is depicted in Figure 21.

In collaboration with the Main Astronomical Observatory of NASU (Kiev, Ukraine), we have studied the stability of compensated-current systems with respect to different wave modes. In particular, we investigated a new triggering

mechanism for the non-resonant reactive instability of Alfvén waves in such systems and found the critical temperature of the ion beams above which the Alfvén mode is generated. The Alfvén-mode

instability is driven by the imbalance of perturbed currents carried by the magnetized background electrons and partially demagnetized beam ions. The instability thus arises at parallel wavelengths that are sufficiently short to demagnetize the beam ions.

As such, the destabilizing effects of the beam temperature and the temperature dependence of the instability threshold and growth rate have been demonstrated for the first time. The beam temperature, density, and bulk speed are all destabilizing and can be combined in a single destabilizing factor triggering the instability above the threshold value α_b^{thr} that varies in a narrow range from 2.43 to 4.87, as is shown in Figure 22.

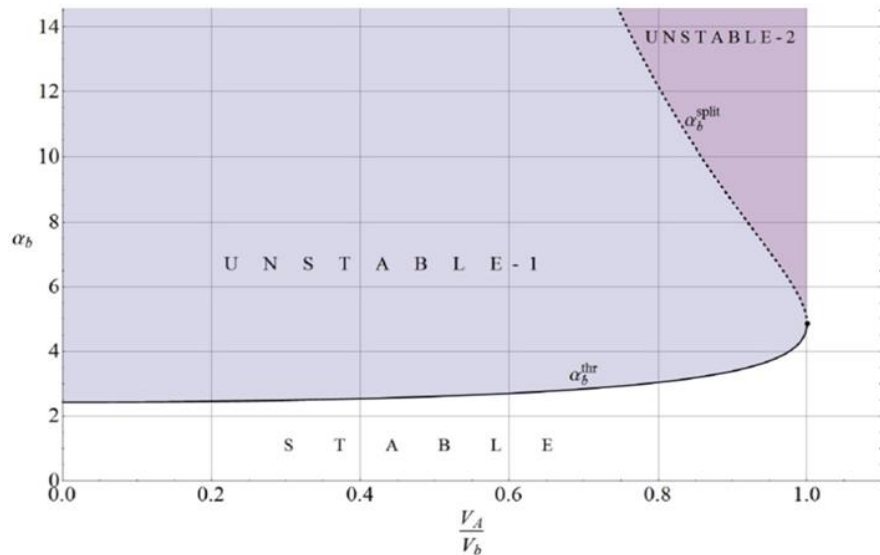


Figure 22: Instability thresholds and unstable ranges of Alfvénic instability in compensated-current systems. Parameter α_b is the product of the normalized beam current and the thermal velocity, V_b is the beam bulk velocity, and V_A is the Alfvén velocity (From Malovichko et al. (2018)).

New analytical expressions for the instability growth rate and its boundary in the parameter space were compared with satellite observations in the terrestrial foreshocks. We found that properties of electromagnetic fluctuations observed in the foreshock region are compatible with theoretical predictions for Alfvénic modes produced by compensated currents. We also found that the ions reflected by supernova shocks can drive stronger instabilities than the instability driven by cosmic rays as suggested by other researchers.

The infant bow shock of comet 67P

A bow shock is the first boundary the solar wind encounters as it flows by a planet or a comet. It is similar to the bow wave that forms in front of the bow of a ship. The Earth’s bow shock has been observed since the beginning of the exploration of interplanetary space, but scientists still do not completely understand the processes involved in its formation.

A comet's appearance changes very much with the distance to the Sun, because the intense heat close to the Sun causes gases to be released from the surface of the comet's nucleus. This also affects the properties of plasma boundaries around the comet, of which the bow shock is one example. Thus, by studying the bow shock at a comet, we

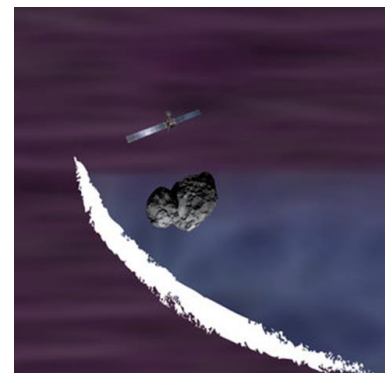


Figure 23: Rosetta observing the infant bow shock (ESA).

look at the same phenomenon under different circumstances. Scientists hope to learn a lot from this.

The Rosetta spacecraft accompanied comet 67P/Churyumov-Gerasimenko during two years from 2014 to 2016. It was long thought that Rosetta had never encountered a bow shock upon approaching the comet. In 2015, when the comet was near its closest approach to the Sun, Rosetta ventured out 1500 km upstream to look for the bow shock, but this turned out not to be far enough. Instead, scientists at BIRA-IASB and co-workers in an international team, found the

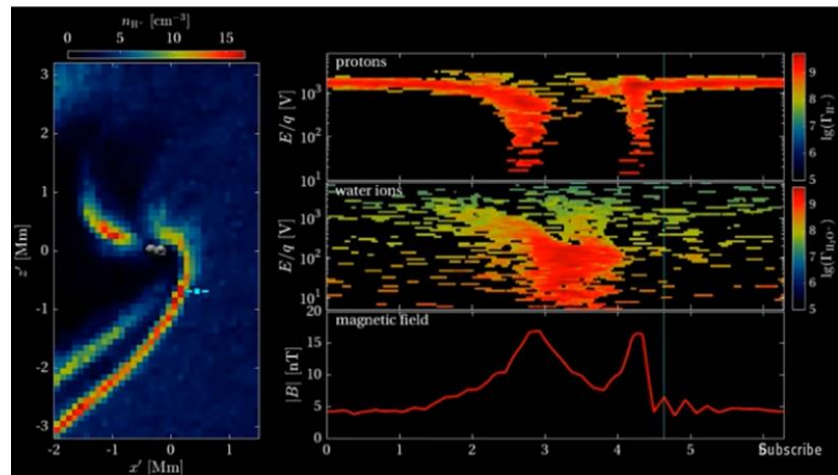


Figure 24: On the left a simulation of Rosetta flying through the bow shock, with on the right the actual measurements by Rosetta on which the simulation was based. The screen shot was taken from a video in the related [ESA News item](#).

bow shock much closer to the nucleus - only about 80 km away. This happened during a time when the comet was a little farther away from the Sun, and the bow shock was in its infancy. The infant bow shock was found to be asymmetric and wider than fully developed bow shocks observed at other comets. Before Rosetta, a bow shock had never been captured during its formation. It is something that can only be seen at comets, since bow shocks at planets are always in a fully developed state.

Cross-validation of GPS tomography models and methodological improvements

Using data from Global Navigation Satellite System (GNSS) networks during severe weather (in March 2010 in Australia and August 2010 in Belgium), an analysis has been carried out regarding the sensitivity of GPS tomography retrieval of water vapour density and wet refractivity. A statistical study has been performed to test and verify 5 models - considering independent observations from radiosonde and radio occultation profiles (Figure 25).

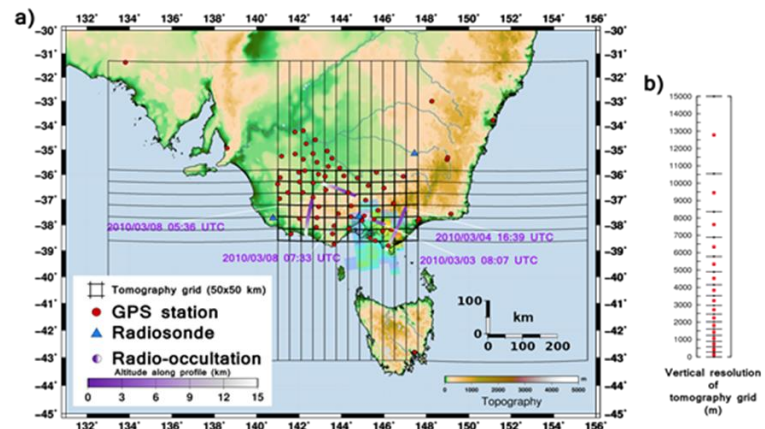


Figure 25: a) GPS stations (red circles), Radiosonde sites (blue triangles), Radio-occultation profiles (white-purple lines), satellite cloud top altitude from OMI sensor at 04:07 on 6 March 2010 (purple-blue-orange pattern; see Figure 25 b) and the tomography grid (inner grid in thick black lines and outer grid in thin black lines); b) Red square represents altitudes above the sea level of the centres of each 3D pixel (voxel) of the tomography grid.

impact. Bad initial conditions, associated with different time-convergence of tomography inversion, can reduce the quality of the tomography solution as compared to radiosonde estimates (by a factor of up to more than 3 for the RMS of bias). This illustrates that the quality of the a priori data in combination with iterative processing is critical, independently of the choice of the tomography model.

The use of data stacking and pseudo-slant observations can significantly improve the quality of the retrievals with respect to non-stacked solutions. This result is due to a better geometrical distribution and a better coverage of mid- and low-tropospheric parts (30% improvement of the coverage). The recommendation of using pseudo-slant observations is illustrated for an episode of heavy rain in Belgium, August 2010 (Figure 26).

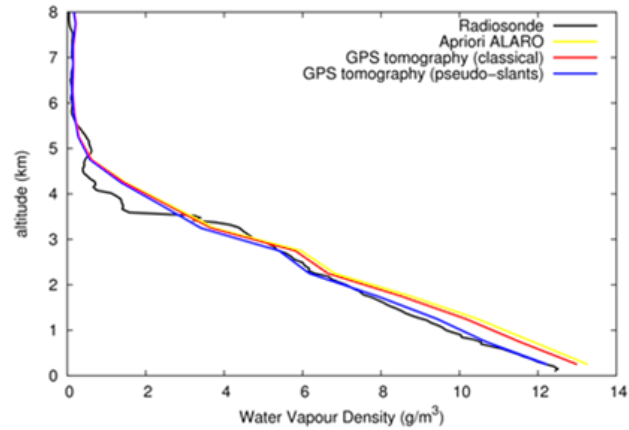


Figure 26: Comparison of water vapour density profiles during severe weather conditions over Belgium (12:00 UTC on 16 August 2010). Radiosonde, launched from Uccle, is compared to ALARO NWP (a priori condition of GPS tomography), GPS tomography (classical retrievals) and GPS tomography using pseudo-slant IWVs observations.

The impact of the uncertainty on GPS observations has also been investigated, showing the importance of using several sets of input data to evaluate the quality of tomography retrievals in comparison to independent external measurements, and to estimate simultaneously the quality of numerical weather prediction (NWP) outputs. A comparison of our multi-model tomography with NWP outputs from the ACCESS-A model shows the relevant use of tomography retrievals to improve the understanding of such severe weather conditions, especially about the initiation of the deep convection.

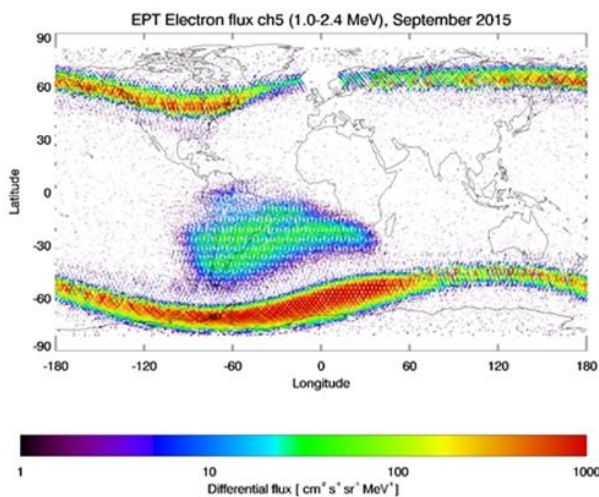


Figure 27: Map of the electron fluxes observed by EPT in channel 5 (1.0-2.4 MeV) during September 2015.

STCE researchers study the inner magnetosphere

The Energetic Particle Telescope (EPT) was launched on the ESA satellite PROBA-V on 7 May 2013 to a LEO polar orbit at an altitude of 820 km. It provides now 5 years of observations, showing strong flux variations, especially for the electron fluxes during geomagnetic storms, associated also with injections in the inner belt. EPT is a detector designed to well discriminate the electrons, protons and helium ions, so that it can make direct unambiguous high quality measurements in the radiation belts and, specifically, in the inner zone, despite the penetrating proton environment. PROBA-V/EPT

observations were combined with LYRA/PROBA2 data for overlapping periods of time to identify electrons with energy > 2 MeV (Katsiyannis et al., 2018). Figure 27 maps the electron fluxes observed by EPT in channel 5 (1.0-2.4 MeV) during September 2015. The fluxes are high at high latitudes corresponding to the penetration of the outer belt at low altitudes, and in the South Atlantic Anomaly corresponding to electrons trapped in the inner belt.

Also in the inner magnetosphere, the influence of the plasmasphere on the radiation belts was studied. The 3-dimensional dynamic model of the plasmasphere developed at BIRA-IASB was provided on the SSA (Space Situational Awareness) Space Weather website of ESA. Comparisons with CLUSTER, CRRES and THEMIS observations confirm that the plasmopause is formed in the post-midnight sector during geomagnetic storms, verifying the assumptions made in the model. A statistical study of the plasmopause position as a function of the MLT (Magnetic Local Time) sector confirms the excellent agreement with the model. MAGION-5 data have been used to determine the thickness of the plasmopause boundary layer.



Life at the STCE - In 2018 there were 2 sessions of the Space Weather Introductory Course (SWIC), a course given to the meteo people of the Dutch military and the KNMI. The SWIC aims at getting the participants acquainted with the space weather jargon so that they can correctly interpret the daily bulletins and can translate this in relevant space weather effects for their own technologies. To ease the digestion of the large amount of knowledge provided, some games have been created. In the picture above, the participants get a card with the name of a space weather feature (e.g. a coronal mass ejection) and they each have to guess what they are by asking questions. These exercises are fun and really help the participants to assimilate the information. No participants got traumatized during the course.

Instrumentation and experiments

Studying the plasmasphere from the ground with the AWDA VLF antennas

In the framework of the STCE, BIRA-IASB operates two VLF antennas for the study of the plasmasphere.

Despite intensive efforts with Belspo and the International Polar Foundation, the VLF antenna at the Princess Elisabeth station in Antarctica is not working satisfactorily: There is strong electromagnetic interference, the source location of which has been found but could not be corrected up to now. Plans for addressing this issue during the next season at the Princess Elisabeth station are taking shape.

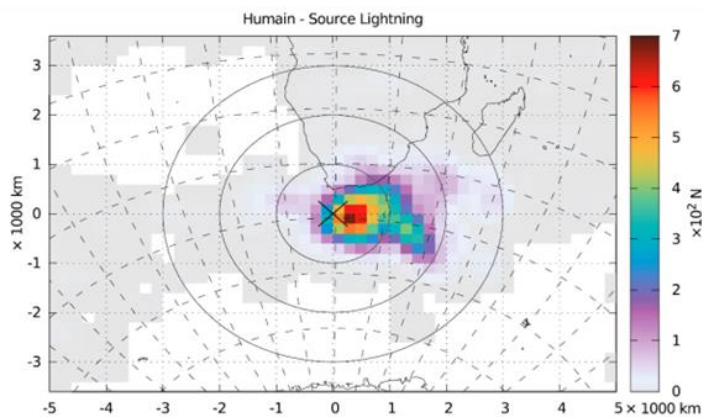


Figure 28: Regional distribution of source lightning (excess matches) detected at Humain, Belgium (showing its conjugate region near South Africa). The concentric circles represent distances of 1000, 2000, and 3000 km from the conjugate points.

The VLF antenna in Humain, however, is producing valuable data. A scientific collaboration with Eotvos University in Hungary on the analysis of the data is ongoing. A new method for identifying the source regions of lightning-generated whistlers has been developed, by calculating the ratio of lightning discharges (from the World Wide Lightning Location Network data) transmitted into ground detectable whistlers as a function of location. The results show that the source region of whistlers corresponding to each station is around the magnetic conjugate point of the respective station. The size of the source region is typically less than 2000

km in radius with a small fraction of sources extending to up to 3500 km. This sets limits on the horizontal propagation distance, across the magnetic field lines, of the waves at ionospheric altitudes.

The joint use of ALC measurements with eddy-covariance measurements

The concentration of atmospheric constituents close to the Earth's surface such as aerosols, ozone and greenhouse gases is governed by turbulent mixing processes in the atmospheric boundary layer (ABL).

The ABL height (BLH), which can be retrieved from ceilometer measurements, determines the volume within which air pollutants emitted from the surface are diluted. The BLH is a key parameter often used by air quality models and atmospheric dispersion models. A detailed understanding of the variability and growth rate of the BLH on diurnal, seasonal and inter-annual timescales is however needed for these applications. The growth of the ABL is linked to the turbulent energy exchange between the Earth's surface and the atmosphere thanks to the solar radiation that is the primary energy source for the Earth-atmosphere system. This solar energy is available to heat the ground and the air in the ABL (sensible heat fluxes) inducing eventually convection and changing the phase of water present at the surface through evaporation (latent heat fluxes). These turbulent energy exchanges at the surface can be measured with the eddy-covariance technique by using a sonic anemometer and a gas analyzer (Figure 29).



Figure 29: Installation of the eddy-covariance system at Uccle in 2018.

At Uccle, since 2011, the BLH has been monitored on a continuous temporal scale by the ceilometer measurements. During the period 2016-2018, the turbulent energy exchanges (sensible and latent heat fluxes) at the surface were measured by an eddy-covariance system. The joint use of both these datasets will strengthen our understanding on surface-atmosphere interactions, in particular on the time evolution of the dependence of the growth of the BLH on the turbulent energy exchanges at the surface during the morning.

One of the main results of this analysis was the linear relationship between the BLH and the sensible heat fluxes (H) with a slope coefficient having an inter-annual variability as illustrated by Figure 30. This variability is likely linked to the development of shallow clouds by convection (especially during the summer) inducing a slight increase of latent heat fluxes at the surface. During the period where less humidity was available at the surface, the impact of this effect on BLH was much lower.

In 2018, RMI purchased a new ceilometer (CL51 VAISALA) to increase its ceilometer network consisting currently of 4 ceilometers in Belgium. Several discussions are ongoing between RMI and the Wing Meteo (Belgium

Defense) in order to retrieve the backscatter signal from the ceilometer network of Wing Meteo and to spatially increase the capacity to monitor aerosol plumes over Belgium.

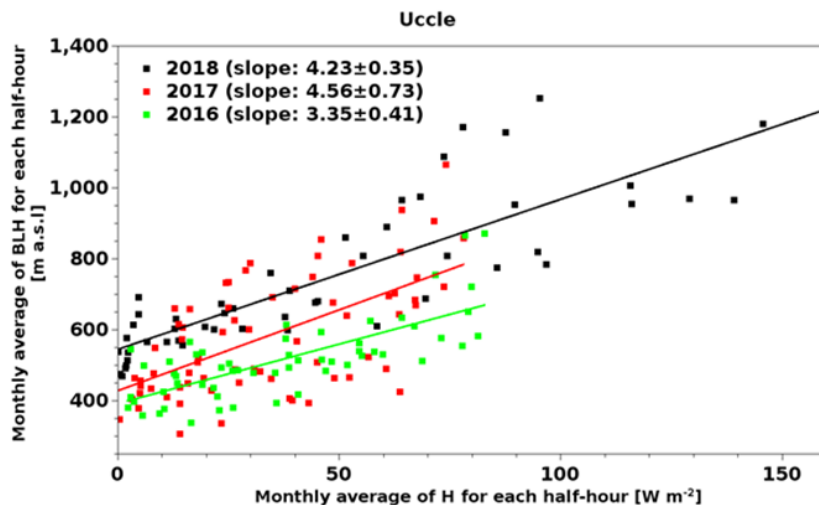


Figure 30: Relationship between the monthly average of sensible heat fluxes (H) and the boundary layer height (BLH) for each half-hour in 2018, 2017 and 2016 at Uccle.

Measurement of polarization of auroral emission lines

We have continued our observing campaigns at the observatory in Skibotn, Norway in order to measure the polarization of auroral emission lines with the dedicated spectropolarimeter, built in collaboration between BIRA-IASB and IPAG in Grenoble. Results from the 2017 campaign have been used to publish

for the first time polarization measurements in the auroral N^2_+ 427.8 nm band. Due to weak signal-to-noise ratios, these measurements still need to be taken with caution since none of the individual data set has a detection with a 3σ confidence level. However, results integrated over the entire observing period each night do show a 3σ detection but due to the long integration period, the origin of this polarization cannot be linked to a specific type of aurora (diffuse vs structured arc) or specific ionospheric or geomagnetic conditions. These observations need to be confirmed with an improved design to increase the signal-to-noise ratio and decrease the exposure time. When available, these improved measurements of the blue line polarization will be important to better understand the physics of auroral processes at altitude below 100 km where the N^2_+ emission occurs and possibly for space weather applications if the polarization varies with ionospheric / geomagnetic conditions.



Figure 31: The photopolarimeter setup as used in Skibotn

In March 2019, we had another campaign in Skibotn using an imaging polarimeter called PLIP (for Polar Lights Imaging Polarimeter). This is a low budget set-up, with two identical cameras (Canon 6D) coupled with also two identical 24 mm lenses opened at $f/2.8$, fixed on a tripod. The two cameras have a linear polarizer in front of the optics, one set horizontally and the other one set vertically, which give us only access to the Q Stokes parameter. The cameras are GPS synchronized. A first version of the pipeline for treating the data was developed at the University of Leiden and will be used to analyze the data from the 2019 campaign.

On meteors: new facilities, BRAMS, and ionospheric observations

Development of a meteor radar facility

In 2018 and early 2019, a lot of work has been done on installing the meteor radar in Dourbes. The transmitting antenna will be similar to the one used for the BRAMS transmitter. The reflector is an 8m x 8m metallic grid and has already been installed on geotextile material to avoid vegetation to grow up around it. The five Yagi antennas forming the interferometric receiving system have all been installed as well. All the cables were installed in gutters and link the antennas to the small container that we procured in 2018. Pictures of the transmitter, the interferometer and of the cables inside the container are shown below.



Figure 32: The future transmitter of the meteor radar (left), the five antennas of the interferometer of the meteor radar (top right), and the RF coaxial cables inside the container (bottom right).

The BRAMS radio meteor network

During the summer 2018, the BRAMS team carried out a careful check of the material and software used by all the 26 receiving stations. Among other things, it was decided to slightly increase the length of each element of the Yagi antenna in order to have the resonant frequency of the antenna very close to 49.97 MHz, the frequency of our transmitter. Indeed, with the specifications given by the antenna provider, the resonant frequency was close to 50.6 MHz instead of 50.0 MHz as claimed. All antennas have also been set vertically such that the reflecting element of the Yagi antenna better

protects from undesired reflections from the ground. This configuration might not be optimal in terms of number of detected meteor echoes for distant receiving stations, but it allows us to make quantitative analyses of the power of meteor echoes since that power depends on the radiation pattern of the antenna which is then close to the theoretical one.

On the other hand, the BRAMS transmitter was also fully characterized, first the power amplifier, then the two crossed-dipole antennas. Due to various conceptual reasons and a bad adaptation of one of the antennas, it was measured that the total power transmitted is about 85 watts instead of the 150 watts expected. The transmitted signal is also not fully circularly polarized but slightly elliptical (phase difference between the two currents at the antenna is 96°). A new design will be installed during summer of 2019 which will allow to emit correctly the 150 watts with a circular polarization. Meanwhile, the radiation pattern of the current transmitter will be fully characterized using a captive weather balloon with a platform. The platform will contain the following payload: (a) two short dipole antennas, two FunCube Dongle Pro+ receivers and one Raspberry Pi to measure the power transmitted by each antenna, (b) an inclinometer and a magnetometer to accurately measure the orientation of the platform, (c) a GPS receiver to accurately measure the position of the platform, and (d) a webcam to double-check the whole procedure.



Figure 33: Receiving antenna at BEHUMB (Humbeek)

In parallel, since most of the ICOM-R75 analog commercial receivers used for the BRAMS network have suffered from a failure in the last 2 years (mostly a capacitor problem resulting in a progressive lack of sensitivity of the receiver) and because these receivers are not produced anymore, it was decided to investigate a new type of digital receiver for the future. After various tests, the choice is to use the SDRplay RSP2 which is cheaper, has a larger dynamic range, and is more sensitive than the ICOM-R75. It also admits a 24 MHz reference signal which will ensure the stability of the local oscillator, which again is not the case with the ICOM-R75. It was also decided to use a Raspberry-Pi with our own code written in Python to sample the data, save the signal in WAV format and put accurate timestamps from the GPS clock on the data. With current receiving stations, it is done using a freeware program called Spectrum Lab which unfortunately works only with Windows, which has obviously created a number of issues that we had to solve over the years. A first test is planned at the station in Uccle (BEUCCL) where a power splitter will be used to equally divide the signal coming from the antenna between the ICOM-R75 and the RSP2 receivers.



Figure 34: The RSP2 receiver and the external sound-card used by the current system to sample the signal going out of the ICOM-R75 receiver (Top). The power splitter used to split the incoming signal from the antenna between the ICOM-R75 and the RSP2 receivers (Bottom). Pictures were taken at the BEUCCL station.

Ionospheric observations of meteors

The sporadic ionospheric E layer (Es) is a thin layer of ions, only a few kilometers thick that is normally observed in the lower ionosphere, at altitudes between 80 and 150 km. When it appears, the Es layer can have a density of electrons and ions many times higher than the background density at such altitudes. The standard theory about the genesis of this phenomenon describes how ions, that are always present in smaller concentrations, get packed together by wind shears between different layers of the neutral thermosphere. The ions involved are mostly long-lived metallic ions, originating from meteors.

Dedicated high time resolution ionosonde observations during the Perseid meteor shower event in August 2018 revealed a different type of sporadic layers that cannot be explained by the aforementioned standard mechanism. The formation of a typical sporadic layer takes some time because ions need to be accumulated, in sufficient quantity, to be able to produce an observable layer. However, we observed sporadic layers appearing within tens of seconds, and quickly disappearing again after a few minutes, at most. These short-lasting, so-called "burst", layers are most likely the signature of direct ionisation by meteoroids, which typically disintegrate at these altitudes.

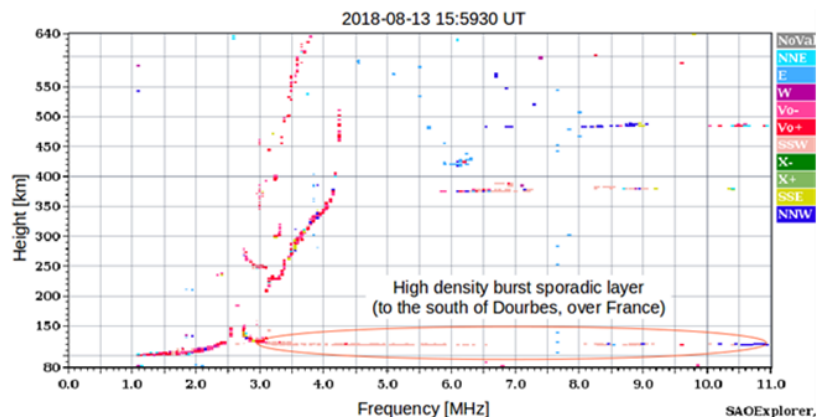


Figure 35: An ionogram, produced by the [Dourbes digisonde](#) on 13/08/2018 at 16:00h, showing a high-density burst sporadic layer detected to the South, over France.

Because the ionosonde can discriminate between echoes coming from different directions, we could also detect, to a reasonable degree of accuracy, the region over which these burst of ionisation appeared. By using data from direct concurrent observations carried out with other ionosondes in Germany, the Czech Republic and Hungary, we were able to also track some of the longer lasting bursts for a few minutes as they moved over Europe.

The success of the 2018 Perseids monitoring campaign is a strong motivation for further research of the effects of meteor showers and for future coordinated campaigns with our European partners during such regularly occurring phenomena.

Characterization of the VIS-NIR detectors for MAJIS/JUICE

The MAJIS (Moons And Jupiter Imaging Spectrometer) instrument is part of the science payload of the ESA L-Class mission JUICE (JUperiter ICy moons Explorer) to be launched in 2022 with an arrival at Jupiter in 2030. JUICE will perform detailed observations of Jupiter and three of its largest moons, Ganymede,

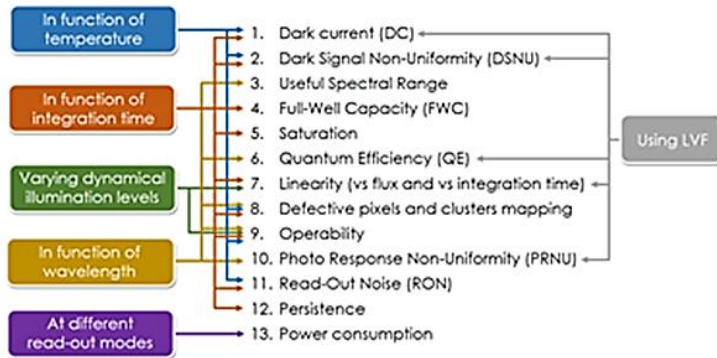


Figure 36: MAJIS VIS-NIR detectors characterization measurements.

Callisto and Europa, for at least three years. MAJIS will perform imaging spectroscopy through two channels: VIS-NIR (0.50 μm - 2.35 μm) and IR (2.25 μm - 5.54 μm), mainly to characterize the Jovian atmosphere and magnetosphere, and to determine the global composition of surface materials of the icy moons. The subsystems of the instrument, and in particular its detectors, need to be characterized in the laboratory before being tested at instrument level after the integration. The STCE

contributes to MAJIS as the characterization of the spare and flight models of the VIS-NIR detectors will be done by the Space optoelectronic and optical Technology and Calibration Laboratories (STCL), a joint BIRA-IASB, KSB-ORB and KMI-IRM activity, whose purpose is to provide facilities and expertise, in particular to support the characterization of space instrumentation.

During 2018, the design and development of the MAJIS facility to characterize the VIS-NIR detectors of MAJIS/JUICE was initiated. The calibration bench must guarantee cleanliness and safety conditions for the detectors in a simulated space environment. The vacuum conditions ($<10^{-5}$ mbar), the thermal environment (116 K to 160 K) and a well-designed optical system for versatile illumination conditions, are needed to characterize the detectors in accordance with the requirements and the planning as reported in Figure 36.

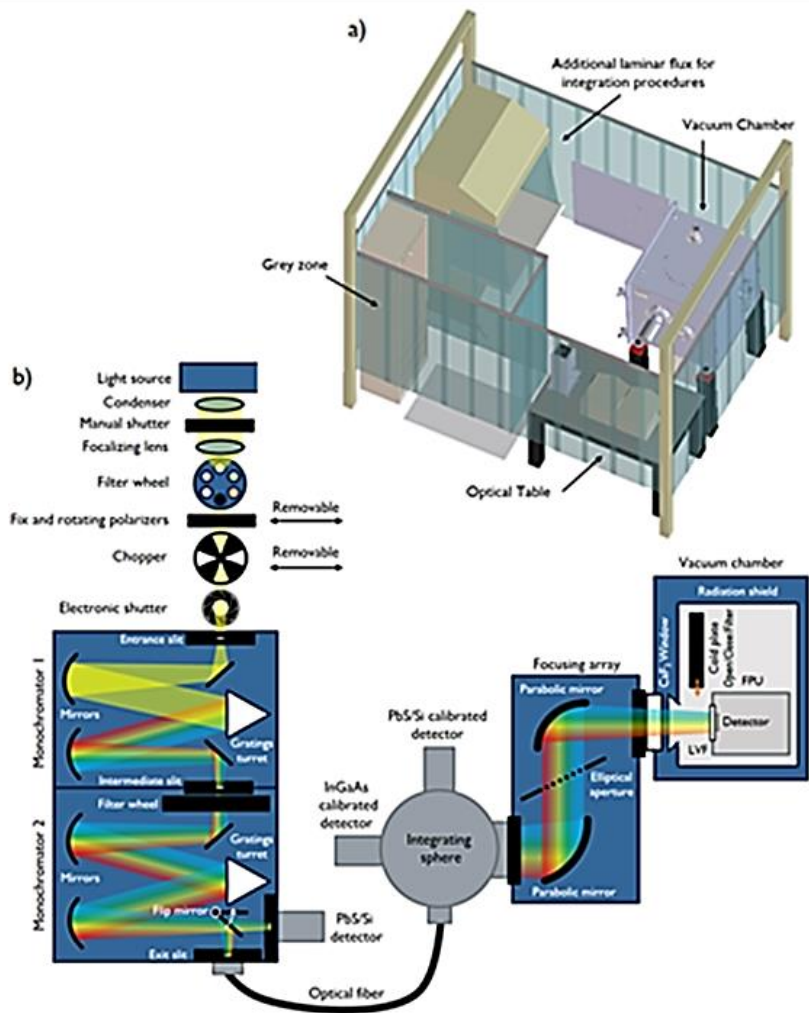


Figure 37: MAJIS VIS-NIR detectors characterization bench: a) schematic model inside the laminar flux, b) optical diagram of the facility at configuration 3.

a collimating optical array that provides the necessary convergent beam to illuminate the detector through a Linear Variable Filter (LVF) installed in front of the detector (for higher diffraction orders rejection), as in the MAJIS instrument. A CaF_2 window interfaces the optical equipment on the table with the detector mount inside the vacuum chamber. Calibrated detectors are used at different points of the optical path to monitor the intensity stability of the light beam and to allow measurements that require an absolute measurement of optical power (as for the Quantum Efficiency). A radiometric modeling was developed to assess the optical performances of the bench.

The next steps for 2019 are the finalization of the Optics Ground Support Equipment (OGSE) for the automatic operation of the calibration bench, and the thermal vacuum validation of the facility by using the VIS-NIR Structural Model and the Engineering Model. Then, finally, the main campaign for the characterization of the spare and flight models of MAJIS VIS-NIR can start.

The facility, presented in Figure 37, was developed in an ISO-5 laminar flux at IASB-BIRA including a vacuum chamber, a cryo-cooling system and optical equipment (QTH lamp, double monochromator). There's also a dedicated detector mount, designed to thermalize the detector and support all the characterization measurements.

Since some parameters require different illumination conditions, beam uniformity, exposure time, and/or data acquisition procedure, three configurations were defined. The first one provides dark conditions for the detector thanks to the radiation shield ($<190\text{K}$) that surrounds it. In the configuration 2, the detector receives a uniform light beam coming from an integrating sphere, itself illuminated by the tunable and monochromatic light beam. Configuration 3 adds



Life at the STCE - Space Pole enthusiasts have started their own greenhouse experiment, i.e. trying to raise some fruit and vegetables in the greenhouses at the ROB. So far, the theory has been proven very successful, yielding rich crops as well as numerous blisters and sweat drops. Picture credits: Nicolas De Coster.

Applications, modeling and services

PECASUS – Pan-European Consortium for Aviation Space weather User Services

The radiation environment at aviation altitudes is shaped mainly by Galactic Cosmic Rays (GCR) and occasional Solar Energetic Particle (SEP) events, both phenomena comprised of high energetic particles (mainly protons with energies >500 MeV) that interact with Earth's atmosphere and generate secondary particles. High energy protons entering the funnel-like cusps in the Earth's magnetic field above the polar caps impact not only the health of crew and passengers, but also electronic devices and HF communications. When, due to a SEP event, an elevated radiation level is recorded on Earth it is known as a Ground Level Enhancement (GLE); it is observed as a short-term enhancement in the GCR background.

The [PECASUS](#) consortium has been established in response to the recent call from the International Civil Aviation Organization (ICAO) to provide a Global Space Weather Information Service. The requested (24/7) service focuses on the dissemination of warning messages (“advisories”) towards aviation actors and corresponds to extreme space weather events with impact on aviation GNSS systems, satellite communications, HF communication and radiation levels at flight altitudes. The PECASUS team consists of a number of European partners with proven space weather service capabilities and expertise, with FMI (Finland) as leader and being responsible for communications towards the aviation sector. The Advisory Messages will be produced by the STCE (Belgium) based on expert interpretation and data streams provided by DLR (Germany), INGV (Italy), Seibersdorf Laboratories (Austria), STCE (Belgium), SRC (Poland) and FU (Cyprus). In addition, the MetOffice (UK) will act as a backup in case of a major failure in the network, while the KNMI (The Netherlands) will take care of user liaison and monitor the PECASUS performance. On basis of expertise in the field of particle radiation and its effects on technology and human health, gained through several projects (e.g. COMESSEP, SEPEM, SPENVIS), the Space Weather Group at BIRA-IASB has been attributed the role of coordinator of the radiation expert group and provider of scientific support for compiling the radiation advisories. The service operation will start in 2019.

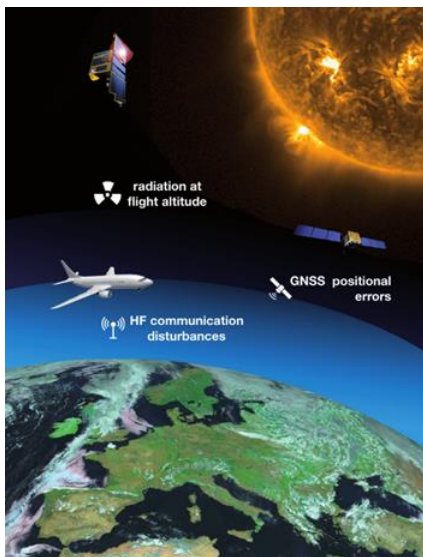


Figure 39: Enhanced solar activity may increase radiation doses at flight altitude, impact communication and navigation.
(Credits: PECASUS)

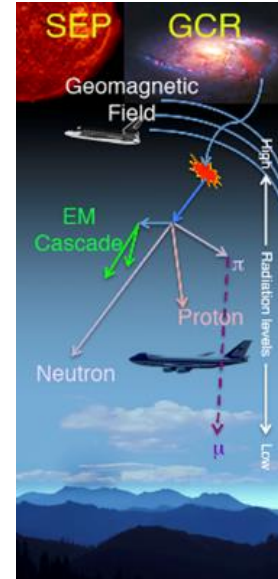


Figure 38: Aviation radiation environment
(Tobiska et al., 2015)

The Advisory Messages will be produced by the STCE (Belgium) based on expert interpretation and data streams provided by DLR (Germany), INGV (Italy), Seibersdorf Laboratories (Austria), STCE (Belgium), SRC (Poland) and FU (Cyprus). In addition, the MetOffice (UK) will act as a backup in case of a major failure in the network, while the KNMI (The Netherlands) will take care of user liaison and monitor the PECASUS performance. On basis of expertise in the field of particle radiation and its effects on technology and human health, gained through several projects (e.g. COMESSEP, SEPEM, SPENVIS), the Space Weather Group at BIRA-IASB has been attributed the role of coordinator of the radiation expert group and provider of scientific support for compiling the radiation advisories. The service operation will start in 2019.

In summary: Space weather can affect aviation by causing degradation of radio/satellite communication, onboard system failure, high radiation doses for air travelers, and disturbances in signal reception from navigation satellites. Air travel is global and the mitigation of traffic disruptions requires international cooperation. The Council of International Civil Aviation Organization has designated the PECASUS consortium as one of three global space weather service centres. The Space Weather

Group at BIRA-IASB will be responsible for the coordination of the radiation expert group and for the provision of scientific support to the on duty operators.

DigiSun : a tool to extract scientific data from sunspot drawings

Sunspot drawings are the base material available for deriving detailed information about the long-term evolution of the solar cycle. In this context, it is important to have the appropriate tools to convert drawings into exploitable scientific data and to extract as much information as possible from these drawings. While such a tool is obviously important for every observatory with historical sunspot drawings and/or still makes daily drawings, there was no generic tool available in the solar physics community. As a side effect, there is a lack of homogeneity among the data and some sunspot drawings collections stay buried in archives due to a lack of manpower to write the appropriate software.

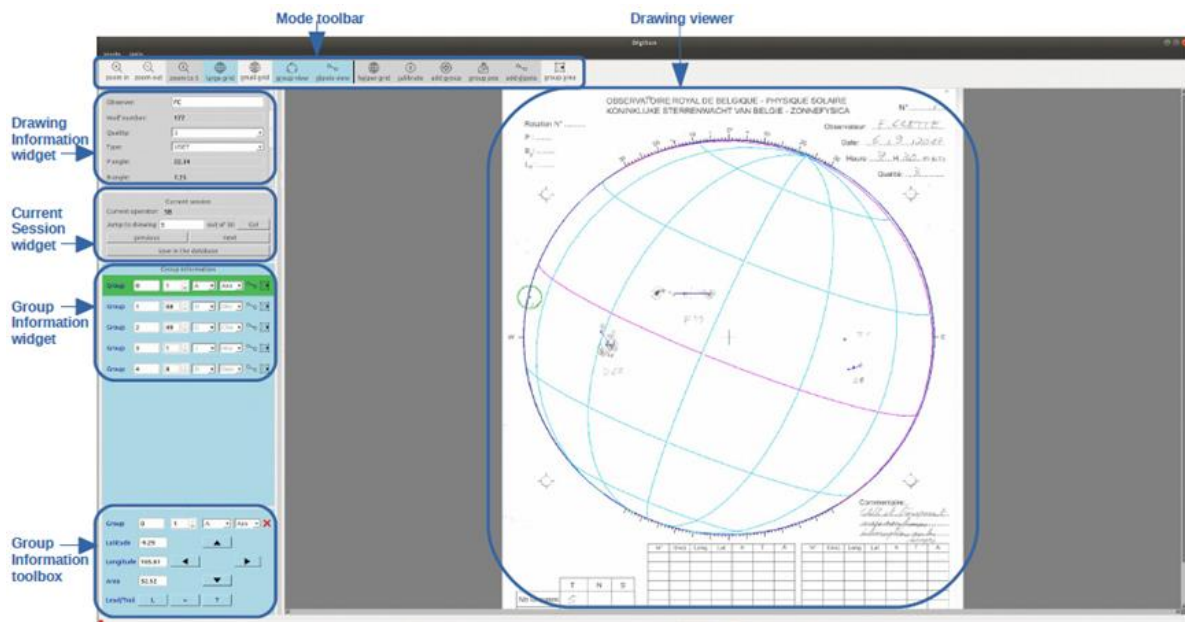


Figure 40: Global view of DigiSun and some of its functionalities.

At ROB, there is a collection of 70 years of sunspot drawings that is still growing with the addition of daily input. The scanning and the first analysis of sunspot drawings are done with an in-house software called DigiSun. In 2018, a new version was developed and the code was rewritten on the basis of a first version which showed its limitation due to its lack of modularity and flexibility. DigiSun is a graphical user interface (GUI) with the following functionalities:

- Sunspot drawings display, variable image scale and image overlay (large grid on Figure 40)
- Calculation of the solar axis angles (P , B_0 , L_0) via an in-house ephemeris module
- Correspondence between pixels position and heliographic coordinates on the solar disk
- Recording of sunspot group parameters (number of spots, splitting, Zurich and McIntosh morphological classification)
- Measurement of the dipole positions and recording of the asymmetry leading/trailing
- Total area sunspot group measurement

All the parameters of the groups are then saved in an external database for relevant scientific analysis. In addition, it contains a functionality to perform the scanning of drawings making it a unique end-to-end tool to transform drawings into scientific data.

The latest module, added in the context of the VAL-U-SUN project, is the sunspot group total area measurement. The total area consists of the umbra and the penumbra area of the sunspot groups. It is an important measure because of its strong correlation with the magnetic field associated to the sunspot. To measure the area, a reduced frame around each sunspot group is considered (Figure 41). A selection and paint toolbox allows a fine-grained selection of the group under consideration. The bottom part of the module (Figure 41) indicates the projected and the de-projected areas, the latter taking into account the foreshortening of the group based the correspondence between pixel positions and heliographic coordinates.

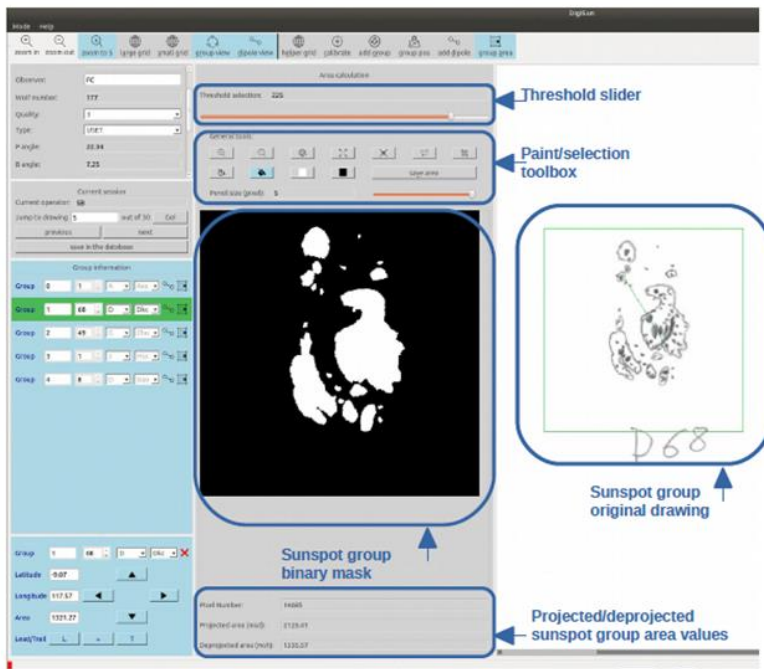


Figure 41: Sunspot area measurement module in DigiSun.

Another important feature of the new version of DigiSun is its adaptability to different drawing formats. This allows the analysis of collections from different observatories. Moreover it was written in a multi-platform programming language making it portable to any computer. A first international collaboration with the Specola Observatory in Locarno was initiated. After a few days of installation and training, the software was perfectly working on-site and is now used for the daily analysis of their sunspot drawings.

We have developed a robust and flexible tool at ROB for the analysis of sunspot drawings. It is

now used for our daily drawings. Moreover it is used to analyze older drawings from our collection in the context of the VAL-U-SUN project, sunspot area measurements being now fast and intuitive. Another achievement is the portability of the software and the fact that it was distributed successfully to another observatory. Hence, software developed for our own needs proved to be useful to the wider, international community. As other institutes already mentioned their interest, we plan to distribute DigiSun further in the near future. This will allow access to new long-term solar data with a much better homogenization.

Next generation of JHelioviewer: browsing the Sun

Solar observatories are providing the worldwide community with a wealth of data, covering wide time ranges (e.g., Solar and Heliospheric Observatory, SOHO), multiple viewpoints (Solar TErrestrial RElations Observatory, STEREO), and returning large amounts of data (Solar Dynamics Observatory, SDO). In particular, the large volume of SDO data presents challenges; the data are available only from a few repositories, and full-disk, full-cadence data for reasonable durations of scientific interest are difficult to download, due to their size and the download rates available to most users. From a scientist's perspective this poses three problems: accessing, browsing, and finding interesting data as efficiently as possible.

JHelioviewer was developed to address these challenges. It is a visualization software tool for solar data based on the JPEG 2000 compression standard and part of the open source ESA/NASA Helioviewer Project. Since the first release of JHelioviewer in 2009, the scientific functionality of the software has been extended significantly under the scope of this project. The JPEG 2000 standard offers useful new features that facilitate the dissemination and analysis of high-resolution image data and offers a solution to the challenge of efficiently browsing petabyte-scale image archives. The JHelioviewer software is open source, platform independent, and extendable via a plug-in architecture. The latest version (and all previous versions) of the JHelioviewer software are available online at <http://www.jhelioviewer.org>, along with a comprehensive [user manual](#).

With JHelioviewer, users can visualize the Sun for any time period between September 1991 and today; they can perform basic image processing in real time, track features on the Sun, and interactively overlay magnetic field extrapolations. The software integrates solar event data and a timeline display. Once an interesting event has been identified, science quality data can be accessed for in-depth analysis. As a first step towards supporting science planning of the upcoming Solar Orbiter mission, JHelioviewer offers a virtual camera model that enables users to set the vantage point to the location of a spacecraft or celestial body at any given time.

Over the last decade, the amount of data returned from space- and ground-based solar telescopes has increased by several orders of magnitude. This constantly increasing volume is both a blessing and a barrier: a blessing for providing data with significantly higher spatial and temporal resolution, but also a barrier for scientists to access, browse, and analyze them.

Since its launch in 2010, the Solar Dynamics Observatory (SDO) has been returning 1.4 terabyte of image data per day, more than three orders of magnitude more than the Solar and Heliospheric Observatory (SOHO). Such staggering volumes of data are accessible only from a few repositories, and users have to deal with data sets that are effectively immobile and practically difficult to download. From a scientist's perspective this poses three problems: accessing, browsing, and finding interesting data as efficiently as possible.

JHelioviewer addresses these three problems using a novel approach: image data is lossily compressed using the JPEG 2000 standard and served on demand in a quality-progressive, region-of-interest-based stream. Together with the [web application](#), it is part of the joint ESA/NASA Helioviewer Project. The aim of the Helioviewer Project is to enable exploration of the Sun and the inner heliosphere for everyone, everywhere, via intuitive interfaces and novel technology. It achieved its first milestone by making data

from SDO and SOHO easily accessible to the scientific community and general public and continues to enjoy popularity in the scientific community, also because of its open source approach.

With the advent of SDO, solar physics has entered the “Big Data” domain: SDO's science data volume of about 0.8 petabyte per year – equivalent to downloading half a million songs per day, every day – is costly to store and can only be delivered to a small number of sites. In a few years, the DKIST will return about 4.5 petabyte per year. Its VBI instrument alone will generate 10^6 images/day, which dwarfs SDO/AIA's 60,000 images/day.

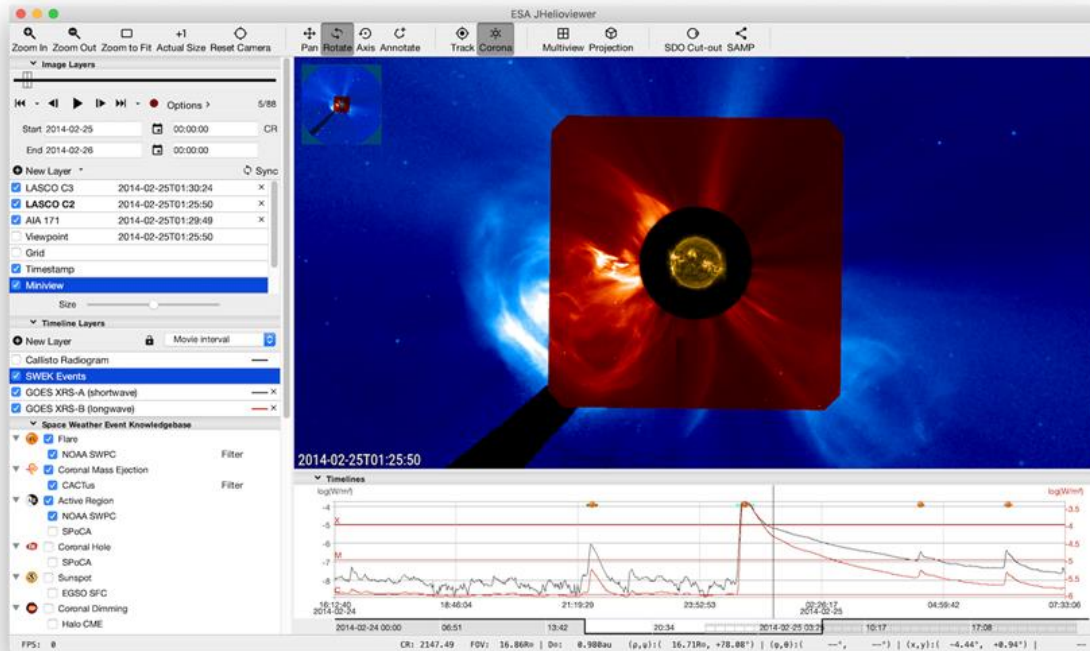


Figure 42: Screenshot of the JHelioviewer application. The left part of the application window hosts expandable sections to manage and display time-dependent image layers, timelines, and event data. The main panel displays image data in a 3D scene that the user can interact with. The timeline panel in the bottom right displays 1D and 2D plots of time series, e.g., disk-integrated X-ray fluxes. Markers for solar events can be overlaid on both panels. This Figure shows the user application interface as of version 2.15.6.

Science quality SDO data for most cadences and durations that users are interested in is too voluminous to download for browsing purposes. The Helioviewer Project addresses this limitation by providing visual browsing data at full 16 megapixel resolution for the entire mission duration, along with co-temporal data from additional data sources. This enables scientists to efficiently browse data from any day of the mission and request archived science data for in-depth analysis once they have identified interesting events.

In light of its popularity in the solar physics community and beyond, our team at ROB - in joint effort with colleagues from the FHNW institute from Switzerland - has enhanced JHelioviewer significantly in this project. We highlight the following new features:

- displaying multi-viewpoint data in a single 3D scene, e.g. from the twin Solar TERrestrial RELations Observatory (STEREO) spacecraft;
- real-time generation and display of difference movies;
- PFSS magnetic field extrapolation models using synoptic magnetograms from the Global Oscillation Network Group (GONG);
- timelines of 1D and 2D data, e.g. disk-integrated X-ray fluxes and radio spectrograms;
- integrating solar event data from the Heliophysics Event Knowledgebase (HEK) and curating it into a Space Weather Event Knowledgebase (SWEK);
- various 2D projections (orthographic, latitudinal, polar, log-polar);
- a split-screen view to display multiple images side by side;
- save and restore scenes;
- interaction with other programs via the SAMP protocol;
- a virtual camera model that enables the user to set the vantage point to the location of a spacecraft or celestial body at a given time, using an ephemeris server.

The last feature in the above list is a first step towards supporting the science planning process for the Solar Orbiter mission, which is a key objective for the future development of JHelioviewer. In parallel, a large number of additional data sets have been added. These include data from the Hinode (XRT), PROBA-2 (SWAP and LYRA), Yohkoh (SXT), and TRACE space missions, as well as data from the ground-based facilities NSO/SOLIS, NSO/GONG, Kanzelhöhe Solar Observatory, ROB-USET, the Nançay Radioheliograph, and the e-CALLISTO network.

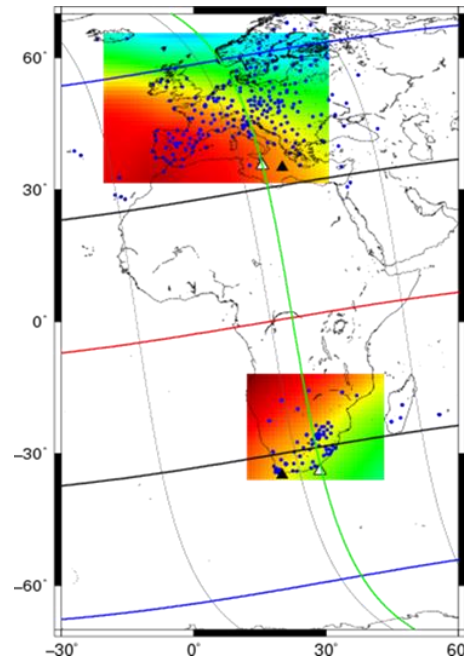


Figure 43: GNSS network used. The blue circles are the GNSS stations used for the period 1998-2017. The red, black, blue lines are the geomagnetic latitudes (0°, +30° and +60°). The green line represents the geomagnetic longitude E95°. The white and black triangles (geographic and geomagnetic coordinates respectively) are the locations considered for inter-hemispheric comparison. The TEC maps are given for year 2015, DoY 076, time 15:00 UTC.

Inter-hemispheric comparison of the ionosphere-plasmasphere

An increasing demand for a better modelling and understanding of the Ionosphere-Plasmasphere system (I/Ps) is required for both scientific and public practical applications using electromagnetic wave signals reflecting on or passing through this layer. In that frame, the BEZA-COM project, a networking project from BELSPO and its South African homologue called NRF (National Research Foundation) has been accepted in 2018. The aim of the BEZA-COM project is to contribute to the actual important scientific questions addressed by the International Steering Committee of the Scientific Committee on Antarctic Research (ISC-SCAR): "What are the differences in the inter-hemispheric conjugacy between the ionosphere and that in the lower, middle and upper atmospheres, and what causes those differences?" (Kennicutt et al. 2014).

During 2018 the ROB-IONO software (Bergeot et al. 2014) was used to reprocess the GNSS data (GPS+GLONASS) of the dense EUREF Permanent GNSS Network and South African TRIGNET networks as well as IGS stations for the period 1998-2017. The output consists in Total Electron Content (TEC expressed in TECu, with $1 \text{ TECu} = 10^{16} \text{ e}^- \cdot \text{m}^{-2}$) maps, estimated every 15 min., and covering the central European and South African regions (Figure 43).

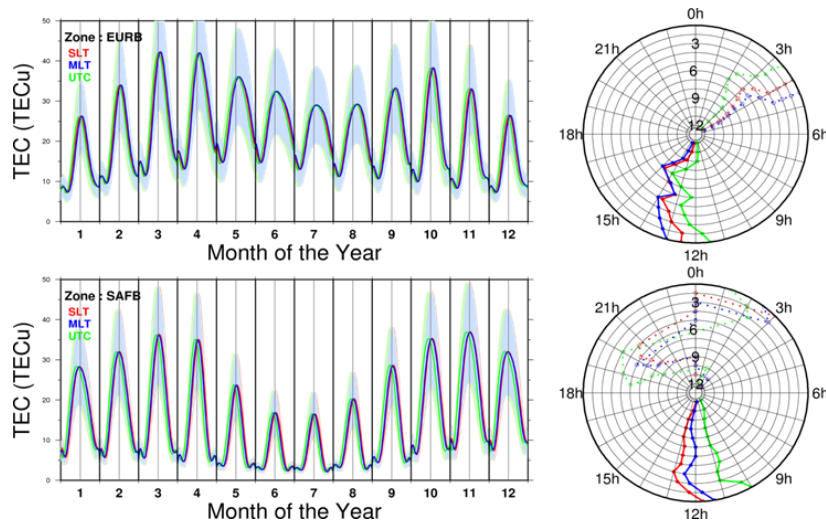


Figure 44: Monthly climatological behaviour of the daily TEC for the two hemispheres and different time definitions: SLT (red), UTC (green) and MLT (blue). Left: The coloured lines are the daily TEC (grey line is noon) for medium solar activity level ($F10.7P = 120 \text{ sfu}$). The spread of the colours stands for low and high solar activity ($F10.7P = 80$ and 160 sfu respectively). Right: Time of occurrence of maximum (bold lines) and minimum TEC (dashed lines). Internal circles: month of the year with December at the centre of the picture. Top: For the European location $E95^\circ; N35^\circ$ in geomagnetic coordinates. Bottom: For the South African location $E95^\circ; S35^\circ$ in geomagnetic coordinates.

resulting model permits to estimate the TEC at a given location, for a given solar activity level and specific time in Coordinated Universal Time (UTC), Solar Local Time (SLT) and Magnetic Local Time (MLT, given by Laundal et Richmond 2016) above each location (Figure 44).

The climatological model based on monthly coefficients allows the description of the climatological behaviour of the I/Ps. From Figure 44, there are clear seasonal and annual variations with a maximum TEC around the equinoxes and minimum around the solstices. The maximum TEC occurs mainly around noon for any of the time definitions and are constant over the year. Some differences are also highlighted: (1) the maximum of the TEC is higher during the daylight (10 to 55% for hours between 10:00 and 15:00) in the Northern hemisphere compare to the Southern for February to September; (2) the minimum TEC (i.e. during low solar zenith angle between 22:00 and 6:00) is also higher in the Northern hemisphere for the period February-September (16 to 80%); (3) the time of occurrence of the minimum TEC is generally constant over the year for the European region but not for South Africa.

The TEC is extracted at different locations in the Northern and Southern hemispheres. The locations are, for the same longitude, symmetric with respect to the equators: the geographic equator and the geomagnetic equator (see the resp. black and white triangles in Figure 43).

The data sets (i.e. TEC at locations symmetric with respect to the equators for the period 1998-2017) are then used to constrain an empirical model to predict the TEC at different locations and time from $F10.7P$ solar index in entrance using a least-square adjustment. The

Thanks to the equatorial symmetry of the locations considered, the difference in TEC climatological behaviour can't be explain by (1) differences in the solar zenithal angle nor (2) different geomagnetic phenomena in European and South African regions. Consequently, one of the main component to be taking into account to explain the differences in the I/Ps is the density of thermospheric neutral winds. In the future, we will check to the thermospheric oxygen/nitrogen differences using, for example, GUVI satellite data.



Life at the STCE - The [CESRA 2018 Summer School](#) took place in the Meridian Room of the Royal Observatory from 10-14 September. Organized by the ROB and STCE, it is aimed at students holding a Master degree, preferentially in Physics or Engineering, who wants an introduction to the science and technics of solar radio physics. Definitely not for the faint-of-heart.

Publications

This overview of publications consists of three lists: the peer-reviewed articles, the presentations and posters at conferences, and the public outreach talks and publications for the general public. It does not include non-refereed articles, press releases, the daily, weekly and monthly bulletins that are part of our public services,... These data are available at the [STCE-website](#) or upon request.

Authors belonging to the STCE have been highlighted in the list of peer reviewed articles.

Peer reviewed articles

1. Afanasyev, A.N.; **Zhukov, A.N.**
Propagation of a global coronal wave and its interaction with large-scale coronal magnetic structures
Astronomy & Astrophysics, 614, A139, 2018, DOI: 10.1051/0004-6361/201731908
2. Aparicio, A.J.P.; **Lefèvre, L.**; Gallego, M.C.; Vaquero, J.M.; **Clette, F.**; Bravo-Paredes, N.; Galaviz, P.; Bautista, L.
A Sunspot Catalog for the Period 1952-1986 from Observations made at the Madrid Astronomical Observatory
Solar Physics, 293, 164, 2018, DOI: 10.1007/s11207-018-1387-1
3. Carrasco, V.M.S.; García-Romero, J.M.; Vaquero, J.M.; Rodríguez, P.G.; Foukal, P.; Gallego, M.C.; **Lefèvre, L.**
The umbra-penumbra area ratio of sunspots during the Maunder Minimum
The Astrophysical Journal, 865, 2, 88, 2018, DOI: 10.3847/1538-4357/aad9f6
4. Cliver, E.W.; **D’Huys, E.**
Size Distributions of Solar Proton Events and Their Associated Soft X-Ray Flares: Application of the Maximum Likelihood Estimator
The Astrophysical Journal, 864, 1, 2018, DOI: 10.3847/1538-4357/aad043
5. Dąbrowski, B.P.; Morosan, D.E.; Fallows, R.A.; Blaszkiewicz, L.; Krankowski, A.; **Magdalenic, J.**; Vocks, C.; Mann, G.; Zucca, P.; Sidorowicz, T.; Hajduk, M.; Kotulak, K.; Fron, A.; Sniadkowska, K.
Observations of the Sun using LOFAR Baldy station
Advances in Space Research, 62, 7, 1895-1903, 2018, DOI: 10.1016/j.asr.2018.06.037
6. **De Keyser, J.**; Lavraud, B.; Prech, L.; **Neefs, E.**; **Berkenbosch, S.**; **Beeckman, B.**; Fedorov, A.; Marcucci, M.F.; De Marco, R.; Brienza, D.
Beam tracking strategies for fast acquisition of solar wind velocity distribution functions with high energy and angular resolutions
Annales Geophysicae, 36, 1285–1302, 2018, DOI: 10.5194/angeo-36-1285-2018
7. **Dominique, M.**; **Zhukov, A.N.**; **Dolla, L.**; Inglis, A.; Lapenta, G.
Detection of Quasi-Periodic Pulsations in Solar EUV Timeseries
Solar Physics, 293, 4, 61, 2018, DOI: 10.1007/s11207-018-1281-x
8. **Dominique, M.**; **Zhukov, A.N.**; Heinzel, P.; **Dammasch, I.E.**; **Wauters, L.**; **Dolla, L.**; **Shestov, S.**; Kretzschmar, M.; Machol, J.; Lapenta, G.; Schmutz, W.
First Detection of Solar Flare Emission in Middle-Ultraviolet Balmer Continuum
The Astrophysical Journal Letters, 867, 2, 2018, DOI: 10.3847/2041-8213/aaeace
9. Forbes, T.G.; **Seaton, D.B.**; Reeves, K.K.
Reconnection in the Post-Impulsive Phase of Solar Flares
The Astrophysical Journal, 858, 70, 2018, DOI: 10.3847/1538-4357/aabad4
10. Fountoulakis I.; Zerefos, C.S.; Bais, A.F.; Kapsomenakis, J.; Koukoulis, M.-E.; Ohkawara, N.; Fioletov, V.; **De Backer, H.**; Kakkala, K.; Karppinen, T.; Webb, A.R.
Twenty-five years of spectral UV-B measurements over Canada, Europe and Japan : Trends and effects from changes in ozone, aerosols, clouds and surface reflectivity
Comptes Rendus Geoscience, 350, 7, 393-402, 2018, DOI: 10.1016/j.crte.2018.07.011
11. Gogoberidze, G.; **Voitenko, Y.M.**; Machabeli, G.
Temperature spectra in the solar wind turbulence
Monthly Notices of the Royal Astronomical Society, 480, 2, 1864-1869, 2018, DOI: 10.1093/mnras/sty1914
12. Goryaev, F.; Slemzin, V.; Rodkin, D.; **D’Huys, E.**; **Podladchikova, O.**; **West, M.**
Brightening and darkening of the extended solar corona observed by SWAP telescope during the superflares on 6 and 10 September 2017

- The Astrophysical Journal Letters, 856, 2, L38, 2018, DOI: 10.3847/2041-8213/aab849
13. Grison, B.; Hanzelka, M.; Breuillard, H.; **Darrouzet, F.**; Santolik, O.; Cornilleau-Wehrin, N.; Dandouras, I. *Plasmaspheric plumes and EMIC rising tone emissions* Journal of Geophysical Research Space Physics, 123, 9443-9452, 2018, DOI: 10.1029/2018JA025796
14. **Gunell, H.**; **Maggiolo, R.**; Nilsson, H.; Stenberg Wieser, G.; Slapak, R.; Lindkvist, J.; Hamrin, M.; **De Keyser, J.** *Why an intrinsic magnetic field does not protect a planet against atmospheric escape* Astronomy & Astrophysics, 614, L3, 2018, DOI: 10.1051/0004-6361/201832934
15. Hahn, M.; **D'Huys, E.**; Savin, D.W. *Density Fluctuations in a Polar Coronal Hole* The Astrophysical Journal, 860, 1, 2018, DOI: 10.3847/1538-4357/aac0f3
16. Harrison, R.A.; Davies, J.; Barnes, D.; Byrne, J.; Perry, C.; Bothmer, V.; Eastwood, J.; Gallagher, P.; Kilpua, E.; Moestl, C.; **Rodriguez, L.**; Rouillard, A.; Odstrcil, D. *Coronal mass ejections in the heliosphere: I. Statistical analysis of the observational properties of coronal mass ejections detected in the heliosphere between 2007 and 2017 by STEREO/HI* Solar Physics, 293, 77, 2018, DOI: 10.1007/s11207-018-1297-2
17. Hosteaux, S.; Chané, E.; **Decraemer, B.**; **Talpeanu, D.-C.**; **Poedts, S.** *Ultra-high-resolution model of a breakout CME embedded in the solar wind* Astronomy & Astrophysics, 620, A57, 2018, DOI: <https://doi.org/10.1051/0004-6361/201832976>
18. Jejič, S.; Heinzl, P.; Labrosse, N.; **Zhukov, A.N.**; Bemporad, A.; Fineschi, S.; Gunár, S. *Visibility of Prominences Using the He I D3 Line Filter on the PROBA-3/ASPIICS Coronagraph* Solar Physics, 293, 2, 2018, DOI: 10.1007/s11207-018-1251-3
19. **Katsiyannis, A.C.**; **Dominique, M.**; **Pierrard, V.**; **Lopez Rosson, G.**; **De Keyser, J.**; **Berghmans, D.**; **Borremans, K.**; **Kruglanski, M.**; **Dammasch, I.E.**; **De Donder, E.** *The detection of ultra-relativistic electrons in low Earth orbit* Journal of Space Weather and Space Climate, 8, A01, 2018, DOI: 10.1051/swsc/2017041
20. Kotova, G.; Verigin, M.; **Lemaire, J.**; **Pierrard, V.**; Bezrukhikh, V.; Smilauer, J. *Experimental study of the plasmasphere boundary layer using MAGION 5 data* Journal of Geophysical Research: Space Physics, 123, 1251-1259, 2018, DOI: 10.1002/2017JA024590
21. López-Solano, J.; Redondas, A.; Carlund, T.; ... ; **De Bock, V.**; ... ; and 23 co-authors *Aerosol optical depth in the European Brewer Network* Atmospheric Chemistry and Physics, 18, 3885-3902, 2018, DOI: 10.5194/acp-18-3885-2018
22. Malovichko, P.; **Voitenko, Y.**; **De Keyser, J.** *Non-resonant Alfvénic instability activated by high temperature of ion beams in compensated-current astrophysical plasmas* Astronomy & Astrophysics, 615, A169, 2018, DOI: <https://doi.org/10.1051/0004-6361/201731710>
23. Mann, G.; Breitling, F.; Vocks, C.; ... ; **Magdalenic, J.**; ... ; and 87 co-authors *Tracking of an electron beam through the solar corona with LOFAR* Astronomy & Astrophysics, 611, A57, 2018, DOI: <https://doi.org/10.1051/0004-6361/201629017>
24. **Marqué, C.**; Klein, K.-L.; Monstein, C.; Opgenoorth, H.; Pulkkinen, A.; Buchert, S.; Krucker, S.; Van Hoof, R.; Thulesen, P. *Solar radio emission as a disturbance of aeronautical radionavigation* Journal of Space Weather and Space Climate, 8, A42, 2018, DOI: 10.1051/swsc/2018029
25. Mathieu, S.; von Sachs, R.; **Delouille, V.**; **Lefèvre, L.** *Uncertainty Quantification in Sunspot Counts* 2018 IEEE Data Science Workshop (DSW), Lausanne, 1-5, 2018, DOI: 10.1109/DSW.2018.8439893
26. Mavromichalaki, H.; Gerontidou, M.; Paschalis, P.; Paouris, E.; Tezari, A.; Sgouropoulos, C.; **Crosby, N.**; **Dierckxsens, M.** *Real-Time Detection of the Ground Level Enhancement on 10 September 2017 by A.Ne.Mo.S.: System Report* Space Weather, 16, 1797-1805, 2018, DOI:10.1029/2018SW001992
27. McLaughlin, J.; Nakariakov, V.; **Dominique, M.**; Jelinek, P.; Takasoa, S. *Modelling Quasi-periodic Pulsations in Solar and Stellar Flares* Space Science Reviews, 214,45, 2018, DOI: 10.1007/s11214-018-0478-5
28. Meftah, M.; Damé, L.; **Bolsée, D.**; Hauchecorne, A.; **Pereira, N.**; **Sluse, D.**; **Cessateur, G.**; ... ; and 10 co-authors *SOLAR-ISS, a new reference spectrum based on SOLAR/SOLSPEC observations* Astronomy & Astrophysics, 611, A1, 2018, DOI: 10.1051/0004-6361/201731316

29. Nemeč, F.; Santolík, O.; Hayosh, M.; **Darrouzet, F.**; Cornilleau-Wehrin, N.
Detailed properties of equatorial noise with quasiperiodic modulation
Journal of Geophysical Research Space Physics, 123, 7, 5344-5355, 2018, DOI: 10.1029/2018JA025382
30. **Pereira, N.**; **Bolsée, D.**; Sperfeld, P.; Pape, S.; **Sluse, D.**; **Cessateur G.**
Metrology of solar spectral irradiance at the top of the atmosphere in the near infrared measured at Mauna Loa Observatory: the PYR-ILIOS campaign
Atmospheric Measurement Techniques, 11, 6605–6615, 2018, DOI: 10.5194/amt-11-6605-2018
31. Philipona, R.; Mears, C.; Fujiwara, M.; Jeannet, P.; Thorne, P.; Bodeker, G.; Haimberger, L.; Hervo, M.; Popp, C.; Romanens, G.; Steinbrecht, W.; Stübi, R.; **Van Malderen, R.**
Radiosondes show that after decades of cooling, the lower stratosphere is now warming
Journal of Geophysical Research: Atmospheres, 123, 12, 509–12, 522, 2018, DOI: <https://doi.org/10.1029/2018JD028901>
32. Raukunen, O.; Vainio, R.; Tylka, A.J.; Dietrich, W.F.; Jiggins, P.; Heynderickx, D.; **Dierckxsens, M.**; **Crosby, N.**; Ganse, U.; Siipola, R.
Two solar proton fluence models based on ground level enhancement observations
Journal of Space Weather and Space Climate, 8, A04, 2018, DOI:10.1051/swsc/2017031
33. Reinisch, B.; Galkin, I.; Belehaki, A.; ... ; **Verhulst, T.**; **Stankov, S.**; ... ; and 14 co-authors
Pilot ionosonde network for identification of travelling ionospheric disturbances
Radio Science, 53, 3, 365-378, 2018, <https://doi.org/10.1002/2017RS006263>
34. Riley, P.; Mays, M.L.; **Andries, J.**; ... ; **Delouille, V.**; ... ; **West, M.J.**; ... ; and 13 co-authors
Forecasting the Arrival Time of Coronal Mass Ejections: Analysis of the CCMC CME Scoreboard
Space Weather, 16, 1245–1260, 2018, DOI: <https://doi.org/10.1029/2018SW001962>
35. **Ritter, B.**; Gérard, J.-C.; Hubert, B.; **Rodriguez, L.**; Montmessin, F.
Observations of the Proton Aurora on Mars with SPICAM on board Mars Express
Geophysical Research Letters, 45, 2, 612-619, 2018, DOI: <https://doi.org/10.1002/2017GL076235>
36. Rodkin, D.; Slemzin, V.; **Zhukov, A.N.**; Goryaev, F.; Shugay, Y.; Veselovsky, I.
Single ICMEs and Complex Transient Structures in the Solar Wind in 2010 - 2011
Solar Physics, 293, 78, 2018, DOI: 10.1007/s11207-018-1295-4
37. Ryan, D.F.; Baumgartner, W.H.; Wilson, M.; **BenMoussa, A.**; Campola, M.; Christe, S.D.; **Gissot, S.**; Jones, L.; Newport, J.; Prydderch, M.; Richards, S.; Seller, P.; Shih, A.Y.; Thomas, S.
Tolerance of the High Energy X-ray Imaging Technology ASIC to potentially destructive radiation processes in Earth-orbit-equivalent environments
Journal of Instrumentation, 13, P02030, 2018, DOI: <https://doi.org/10.1088/1748-0221/13/02/P02030>
38. **Scolini, C.**; Messerotti, M.; Poedts, S.; **Rodriguez, L.**
Halo Coronal Mass Ejections during Solar Cycle 24: reconstruction of the global scenario and geoeffectiveness
Journal of Space Weather and Space Climate, 8, A09, 2018, DOI: 10.1051/swsc/2017046
39. **Scolini, C.**; Verbeke, C.; Poedts, S.; Chané, E.; Pomoell, J.; Zuccarello, F.P.
Effect of the Initial Shape of Coronal Mass Ejections on 3-D MHD Simulations and Geoeffectiveness Predictions
Space Weather, 16, 754-771, 2018, DOI: <https://doi.org/10.1029/2018SW001806>
40. **Shestov, S.V.**; **Zhukov, A.N.**
Influence of misalignments on the performance of externally occulted solar coronagraphs
Astronomy & Astrophysics, 612, A82, 2018, DOI: 10.1051/0004-6361/201732386
41. **Termonia, P.**; **Van Schaeckbroeck, B.**; **De Cruz, L.**; **De Troch, R.**; ... ; **Giot, O.**; **Hamdi, R.**; **Vannitsem, S.**; **Duchêne F.**; ... ; **Stavrakou, T.**; **Bauwens, M.**; **Müller, J.-F.**; **Luyten, P.**; ... ; **Pottiaux, E.**; and 20 co-authors
The CORDEX.be initiative as a foundation for climate services in Belgium
Climate Services, 11, August 2018, Pages 49-61, <https://doi.org/10.1016/j.cliser.2018.05.001>
42. Thiemann, E.M.B.; Eparvier, F.G.; Bougher, S.W.; **Dominique, M.**; Andersson, L.; Girazian, Z.; Pilinski, M.D.; Templeman, B.; Jakosky, B.M.
Mars Thermospheric Variability Revealed by MAVEN EUVM Solar Occultations: Structure at Aphelion and Perihelion, and Response to EUV Forcing
Journal of Geophysical Research: Planets, 123, 2248-2269, 2018, DOI: 10.1029/2018JE005550
43. **Vandaele, A. C.**; Lopez-Moreno, J.-J.; Patel, M. R.; ... ; **Daerden, F.**; **Ristic, B.**; **Robert, S.**; **Thomas, I. R.**; **Wilquet, V.**; ... ; **Aoki, S.**; **Bolsé, D.**; ... ; **Depiesse, C.**; **Drummond, R.**; ... ; **Hetey, L.**; ... ; **Karatekin, O.**; ... ; **Mahieux, A.**; ... ; **Neary, L.**; **Neefs, E.**; ... ; **Viscardy, S.**; ... ; **Willame, Y.**; ... ; the NOMAD Team; and 34 co-authors

NOMAD, an Integrated Suite of Three Spectrometers for the ExoMars Trace Gas Mission: Technical Description, Science Objectives and Expected Performance
Space Science Reviews, 214, 2018, DOI: 10.1007/s11214-018-0517-2

44. Verbanac, G.; Bandic, M.; **Pierrard, V.**; Cho, J.
MLT plasmopause characteristics: comparison between THEMIS observations and numerical simulations
Journal of Geophysical Research: Space Physics, 123, 2000-2017, 2018, DOI: 10.1002/2017JA024573

45. Verhulst, T.G.W. ; Stankov, S.M.
Ionospheric wave signature of the American solar eclipse on 21 August 2017 in Europe
Advances in Space Research, Vol.61, No.9, pp.2245–2251, doi:10.1016/j.asr.2018.02.007

46. Vocks, C.; Mann, G.; Bisi, M.; Dabrowski, B.; Fallows, R.; Gallagher, P.T.; Krankowski, A.; **Magdalenic, J.**; **Marqué, C.**; Morosan, D.; Rucker, H.O.
LOFAR observations of the quiet solar corona

Astronomy & Astrophysics, 614, A54, 2018, DOI: 10.1051/0004-6361/201630067

47. Ying, B.; Feng, L.; Lu, L.; Zhang, J.; **Magdalenic, J.**; Su, Y.; Su, Y.; Gan, W.
Properties of a Small-scale Short-duration Solar Eruption with a Driven Shock
The Astrophysical Journal, 856, 24, 2018, DOI: 10.3847/1538-4357/aaadaf

48. Zhao, J.S.; **Voitenko, Y.**; **De Keyser, J.**; Wu, D.J.
Nonlinear Decay of Alfvén Waves Driven by Interplaying Two- and Three-dimensional Nonlinear Interactions
The Astrophysical Journal, 857, 42, 2018, DOI: 10.3847/1538-4357/aab555

49. Zucca, P.; Morosan, D.E.; Rouillard, A.P.; ... ; **Magdalenic, J.**; ... ; and 61 co-authors
Shock location and CME 3D reconstruction of a solar type II radio burst with LOFAR
Astronomy & Astrophysics, 615, A89, 2018, DOI: 10.1051/0004-6361/201732308

Presentations and posters at conference

1. Altadill, D.; Blanch, E.; Zornoza, M.J.; Paznukhov, V.; Belehaki, A.; Galkin, I.; Buresova, D.; Verhulst, T.; Sanz, J. Characterization of large scale TIDs by analysis of classical ionospheric data in European region
COSPAR 42nd Assembly, Pasadena, California, USA, 14-22 July 2018
2. Belehaki, A.; ... ; Haralambous, H.; and 10 others
Comparison of Travelling Ionospheric Disturbances characteristics extracted from Digisonde-to-Digisonde operations and GNSS-TEC de-trending and gradient techniques
EGU General Assembly 2018, Vienna, Austria, 8-13 April 2018
3. Belehaki, A.; ... ; Haralambous, H.; and 11 others
Detection of travelling ionospheric disturbances in TechTIDE EC H2020 project and perspectives for the development of mitigation strategies
EGU General Assembly 2018, Vienna, Austria, 8-13 April 2018
4. Belehaki, A.; ... ; Haralambous, H.; and 10 others
HF-based TID nowcast methodology and its validation with GNSS-TEC analysis techniques
2nd URSI AT-RASC, Gran Canaria, Spain, 28 May-1 June 2018
5. Bergeot, N. ; Darrouzet, F. ; Pierrard, V. ; Chevalier, J.-M.
Climatological behavior of the topside ionospheric-plasmaspheric electron content above Antarctica
2nd URSI AT-RASC, Gran Canaria, Spain, 28 May-1 June 2018 (invited talk)
6. Bergeot, N.; Chevalier J.-M.
Climatological Behaviours of the Total Electron Content over Antarctica
POLAR2018: A SCAR/IASC Open Science Conference, Davos, Switzerland, 19-23 June 2018
7. Bergeot, N.; ... ; Spogli, L.; and 40 others
RESOURCE: an International Initiative for Radio Sciences Research on Antarctic Atmosphere
AGU Fall Meeting, Washington, D.C., USA, 10-14 December 2018 (talk and poster)
8. Bergeot, N.; Habarulema, J.B.; Chevalier, J.-M.
Inter-hemispheric comparison of the ionosphere-plasmasphere system
2nd URSI AT-RASC, Gran Canaria, Spain, 28 May-1 June 2018 (poster)
9. Berghmans, D.; Seaton, D.; West, M.
Zooming in on the coronal poles with Solar Orbiter
Polar Perspectives Conference, Boulder Colorado, USA, 25-27 September 2018
10. Berghmans, D.; Rochus, P.; Auchere, F.; Harra, L.; Schmutz, W.; Schuhle, U.
The EUV instrument onboard Solar Orbiter: the EUV corona imaged differently
SDO Science Workshop, Ghent, Belgium, 29 October-2 November 2018
11. Bolsée, D.; Van Optsal, B.; Pereira, N.
The Solar UV-VIS Spectral Irradiance Measurements. Overview of Recent Space and Ground-based Activities from Belgium
European conference on solar UV monitoring, Vienna, Austria, 12-14 September 2018
12. Bolsée, D.; Pereira, N.; Sluse, D.; Cessateur, G.; Meftah, M.; Damé, L.; Hauchecorne, A.; Bekki, S.; Marchand, M.
The Measurement of the Solar Spectral Irradiance during the Solar Cycle 24 using SOLAR/SOLSPEC on ISS
EGU General Assembly 2018, Vienna, Austria, 8-13 April 2018 (poster)
13. Bolsée, D.; Pereira, N.; Cessateur, G.; Meftah, M.; Damé, L.; Bekki, S.; Irbah, A.; Hauchecorne, A.; Sluse, D.
SOLAR/SOLSPEC UV spectrometer. Lessons learned from the 9-year SOLAR mission
Ultra-Violet Detectors and Instruments Workshop, Toulouse, France, 28-29 November 2018
14. Bolsée, D.; ... ; Bekki, S. and 7 others
SOLAR/SOLSPEC : highlights of the 9-year SOLAR mission
INSPIRE and Small Sat workshop, Paris, France, 27-29 August 2018
15. Bruyninx, C.; Legrand, J.; Fabian, A.; Roosbeek, F.
Multi-GNSS Capability of the EUREF Permanent Tracking Network
EUREF symposium, Amsterdam, The Netherlands, 30 May-01 June 2018
16. Bruyninx, C.; Pottiaux, E.; Annaert, N.
Real-time Distribution of EPN Data - Experiences from the ROB Broadcaster
EUREF symposium, Amsterdam, The Netherlands, 30 May-01 June 2018
17. Bruyninx, C.; Legrand, J.; Fabian, A.; Pottiaux, E.
Monitoring of Permanent GNSS Networks Used for Accessing the Terrestrial Reference Frame

COSPAR 42nd Assembly, Pasadena, California, USA, 14-22 July 2018

18. Bruyninx, C.; Bergeot, N.; Chatzinikos, M.; Chevalier, J.-M.; Fabian, A.; Legrand, J.; Pottiaux, E.; Voet, P.; De Doncker, P.
National report of Belgium to EUREF
EUREF symposium, Amsterdam, The Netherlands, 30 May-01 June 2018

19. Bruyninx, C.; Fabian, A.; Legrand, J.; Pottiaux, E.; Roosbeek, F.
ROB's GNSS Contribution to EPOS
EUREF symposium, Amsterdam, The Netherlands, 30 May-01 June 2018

20. Bruyninx, C.; Fabian, A.; Legrand, J.
EPOS-GNSS Network Management and Implementation in M³G
EPOS TCS GNSS Data and Products Workshop, Coimbra, Portugal, 16-17 January 2018

21. Bruyninx, C.
The EUREF Permanent GNSS Network
POSKEN Communication Workshop, Brussels, Belgium, 26-27 April 2018

22. Calders, S.; and the SPENVIS team
SPENVIS Next Generation
9th CCMC Workshop, College Park, Maryland, USA, 23-27 April 2018

23. Calders, S.; Lamy, H.; Anciaux, M.; Ranvier, S.; Martinez Picar, A.; Verbeeck, C.
Towards an autonomous BRAMS network
International Meteor Conference 2018, Pezinok-Modra, Slovakia, 30 August-02 September 2018

24. Calders, S.; Lamy, H.; Martínez Picar, A.; Verbeeck, C.; Anciaux, M.; Ranvier, S.
Towards an autonomous BRAMS network
International Meteor Conference 2018, Pezinok-Modra, Slovakia, 30 August-02 September 2018 (poster)

25. Calders, S.; Messios, N.; Botek, E.; De Donder, E.; Kruglanski, M.; Evans, H.; Rodgers, D.
Modeling the space environment and its effects on spacecraft and astronauts using SPENVIS
SpaceOps 2018 - The 15th International Conference on Space Operations, Marseille, France, 28 May-1 June 2018

26. Calders, S.
SPace ENVIRONMENT Information System (SPENVIS - R.103)
Thematic Workshop, Frankfurter Press Club, Germany, 15-17 October 2018

27. Calders, S.; Lamy, H.; De Keyser, J.; Verbeeck, C.; Martínez Picar, A.; Tétard, C.

The Radio Meteor Zoo: involving citizen scientists in radio meteor research
EPSC 2018, Berlin, Germany, 16-21 September 2018

28. Calders, S.; Zheng, Y.
How to engage the public in space weather research
ESWW15, Leuven, Belgium, 5-9 November 2018

29. Cessateur, G.; Barthélémy, M.; De Keyser, J.; Maggiolo, R.; Rubin, M.; Loreau, J.
Solar UV variability impact on airglow emissions from comets and Galilean moons
EGU General Assembly 2018, Vienna, Austria, 8-13 April 2018 (poster)

30. Cessateur, G.; Maggiolo, R.; Hamrin, M.; De Keyser, J.; Gunell, H.; Maes, L.; Pitkänen, T.
New insights for solar wind-magnetosphere coupling functions
EGU General Assembly 2018, Vienna, Austria, 8-13 April 2018 (poster)

31. Chabanski, S.; De Donder, E.; Borries, C.; Crosby, N.; Andries, J.; Perry, C.
SSA Space Weather Network User Test Campaigns: validating SSA space weather prototype service performance together with end users
COSPAR 42nd Assembly, Pasadena, California, USA, 14-22 July 2018

32. Chabanski, S.; O'Hara, J.; Glover, A.
ESA SSA Space Weather Service Network: Case Study of the September 2017 Space Weather Events
ESWW15, Leuven, Belgium, 5-9 November 2018

33. Chabanski, S.
Migration of SWE Network towards more operational system
Thematic Workshop, Frankfurter Press Club, Germany, 15-17 October 2018

34. Cisnero-González, M.; ... ; Filacchione, G.; and 14 others; and the MAJIS team
Design of the calibration facility for the characterization of MAJIS/JUICE VIS-NIR detectors
INSPIRE and Small Sat workshop, Paris, France, 27-29 August 2018 (talk and poster)

35. Cisnero-González, M.; ... ; Filacchione, G.; and 14 others; and the MAJIS team
Design of the calibration bench for the characterization of MAJIS/JUICE VIS-NIR detectors
EPSC 2018, Berlin, Germany, 16-21 September 2018 (poster)

36. Clerbaux, C.; George, M.; Clarisse, L.; Laffineur, Q.; Froom, M.D.; Parrington, M.

- Pollution transported by hurricane Ophelia: 3D observations by ground-based, aircraft and satellite data compared with CAMS atmospheric composition analyses*
AGU Fall Meeting, Washington, D.C., USA, 10-14 December 2018
37. Cliver, E.W.; D'Huys, E.
Size Distributions of Solar Proton Events and Their Associated Soft X-Ray Flares: Application of the Maximum Likelihood Estimator
ESWW15, Leuven, Belgium, 5-9 November 2018 (poster)
38. Cornilleau-Wehrlin, N.; Nemeč, F.; Santolik, O.; Hayosh, M.; Darrouzet, F.
Detailed Properties of Equatorial Noise with Quasiperiodic Modulation
5th Cluster-THEMIS Workshop, Chania, Crete, Greece, 24-28 September 2018
39. Crapolicchio, R.; Casella, D.; Marqué, C.; Bergeot, N.; Chevalier, J.-M.
Solar radio observation from Soil Moisture and Ocean Salinity (SMOS) mission: a potential new dataset for space weather services
ESWW15, Leuven, Belgium, 5-9 November 2018 (poster)
40. Crocker, P.; ... ; Vaclavovic, P.; and 14 others; and the EPOS-GNSS Team
GLASS, a Tool for Quality-Controlled GNSS Data and Products Dissemination
AGU Fall Meeting, Washington, D.C., USA, 10-14 December 2018 (poster)
41. Dabrowski, B.; ... ; Sniadkowska, K.; and 12 others
Solar observations with Baldy LOFAR station
EGU General Assembly 2018, Vienna, Austria, 8-13 April 2018 (poster)
42. Damé, L.; Meftah, M.; Hauchecorne, A.; Irbah, A.; Bekki, S.; Bolsée, D.; Pereira, N.; Sluse, D.; Cessateur, G.
SOLAR/SOLSPEC: a new solar reference spectrum, SOLAR-ISS 165-3000 nm and 9 years observations of solar spectral irradiance from space from the ISS
EGU General Assembly 2018, Vienna, Austria, 8-13 April 2018 (poster)
43. Damé, L.; Bolsée, D.; Hauchecorne, A.; Meftah, M.; Irbah, A.; Bekki, S.; Pereira, N.; Sluse, D.; Cessateur, G.
Cycle 24 variability of the ultraviolet solar spectral irradiance with the SOLAR/SOLSPEC 9 years of data from the International Space Station
COSPAR 42nd Assembly, Pasadena, California, USA, 14-22 July 2018 (poster)
44. Dammasch, I.E.; Dominique, M.; Zhukov, A.N.; Heinzl, P.; Wauters, L.
Multi-instrument observations of an X9.3 flare
ISEST Workshop 2018 / XVIth HAC, Hvar, Croatia, 24-28 September 2018
45. Dandouras, I.; Yamauchi, M.; Rème, H.; De Keyser, J.; Marghitu, O.; Hirahara, M.; and the ESCAPE team
European SpaceCraft for the study of Atmospheric Particle Escape: follow-on mission
ESWW15, Leuven, Belgium, 5-9 November 2018
46. Dandouras, I.; Yamauchi, M.; Rème, H.; De Keyser, J.; Marghitu, O.; and the ESCAPE team
European SpaceCraft for the study of Atmospheric Particle Escape (ESCAPE): a planetary mission to Earth, proposed to ESA in response to the M5-call
Europlanet Workshop: Planetary Atmospheric Erosion, Murighiol, Romania, 11-15 June 2018 (invited talk)
47. Dandouras, I.; ... ; Tian, F.; and 18 others; and the ESCAPE Team
European SpaceCraft for the study of Atmospheric Particle Escape (ESCAPE): a planetary mission to Earth, proposed to ESA in response to the M5-call
EGU General Assembly 2018, Vienna, Austria, 8-13 April 2018 (poster)
48. Dandouras, I.; ... ; Daglis, I.; and 19 others
ESCAPE (European SpaceCraft for the study of Atmospheric Particle Escape): a planetary mission to Earth, proposed to ESA in response to the M5-call
52nd ESLAB Symposium: Comparative Aeronomy and Plasma Environment of Terrestrial Planets, ESA/ESTEC, Noordwijk, The Netherlands, 14-18 May 2018 (poster)
49. Darrouzet, F.; Pierrard, V.; Benck, S.; Décréau, P.; Ganuskina, N.; De Keyser, J.
Links between the plasmopause and the radiation belts boundaries as observed by Cluster instruments
EGU General Assembly 2018, Vienna, Austria, 8-13 April 2018 (talk & poster)
50. Darrouzet, F.; De Keyser, J.; Lemaire, J.F.; Décréau, P.M.E.; Gallagher, D.
Plasmasphere observations with Cluster completed by new data from an old mission, Dynamic Explorer-1
Workshop "The Plasmasphere and Warm Plasma Cloak", Los Alamos, New Mexico, USA, 18-20 September 2018 (invited talk)
51. Darrouzet, F.; De Keyser, J.; Lemaire, J.F.; Décréau, P.M.E.; Gallagher, D.
Plasmasphere observations with Cluster completed by new data from an old mission, Dynamic Explorer-1
5th Cluster-THEMIS Workshop, Chania, Crete, Greece, 24-28 September 2018
52. Dasso, S.; Masias-Meza, J.; Lanabere, V.; Demoulin, P.; Janvier, M.; Rodriguez, L.

Manifestation of Coronal Mass Ejections near Earth: A review

COSPAR 42nd Assembly, Pasadena, California, USA, 14-22 July 2018 (invited talk)

53. De Bock, V.

Analysis and interpretation of Aerosol Optical Depth values retrieved from a Brewer spectrophotometer at Uccle, Belgium

PhD public defense at ULB, Brussels, Belgium, 12 October 2018

54. De Bock, V.; Mangold, A.; De Backer, H.; Delcloo, A. *UV measurements at Uccle, Belgium (1990-2018) and Utsteinen, Antarctica (2011-2018)*

European conference on solar UV monitoring, Vienna, Austria, 12-14 September 2018

55. Decraemer, B.; Van Doorselaere, T.; Zhukov, A.N.

Streamer wave events observed with STEREO/COR2
BUKS 2018 Workshop, Tenerife, Spain, 3-7 September 2018 (poster)

56. Decraemer, B.; Zhukov, A.N.; Van Doorselaere, T. *Three-dimensional structure of coronal streamers observed by SOHO/LASCO and STEREO/COR2*

COSPAR 42nd Assembly, Pasadena, California, USA, 14-22 July 2018 (poster)

57. Decraemer, B.; Zhukov, A.N.; Van Doorselaere, T. *Three-dimensional structure of coronal streamers observed by SOHO/LASCO and STEREO/COR2*

SDO Science Workshop, Ghent, Belgium, 29 October-2 November 2018

58. De Donder, E.; Crosby, N.; Andries, J.; Perry, C.; Borries, C.; Martini, D.; Thorn, P.; Glover, A.; Luntama, J.-P. *Services for Spacecraft Operations support within the ESA Space Situational Awareness Space Weather Service Network*

SpaceOps 2018 - The 15th International Conference on Space Operations, Marseille, France, 28 May-1 June 2018

59. De Donder, E.; Vansintjan, R.; Glover, A. *ESA SSA Space Weather Service Network: User Support Test Campaign*

ESWW15, Leuven, Belgium, 5-9 November 2018

60. De Donder, E.

Combination of SSA SWE Network products: SSCC user support test campaigns

Thematic Workshop, Frankfurter Press Club, Germany, 15-17 October 2018

61. De Donder, E.; Latocha, M.; Beck, P.; Dierckxsens, M.; Crosby, N.; Calders, S.

Pan-European Consortium for Aviation Space weather User Services (PECASUS): Radiation Expert Group and Service

ESWW15, Leuven, Belgium, 5-9 November 2018 (poster)

62. De Keyser, J.; Yamauchi, M.; Dandouras, I.; Gunell, H.; Maggiolo, R.

Atmospheric escape: sculpting the conditions favorable for the existence of life

FRS-FNRS Contact Group symposium "Astrobiology: from stars and planets to extreme life", Liège, Belgium, 18 December 2018

63. De Keyser, J.; ... ; Génot, V.; and 11 others

Assessment of beam tracking strategies for plasma spectrometers

EGU General Assembly 2018, Vienna, Austria, 8-13 April 2018 (poster)

64. De Keyser, J.; Lavraud, B.; Prech, L.; Maggiolo, R.; Dandouras, I.

Plasma spectrometers with beam tracking strategies for space weather science applications

ESWW15, Leuven, Belgium, 5-9 November 2018 (poster)

65. Delcloo, A.; Laffineur, Q.; De Backer, H.

Confusing situation of the European air traffic on October 2017: joint use of ceilometer measurements together with dispersion model output and CAMS forecasts are an asset for making critical decisions

EUNADICS-AV scientific conference, Rome, Italy, 18-19 June 2018 (poster)

66. Delouille, V.; Hofmeister, S.; Reiss, M.; Temmer, M.; Mampaey, B.

Coronal holes detection using supervised classification

ESWW15, Leuven, Belgium, 5-9 November 2018 (poster)

67. Delouille, V.; Hofmeister, S.; Reiss, M.; Temmer, M.; Mampaey, B.

Coronal holes detection using supervised classification

SDO Science Workshop, Ghent, Belgium, 29 October-2 November 2018 (poster)

68. Delouille, V.; Hofmeister, S.; Reiss, M.; Temmer, M.; Mampaey, B.

Coronal holes detection using supervised classification

ADA IX, Valencia, Spain, 20-22 May 2018 (poster)

69. Depiesse, C.; ... ; Thibert, T.; and 16 others

Calibration of the NOMAD-UVIS channel

EPSC 2018, Berlin, Germany, 16-21 September 2018 (poster)

70. D'Huys, E.; West, M.; Berghmans, D.; Mierla, M.; O'Hara, J.

The SWAP EUV Imager onboard PROBA2: 9 Years of Observations

Solar Wind 15, Brussels, Belgium, 18-22 June 2018 (poster)

71. Dierckxsens, M.; Crosby, N.; Calders, S.; Zychová, L.

Operational Performance of the COMESEP Alert System
ESWW15, Leuven, Belgium, 5-9 November 2018 (poster)

72. Dolla, L.; Voitenko, Y.; Pierrard, V.; Zhukov, A.N.
What Heats the Minor Ions of the Solar Corona?
Solar Wind 15, Brussels, Belgium, 18-22 June 2018

73. Dolla, L.
Subtraction of the continuum contribution in the narrowband filters of PROBA-3/ASPIICS
PROBA3 SWT7 meeting, ESTEC, Noordwijk, The Netherlands, 28-29 September 2018

74. Dolla, L.; Zhukov, A.N.
The Science Activity Plan of PROBA-3/ASPIICS
PROBA3 SWT7 meeting, ESTEC, Noordwijk, The Netherlands, 28-29 September 2018

75. Dolla, L.; Voitenko, Y.; Pierrard, V.; Zhukov, A.N.
Hinode/EIS measurements of the preferential heating of minor ions in the low corona (to test the role of different wave-particle mechanisms)
Hinode-12, Granada, Spain, 10-13 September 2018

76. Dominique, M.; Katsiyannis, A.C.; Berghmans, D.; Wauters, L.; Thiemann, E.; Dammasch, I.E.
Building on the heritage of PROBA2/LYRA for future small-sat missions
INSPIRE and Small Sat workshop, Paris, France, 27-29 August 2018

77. Dominique, M.; Wauters, L.; Katsiyannis, A.C.; Dammasch, I.E.
LYRA status update
PROBA2 SWT-16, Brussels, Belgium, 6 August 2018

78. Dominique, M.; Wauters, L.; Katsiyannis, A.C.; Dammasch, I.E.
LYRA status update
PROBA2 SWT-17, Brussels, Belgium, 13 November 2018

79. Dominique, M.; Zhukov, A.N.; Dolla, L.; Wauters, L.; Dammasch, I.E.; Thiemann, E.; Heinzl, P.; Lapenta, G.
Joint observations of the X9.3 and X8.2 flares on 2017 September 6 and 10 by PROBA2/LYRA, SDO/EVE, and MAVEN/EUVIM
SDO Science Workshop, Ghent, Belgium, 29 October-2 November 2018

80. Dominique, M.; Zhukov, A.N.; Dammasch, I.E.; Wauters, L.; Dolla, L.; Shestov, S.; Heinzl, P.; Lapenta, G.
Observation of the X9.3 flare on September 6 2017 in UV/EUV by PROBA2/LYRA
Triennial Earth-Sun Summit 2018, Leesburg, Virginia, USA, 20-24 May 2018

81. Douša, J.; ... ; Václavovič, P.; and 13 others

New way of GNSS data dissemination within the European Plate Observing System (EPOS)
CzechGeo/EPOS Workshop, Prague, Czech Republic, 5 December 2018 (poster)

82. Fabian, A.; Bruyninx, C.; Legrand, J.
GNSS Metadata Management and Distribution System (M3G)
EUREF symposium, Amsterdam, The Netherlands, 30 May-1 June 2018 (poster)

83. Fazakerley, A.; Berthomier, M.; and the Alfvén team
The Alfvén Mission for the ESA M5 Call
EGU General Assembly 2018, Vienna, Austria, 8-13 April 2018 (poster)

84. Fernandes, R.; ... ; Vaclavovic, P.; and 29 others
The EPOS Thematic Core Service (TCS) "GNSS"
EUREF symposium, Amsterdam, The Netherlands, 30 May-01 June 2018

85. Fernandes, R.; ... ; Soehne, W.; and 15 others
EPOS-GNSS - Current status of service and product implementation
EGU General Assembly 2018, Vienna, Austria, 8-13 April 2018 (poster)

86. Fernandes, R.; ... ; Vaclavovic, P.; and 29 others
The contribution of EPOS to disseminate GNSS data & products in Europe
EPOS-PL Workshop, Jachranka, Poland, 19-20 November 2018

87. Galkin, I.; Reinisch, B.; Belehaki, A.; Borries, C.; Altadill, D.; Sanz, J.; Buresova, D.; Verhulst, T.; Mielich, J.; Katamzi, Z.; Haralambous, H.
TechTIDE: Warning and mitigation technologies for travelling ionospheric disturbance effects
COSPAR 42nd Assembly, Pasadena, California, USA, 14-22 July 2018

88. García-Rigo, A.; ... ; Orus-Perez R.; and 27 others
Assessment of global and regional VTEC ionospheric maps within IAG's RTIM-WG
EGU General Assembly 2018, Vienna, Austria, 8-13 April 2018

89. Gissot, S.; Giordanengo, B.; BenMoussa, A.; Meynants, G.; Koch, M.; Schühle, U.; Gottwald, A.; Laubis, C.; Kroth, U.; Scholtze, F.
Space-grade 3Kx3K Backside Illuminated CMOS Image Sensor for EUV Observation of the Sun
Ultra-Violet Detectors and Instruments Workshop, Toulouse, France, 28-29 November 2018

90. Gunell, H.; Maggiolo, R.; Nilsson, H.; Stenberg Wieser, G.; Slapak, R.; Lindkvist, J.; Hamrin, M.; De Keyser, J.

Why an intrinsic magnetic field does not protect a planet against atmospheric escape

Europlanet Workshop: Planetary Atmospheric Erosion, Murighiol, Romania, 11-15 June 2018

91. Gunell, H.; Maggiolo, R.; Nilsson, H.; Stenberg Wieser, G.; Slapak, R.; Lindkvist, J.; Hamrin, M.; De Keyser, J.

Why an intrinsic magnetic field does not protect a planet against atmospheric escape

5th Cluster-THEMIS Workshop, Chania, Crete, Greece, 24-28 September 2018

92. Hahn, M.; D'Huys, E.

Density Fluctuations in a Polar Coronal Hole

SHINE, Cocoa Beach, Florida, USA, 30 July-3 August 2018 (poster)

93. Hinterreiter, J.; Temmer, M.; Verbeke, C.; Poedts, S.; Pomoell, J.; Magdalenic, J.; Scolini, C.; Rodriguez, L.; Kilpua, E.; Asvestari, E.; Jebaraj, I.; Isavnin, A.

Validation of the background solar wind modeled by EUHFORIA

EGU General Assembly 2018, Vienna, Austria, 8-13 April 2018 (poster)

94. Hinterreiter, J.; Temmer, M.; Verbeke, C.; Poedts, S.; Pomoell, J.; Magdalenic, J.; Camilla, C.; Rodriguez, L.; Kilpua, E.; Asvestari, E.; Jebaraj, I.; Isavnin, A.

Testing the performance of EUHFORIA background solar wind modeling

Solar Wind 15, Brussels, Belgium, 18-22 June 2018 (poster)

95. Isavnin, A.; Moestl, C.; Poedts, S.; Scolini, C.; Pomoell, J.; Magdalenic, J.; Palmerio, E.; Kilpua, E.; Winslow, R.

Capacity of the FRI3D model of coronal mass ejections for usage in space weather forecasting

EGU General Assembly 2018, Vienna, Austria, 8-13 April 2018 (poster)

96. Janssens, J.

Status manuscripts Journal of SWSC

ESWW15, Leuven, Belgium, 5-9 November 2018 (invited talk)

97. Jebaraj, I.C.; Magdalenic, J.; Scolini, C.; Rodriguez, L.; Poedts, S.; Krupar, V.; Pomoell, J.; Temmer, M.

CME and associated shock wave observed on September 27, 2012

Solar Wind 15, Brussels, Belgium, 18-22 June 2018 (poster)

98. Jones, J.; Guerova, G.; Dousa, J.; Dick, G.; De Haan, S.; Pottiaux, E.; Bock, O.; Pacione, R.

COST Action ES1206: GNSS4SWEC - Advanced GNSS Tropospheric Products for Severe Weather Events and Climate

EGU General Assembly 2018, Vienna, Austria, 8-13 April 2018

99. Katsiyannis, A.C.; Dominique, M.; Pierrard, V.; Lopez Rosson, G.

The detection of ultra-relativistic electrons in low Earth orbit by the LYRA instrument on board the PROBA2 satellite

Triennial Earth-Sun Summit 2018, Leesburg, Virginia, USA, 20-24 May 2018 (poster)

100. Katsiyannis, A.C.; Dominique, M.; Pierrard, V.; Lopez Rosson, G.

The detection of ultra-relativistic electrons in low Earth orbit by the LYRA instrument on board the PROBA2 satellite

ESWW15, Leuven, Belgium, 5-9 November 2018

101. Katsiyannis, A.C.; Dominique, M.

The detection of ultra-relativistic electrons in low Earth orbit by the LYRA instrument on board the PROBA2 satellite

INSPIRE and Small Sat workshop, Paris, France, 27-29 August 2018

102. Katsiyannis, A.C.; Dominique, M.

The in-situ detection of ultra-relativistic electrons by LYRA, an UV radiometer on board PROBA2

ESWW15, Leuven, Belgium, 5-9 November 2018 (poster)

103. Kauristie, K.; ... ; Osterberg, K.; and 23 others

PECASUS, a European Space Weather Service Network for Aviation

ESWW15, Leuven, Belgium, 5-9 November 2018

104. Klos A.; ... ; Tornatore V.; and 12 others

Homogenisation of tropospheric data: evaluating the algorithms under the presence of autoregressive process

IX Hotine-Marussi Symposium, Rome, Italy, 18-22 June 2018

105. Koukras, A.; Marqué, C.; Dolla, L.

Studying the kinematics of EUV waves

PROBA2 SWT-16, Brussels, Belgium, 6 August 2018 (Science Working Team)

106. Koukras, A.; Marqué, C.; Downs, C.; Dolla, L.

Analyzing the kinematics of EUV waves by combining simulations and multi-instrument observations

CESRA Summer School, Brussels, Belgium, 10-14 September 2018

107. Koukras, A.; Marqué, C.; Downs, C.; Dolla, L.

Analyzing the kinematics of EUV waves by combining simulations and multi-instrument observations

SDO Science Workshop, Ghent, Belgium, 29 October-2 November 2018

108. Krupar, V.; Eastwood, J.P.; Magdalenic, J.;

Gopalswamy, N.; Kruparova, O.; Szabo, A.

- Interplanetary type II radio bursts: STEREO observations and Monte Carlo Simulations*
EGU General Assembly 2018, Vienna, Austria, 8-13 April 2018 (poster)
109. Laffineur, Q.; Delclocq, A.; Mangold, A.; De Bock, V.; De Backer, H.
Misidentification of smoke plumes over Europe: joint use of ceilometer measurements with dispersion model increases their identification
EGU General Assembly 2018, Vienna, Austria, 8-13 April 2018 (poster)
110. Laitinen, T.; ... ; Kriegel, M.; and 20 others
PECASUS: Space Weather instrumentation for a global space weather service to support civil aviation
ESWW15, Leuven, Belgium, 5-9 November 2018 (talk & poster)
111. Lamy, H.; Echim, M.; Cessateur, G.; Simon Wedlund, C.; Gustavsson, B.; Maggiolo, R.; Darrouzet, F.; De Keyser, J.
From optical ground-based observations of discrete auroral arcs to the magnetospheric generator: fine-tuning model and time evolution
EGU General Assembly 2018, Vienna, Austria, 8-13 April 2018 (talk & poster)
112. Lamy, H.; Calders, S.; Tétard, C.; Verbeeck, C.; Martinez Picar, A.
The Radio Meteor Zoo : a Citizen Science project using BRAMS data
ESWW15, Leuven, Belgium, 5-9 November 2018
113. Lamy, H.; Verbeeck, C.; Calders, S.; Martínez Picar, A.; Tétard, C.
Study of the Quadrantids 2016 using BRAMS data
EGU General Assembly 2018, Vienna, Austria, 8-13 April 2018
114. Lamy, H.; Anciaux, M.; Verbeeck, C.; Calders, S.; Martinez Picar, A.; Tetard, C.
Computing mass indices of meteor showers with BRAMS data
EPSC 2018, Berlin, Germany, 16-21 September 2018
115. Lefèvre, L. ; Clette, F.; Delouille, V. ; Mathieu, S.; von Sachs, R.
The Sunspot Number Recalibration
SDO Science Workshop, Ghent, Belgium, 29 October-2 November 2018 (poster)
116. Lefèvre, L.; Clette, F.
The Sunspot Number Revision and Recalibration: an ongoing effort
COSPAR 42nd Assembly, Pasadena, California, USA, 14-22 July 2018 (invited talk)
117. Lefèvre, L.; Clette, F.; Cliver, E.
Sunspot Number revision
EGU General Assembly 2018, Vienna, Austria, 8-13 April 2018 (invited talk)
118. Lefèvre, L.
Assessment of ADF method
ISSI team workshop "Recalibration of the Sunspot Number Series", Bern, Switzerland, 22-26 January 2018 (invited talk)
119. Legrand, J.; Bruyninx C.
Quality Assessment of the EPN Multi-year Position and Velocity Solution
COSPAR 42nd Assembly, Pasadena, California, USA, 14-22 July 2018
120. Lidberg, M.; Bruyninx, C.; Kenyeres, A.; Poutanen, M.; Söhne, W.
EUREF and the infrastructure for high performance GNSS applications in Europe
European Navigation Conference 2018, Gothenburg, Sweden, 14-17 May 2018
121. Lopez Rosson, G.
Van Allen radiation belts dynamics revealed from PROBA V/EPT observations
PhD public defense at UCL, Leuven, Belgium, 23 October 2018
122. Mangold, A.; Laffineur, Q.; Van Malderen, R.; Hermans, C.; Nys, K.; Verbruggen, M.; De Backer, H.
Total ozone, UV and radio sounding measurements in the Sør Rondane Mountains
POLAR2018: A SCAR/IASC Open Science Conference, Davos, Switzerland, 19-23 June 2018
123. Mathieu, S.; von Sachs, R.; Ritter, C.; Delouille, V.; Lefèvre, L.
Uncertainty Quantification in Sunspot Counts
RSSB Annual Meeting, Ovat, Belgium, 17-19 October 2018 (poster)
124. Mathieu, S.; von Sachs, R.; Delouille, V.; Lefèvre, L.
Uncertainty quantification in sunspot counts
IEEE Data Science Workshop, Lausanne, Switzerland, 4-6 June 2018 (poster)
125. Morel, L.; Pottiaux, E.; Durand, F.; Follin, J.-M.; Durand, S.; Van Baelen, J.
Global validity and behaviour of tropospheric gradients estimated by GPS
EGU General Assembly 2018, Vienna, Austria, 8-13 April 2018 (poster)
126. Magdalenic, J.
Radio Observations and Space Weather

CESRA Summer School, Brussels, Belgium, 10-14 September 2018 (invited talk)

127. Magdalenic, J.

The role of Solar Radio Science in the Space Weather Research

EGU General Assembly 2018, Vienna, Austria, 8-13 April 2018 (invited talk)

128. Magdalenic, J.; Jebaraj, I.; Harra, L.; Matthews, S.; Berghmans, D.; Krupar, V.

Active region jets on August 25, 2011

Solar Wind 15, Brussels, Belgium, 18-22 June 2018

129. Magdalenic, J.; Marqué, C.; Fallows, R.; Mann, G.; Vocks, C.

Fine structures of type II radio burst observed by LOFAR

EGU General Assembly 2018, Vienna, Austria, 8-13 April 2018 (poster)

130. Magdalenic, J.; ... ; Zhukov, A.; and 11 others

Constraining CMEs and shocks by observations and modeling throughout the inner heliosphere - CCSOM

Solar Wind 15, Brussels, Belgium, 18-22 June 2018 (poster)

131. Maggiolo, R. ; Hamrin, M. ; Cessateur, G. ; De Keyser, J. ; Gunell, H.; Maes, L. ; Pitkänen, T.

The time response of the plasmashet composition to the solar wind

EGU General Assembly 2018, Vienna, Austria, 8-13 April 2018 (poster)

132. Marqué, C.; Martínez Picar, A. ; Magdalenic, J.; Ergen, A.

Software defined radio technologies for monitoring of the solar activity

ESWW15, Leuven, Belgium, 5-9 November 2018 (poster)

133. Martínez Picar, A.; Marqué, C.

Using SPADE for radio meteor observations

International Meteor Conference 2018, Pezinok-Modra, Slovakia, 30 August-02 September 2018

134. Martínez Picar, A.; Marqué, C.; Magdalenic, J.

New Capabilities of the Humain Radio-Astronomy Station

17th RHESSI Workshop, Dublin, Ireland, 18-23 June 2018

135. Meftah, M.; Damé, L.; Hauchecorne, A.; Irbah, A.;

Bekki, S.; Bolsée, D.; Pereira, N.; Sluse, D. ; Cessateur, G.

Recent variability of the solar spectral irradiance by using SOLAR/SOLSPEC data

EGU General Assembly 2018, Vienna, Austria, 8-13 April 2018 (poster)

136. Micera, A.; Zhukov, A.N.; Boella, E.; Lapenta, G.

Fully kinetic simulations of electron and ion firehose instability in the solar wind using the ECSIM code

12th Heliophysics Summer School, Boulder, Colorado, USA, 24-31 July 2018

137. Micera, A.; Zhukov, A.N.; Boella, E.; Lapenta, G.

Fully kinetic simulations of electron and ion firehose instability in the solar wind using the ECSIM code

ISSS-13 conference, Los Angeles, USA, 6-14 September 2018 (poster)

138. Micera, A.; Boella, E.; Zhukov, A.N.; Gonzalez-Herrero, D.; Lapenta, G.

Kinetic simulations of electron and ion temperature-anisotropy instabilities in the solar wind using the ECSIM code

Solar Wind 15, Brussels, Belgium, 18-22 June 2018 (poster)

139. Micera, A.; Boella, E.; Zhukov, A.N.; Gonzalez-Herrero, D.; Lapenta, G.

Kinetic simulations of electron and ion temperature-anisotropy instabilities in the solar wind using the ECSIM code

19th Meeting of the FNRS Contact Group Astronomie & Astrophysique, Planetarium, Brussels, Belgium, 4 June 2018

140. Micera, Alfredo; Gonzalez-Herrero, Diego; Boella, Elisabetta; Zhukov, Andrei ; Lapenta, Giovanni

First principle simulations of tangential discontinuities at the magnetopause using the new Energy Conserving Semi-Implicit Method

EGU General Assembly 2018, Vienna, Austria, 8-13 April 2018 (poster)

141. Mierla, M.; Talpeanu, D.; Rodriguez, L.; Zhukov, A.N.; D'Huys, E.; Zuccarello, F.

3D Reconstruction and Simulation of Stealth CMEs

ISSI meeting "Understanding the Origins of Problem Geomagnetic Storms", Bern, Switzerland, 16-20 April 2018

142. Mierla, M.; Inhester, B.; Zhukov, A.N.

Calculation of polarization angle deviations using SECCHI/COR1

PROBA3 SWT7 meeting, ESTEC, Noordwijk, The Netherlands, 28-29 September 2018

143. Mierla, M.; D'Huys, E.; Seaton, D.; Berghmans, D.; West, M.; Podladchikova, O.; Wauters, L.; Janssens, J.

Long-term evolution of the solar corona using SWAP data

ESWW15, Leuven, Belgium, 5-9 November 2018 (poster)

144. Mierla, M.; D'Huys, E.; Seaton, D.; Berghmans, D.; West, M.; Podladchikova, O.; Wauters, L.; Janssens, J.

Long-term evolution of the solar corona using SWAP data

SDO Science Workshop, Ghent, Belgium, 29 October-2 November 2018 (poster)

145. O'Hara, J.; Mierla, M.; Podladchikova, O.; D'Huys, E.; West, M.

Exceptional Extended Field of View Observations by SWAP on 1 and 3 April 2017

ESWW15, Leuven, Belgium, 5-9 November 2018 (poster)

146. O'Hara, J.; Mierla, M.; Podladchikova, O.; D'Huys, E.; West, M.

Exceptional Extended Field of View Observations by SWAP on 1 and 3 April 2017

SDO Science Workshop, Ghent, Belgium, 29 October-2 November 2018 (poster)

147. Palmerio, E.; ... ; Nieves-Chinchilla, T.; and 12 others
Magnetic structure and propagation of a solar flux rope from the Sun to Saturn

EGU General Assembly 2018, Vienna, Austria, 8-13 April 2018 (poster)

148. Palmerio, E.; ... ; Turc, L.; and 15 others
Evolution of a coronal mass ejection from the Sun to Saturn
AGU Fall Meeting, Washington, D.C., USA, 10-14 December 2018 (poster)

149. Palmerio, E.; ... ; Turc, L.; and 15 others
Evolution of a coronal mass ejection from the Sun to Saturn
SDO Science Workshop, Ghent, Belgium, 29 October-2 November 2018 (poster)

150. Palmerio, E.; Scolini, C.; Rodriguez, L.; West, M.; Good, S.; Mierla, M.
Multipoint study of an Earth-impacting CME erupting from the solar limb
ESWW15, Leuven, Belgium, 5-9 November 2018 (poster)

151. Pereira, N.; Bolsée, D.; Sluse, D.; Cessateur, G.; Sperfeld, P.; Pape, S.
Metrology of the Solar Spectral Irradiance at the Top of Atmosphere in the Near Infrared using Ground Based Instruments: The PYR-ILIOS campaign
INSPIRE and Small Sat workshop, Paris, France, 27-29 August 2018

152. Pereira, N.; Vandaele, A.C.; Mahieux, A.; Bolsée, D.; Sluse, D.; Dekemper, E.; Cessateur, G.; Trompet, L.
Prospects on future instrumentation for the Solar Spectrum measurement
INSPIRE and Small Sat workshop, Paris, France, 27-29 August 2018

153. Pierrard, V.; Darrouzet, F.; Voitenko, Y.; Lamy, H.; De Keyser, J.
Radio Observations for Space Weather: Space Applications From the Solar Corona to the Inner Magnetosphere
2nd URSI Atlantic Radio Science Meeting, Gran Canaria, 28 May-1 June 2018 (invited talk)

154. Pierrard, V.; Lemaire, J.; Darrouzet, F.; Lopez Rosson, G.

What new observations and dynamic simulations of the plasmasphere reveal on the inner magnetosphere
Workshop "Gringauz 100: Plasmas in the Solar System", Moscow, Russia, 13-15 June 2018 (invited talk)

155. Pierrard, V.; Darrouzet, F.
Recent Advances in the Kinetic 3D Dynamical Model of Plasmasphere
Workshop "The Plasmasphere and Warm Plasma Cloak", Los Alamos, New Mexico, USA, 18-20 September 2018 (invited talk)

156. Podladchikova, O.; Marqué, C.; Berghmans, D.; Stegen, K.
The Self-Adjusted Solar Flux Forecasting Tool (SASFF)
ESWW15, Leuven, Belgium, 5-9 November 2018 (poster)

157. Podladchikova, O.; Marqué, C.
Statistical approaches for the forecast of the F10.7 index
ESWW15, Leuven, Belgium, 5-9 November 2018 (poster)

158. Podladchikova, O.; Verbeeck, C.; Kraaikamp, E.
Broken Self-Organized-Criticality Scenario for Solar Flares Energy Release Observed by SDO/AIA
SDO Science Workshop, Ghent, Belgium, 29 October-2 November 2018

159. Podladchikova, O.; Kraaikamp, E.; Verbeeck, C.
A Model of Turbulent Dynamo for Particle Acceleration in Low Corona: Evidences Deduced from the SDO EUV Flares Database
Solar Wind 15, Brussels, Belgium, 18-22 June 2018

160. Poedts, S.; ... ; Luntama, J.-P.; and 20 others
The ESA Virtual Space Weather Modelling Centre
ESWW15, Leuven, Belgium, 5-9 November 2018 (poster)

161. Poedts, S.; ... ; Luntama, J.-P.; and 21 others
The ESA Virtual Space Weather Modelling Centre – Part 2
ESWW15, Leuven, Belgium, 5-9 November 2018 (poster)

162. Ritter, B.; Gerard, J.-C.; Hubert, B.; Rodriguez, L.; Gkouvelis, L.
Proton Aurora on Mars
ESWW15, Leuven, Belgium, 5-9 November 2018 (poster)

163. Ritter, B.; Gérard, J.-C.; Hubert, B.; Rodriguez, L.; Gkouvelis, L.
Proton Aurora on Mars
52nd ESLAB Symposium: Comparative Aeronomy and Plasma Environment of Terrestrial Planets, ESA/ESTEC, Noordwijk, The Netherlands, 14-18 May 2018 (poster)

164. Rodriguez, L.; Scolini, C.; Mierla, M.; Zhukov, A.N.; West, M.
Space weather monitor at the L5 point: a case study of a CME observed with STEREO B

- EGU General Assembly 2018, Vienna, Austria, 8-13 April 2018 (poster)
165. Rodriguez, L.; Zhukov, A.N.; Mierla, M.; Talpenau, D.
Linking CMEs to ICMEs
ISSI meeting "Understanding the Origins of Problem Geomagnetic Storms", Bern, Switzerland, 16-20 April 2018
166. Rodriguez, L.; Masias-Meza, J.; Dasso, S.; Demoulin, P.; Zhukov, A.N.; Gulisano, A.; Mierla, M.; Kilpua, E.; West, M.; Lacatus, D.; Paraschiv, A.; Janvier, M.
Typical Profiles and Distributions of Plasma and Magnetic Field Parameters in Magnetic Clouds at 1 AU
Solar Wind 15, Brussels, Belgium, 18-22 June 2018
167. Santolik, O.; Kolmasova, I.; Darrouzet, F.; Pickett, J.S.; Cornilleau-Wehrin, N.
Case studies of chorus in plasmaspheric plumes
5th Cluster-THEMIS Workshop, Chania, Crete, Greece, 24-28 September 2018
168. Sapundjiev, D.; Stankov, S.
Cosmic ray cutoff rigidity estimations based on the World Magnetic Model
Latin American Conference on Space Geophysics (COLAGE), 16-20 April 2018, Buenos Aires, Argentina
169. Sarkar, R.; Srivastava, N.; Mierla, M.; West, M.; D'Huys, E.
Evolution of Coronal Cavity from Quiescent to Eruptive Phase in Association with Coronal Mass Ejection
AGU Fall Meeting, Washington, D.C., USA, 10-14 December 2018
170. Scolini, C.; Zuccarello, F.P.; Rodriguez, L.; Poedts, S.; Mierla, M.; Verbeke, C.; Pomoell, J.
Observation-based modelling of magnetised CMEs with EUHFORIA and implications for geo-effectiveness predictions
ESWW15, Leuven, Belgium, 5-9 November 2018
171. Scolini, C.; Verbeke, C.; Poedts, S.; Zuccarello, F.P.; Chané, E.; Rodriguez, L.; Mierla, M.; Pomoell, J.; Cramer, W.; Raeder, J.; Gopalswamy, N.
Sun-to-Earth simulation of the July 12, 2012 geo-effective CME with EUHFORIA+OpenGGCM
Triennial Earth-Sun Summit 2018, Leesburg, Virginia, USA, 20-24 May 2018
172. Scolini, C.; Verbeke, C.; Poedts, S.; Rodriguez, L.; Mierla, M.; Pomoell, J.; Cramer, W.; Raeder, J.; Gopalswamy, N.
Sun-to-Earth simulations of geo-effective Coronal Mass Ejections with EUHFORIA: a heliospheric-magnetospheric model chain approach
EGU General Assembly 2018, Vienna, Austria, 8-13 April 2018 (poster)
173. Scolini, C.; Verbeke, C.; Zuccarello, F. P.; Poedts, S.; Rodriguez, L.; Mierla, M.; Pomoell, J.; Raeder, J.; Cramer, W. D.
Sun-to-Earth simulations of geoeffective CMEs, EUHFORIA: A heliospheric-magnetospheric model chain approach
Solar Wind 15, Brussels, Belgium, 18-22 June 2018
174. Scolini, C.; Zuccarello, F.P.; Rodriguez, L.; Poedts, S.; Verbeke, C.; Palmerio, E.; Mierla, M.; Pomoell, J.
Observation-based Sun-to-Earth simulations of geo-effective CMEs with EUHFORIA
ISEST Workshop 2018 / XVIth HAC, Hvar, Croatia, 24-28 September 2018 (invited talk)
175. Scolini, C.; Zuccarello, F.P.; Rodriguez, L.; Poedts, S.; Mierla, M.; Verbeke, C.; Pomoell, J.; Cramer, W.D.; Raeder, J.
Observation-based Sun-to-Earth simulations of geo-effective Coronal Mass Ejections with EUHFORIA
AGU Fall Meeting, Washington, D.C., USA, 10-14 December 2018 (poster)
176. Seaton, D.; ... ; Zhukov, A.N.; and 29 others
New High-Altitude Observations of the IR and Visible Solar Corona from the 2017 Eclipse
AGU Fall Meeting, Washington, D.C., USA, 10-14 December 2018
177. Shestov, S.; Zhukov, A.N.; Van Doorselaere, T.
Simulation of dynamics of hot plasma in post-flare loops
SDO Science Workshop, Ghent, Belgium, 29 October-2 November 2018
178. Shestov, S.; Zhukov, A.N.
ASPIICS data pipeline and data products
ASPIICS Science Working Team meeting 7, ESTEC, Noordwijk, The Netherlands, 27-28 September 2018
179. Shestov, S.; Zhukov, A. N.
ASPIICS: modeling and removal of ghosts
ASPIICS Science Working Team meeting 7, ESTEC, Noordwijk, The Netherlands, 27-28 September 2018
180. Shestov, S.; Voitenko, Y.; Zhukov, A.N.
Initiation of Alfvénic turbulence by Alfvén wave collisions: a numerical study
BUKS 2018 Workshop, Tenerife, Spain, 3-7 September 2018
181. Shestov, S.; Voitenko, Y.; Zhukov, A.N.
Initiation of Alfvénic Turbulence by Alfvén Wave Collisions: A Numerical Study
Solar Wind 15, Brussels, Belgium, 18-22 June 2018 (talk & poster)
182. Talpeanu, D.-C.; Zuccarello, F.P.; Chané, E.; Poedts, S.; D'Huys, E.; Hosteaux, S.; Mierla, M.

Numerical Modelling of Stealth Solar Eruptions; Simulated and In-Situ Signatures at 1AU
BAMC-UKMHD 2018, St. Andrews, UK, 26-29 March 2018

183. Talpeanu, D.-C.; Zuccarello, F.P.; Chané, E.; Poedts, S.; D'Huys, E.; Hosteaux, S.; Mierla, M.
Numerical Modelling of Stealth Solar Eruptions and Comparison with In-Situ Signatures at 1AU
Solar Wind 15, Brussels, Belgium, 18-22 June 2018 (poster)

184. Talpeanu, D.-C.; Zuccarello, F.P.; Chané, E.; Poedts, S.; D'Huys, E.; Hosteaux, S.; Mierla, M.; Roussev, I.
Initiation of Stealth CMEs: Clues from Numerical Modelling and In-Situ Comparisons
SDO Science Workshop, Ghent, Belgium, 29 October-2 November 2018

185. Talpeanu, D.-C.; Zuccarello, F.P.; Chané, E.; Poedts, S.; D'Huys, E.; Hosteaux, S.; Mierla, M.; Roussev, I.
Numerical Modelling of Stealth Solar Eruptions Inserted in Different Solar Wind Speeds and Comparison with In-Situ Signatures
ESWW15, Leuven, Belgium, 5-9 November 2018 (poster)

186. Temmer, M.; Heinemann, S.; Hinterreiter, J.; Magdalenic, J.; Jebaraj, I.; Verbeke, C.; Poedts, S.; Pomoell, J.; Scolini, C.; Rodriguez, L.; Kilpua, E.; Asvestari, E.
Validating the background solar wind using the EUHFORIA model
ESWW15, Leuven, Belgium, 5-9 November 2018 (poster)

187. Temmer, M.; Thalmann, J.K.; Dissauer, K.; Veronig, A.M.; Tschernitz, J.; Hinterreiter, J.; Rodriguez, L.
Combining remote-sensing image data with in-situ measurements supported by modeling for Earth-affecting CME events
EGU General Assembly 2018, Vienna, Austria, 8-13 April 2018

188. Temmer, M.; Thalmann, J.K.; Dissauer, K.; Veronig, A.M.; Tschernitz, J.; Hinterreiter, J.; Rodriguez, L.
Combining remote-sensing image data with in-situ measurements supported by modeling for Earth-affecting CME events
14th Quadrennial Solar-Terrestrial Physics Symposium, Toronto, Canada, 9-13 July 2018

189. Van Lil, E.H.; Van Malderen, R.
On the worst case trajectories of microwave links above Belgium
2nd URSI AT-RASC, Gran Canaria, Spain, 28 May-1 June 2018 (talk & poster)

190. Van Malderen R.; Berckmans J.; Pottiaux E.; Pacione R.
Evaluation of the atmospheric water vapor content in the regional climate model ALARO-0 using GNSS observations from EPN Repro2

EGU General Assembly 2018, Vienna, Austria, 8-13 April 2018

191. Verbeeck, C.
New SOOPs (Solar Orbiter Operation Plans) proposed by EUI
11th Solar Orbiter Science Operations Working Group meeting, ESAC, Madrid, Spain, 16-18 January 2018

192. Verbeeck, C.
New SOOPs (Solar Orbiter Operation Plans) proposed by EUI
21st EUI Consortium Meeting, PMOD, Davos, Switzerland, 5-7 March 2018

193. Verbeeck, C.
Onboard science programs
21st EUI Consortium Meeting, PMOD, Davos, Switzerland, 5-7 March 2018

194. Verbeeck, C.
Commissioning Phase details
22nd EUI Consortium Meeting, MPS, Göttingen, Germany, 24-26 September 2018

195. Verbeeck, C.; Kraaikamp, E.; Podladchikova, O.
Solar flare distributions: lognormal instead of power law?
SDO Science Workshop, Ghent, Belgium, 29 October-2 November 2018

196. Verbeeck, C.; Lamy, H.; Calders, S.; Tétard, C.; Martínez Picar, A.
BRAMS radio observations: activity of some recent major meteor showers
International Meteor Conference 2018, Pezinok-Modra, Slovakia, 30 August-02 September 2018

197. Verbeeck, C.; Rendtel, J.; Veljković, K.; Perlerin, V.; Hankey, M.; Weiland, T.; Knöfel, A.
Visual Workshop 2018: analyzing the Perseids 2018
International Meteor Conference 2018, Pezinok-Modra, Slovakia, 30 August-02 September 2018

198. Verbeke, C.; Scolini, C.; Pomoell, J.; Poedts, S.
Modeling Coronal Mass Ejections with EUHFORIA: A Parameter Study of a magnetized Flux Rope Model
COSPAR 42nd Assembly, Pasadena, California, USA, 14-22 July 2018

199. Verhulst, T.
New opportunities for ionospheric research and applications made possible by modern ionosondes
2nd OIC Workshop on Geomagnetism and Ionosphere, Sonmiani, Pakistan, 10-17 November 2018

200. Verhulst, T.; Altadill, D.; Galkin, I.; Blanch, E.; Stankov, S.; Reinisch, B.; Kozlov, A.; Belehaki, A.

Improving signal-to-noise ratio in oblique ionosonde soundings using new hardware capability of the DPS4D ionosonde

2nd URSI AT-RASC, Gran Canaria, Spain, 28 May-1 June 2018

201. Verhulst, T.; Stankov, S.

Ionospheric disturbances due to the 2017 American solar eclipse detected at a European observatory

2nd URSI AT-RASC, Gran Canaria, Spain, 28 May-1 June 2018

202. Verhulst, T.; Stankov, S.

The importance of the three-dimensional geometry of solar eclipses for analysis of the impact on the ionosphere

COSPAR 42nd Assembly, Pasadena, California, USA, 14-22 July 2018

203. Voitenko, Y.; Brazhenko, A.; Melnik, V.; Frantsuzenko, A.; Pierrard, V.

Faint Coronal Radio Bursts Generated by Alfvén Waves

2nd URSI AT-RASC, Gran Canaria, Spain, 28 May-1 June 2018

204. Voitenko, Y.; Gogoberidze, G.; De Keyser, J.

Imbalanced Alfvénic Turbulence in the Solar Wind

Solar Wind 15, Brussels, Belgium, 18-22 June 2018

205. Voitenko, Y.; Gogoberidze, G.; De Keyser, J.; Pierrard, V.

Imbalanced Alfvénic Turbulence and Anisotropic Energy Release in the Solar Wind

18th Ukrainian Conference on Space Research, Kiev, Ukraine, 17-20 September 2018

206. Voitenko, Y.; Melnik, V.; Pierrard, V.; Brazhenko, A.; Frantsuzenko, A.

Radio Diagnostics of Plasma and Waves Above Active Regions of Solar Corona

Dynamic Sun II: Solar Magnetism from Interior to the Corona, Siem Reap, Angkor Wat, Cambodia, 12-16 February 2018 (invited talk)

207. Wagner, T.; Beirle, S.; Dörner, S.; Wang, Y.; Loyola, D.; Van Malderen, R.

Global maps of water vapor trends and correlation of the water vapor distribution to different teleconnection indices derived from 20 years of combined GOME-SCIAMACHY-GOME-2 observations

EGU General Assembly 2018, Vienna, Austria, 8-13 April 2018

208. Wauters, L.; Dominique, M.; Dammasch, I.; Meftah, M.

Tracking of predominant periodicities evolution for PROBA2/LYRA and other long-term solar time series

INSPIRE and Small Sat workshop, Paris, France, 27-29 August 2018

209. Wauters, L.; Dominique, M.; Dammasch, I.; Meftah, M.

Tracking of predominant periodicities evolution for PROBA2/LYRA and other long-term solar time series
SDO Science Workshop, Ghent, Belgium, 29 October-2 November 2018 (poster)

210. West, M.

Exploring the Solar Poles from the L1 perspective
SDO Science Workshop, Ghent, Belgium, 29 October-2 November 2018 (poster)

211. West, M.; Andries, J.

CCMC & ROB Partnership Outlook

9th CCMC Workshop, College Park, Maryland, USA, 23-27 April 2018 (invited talk)

212. West, M.; Nicula, B.; Verstringe, F.; Bourgoignie, B.; Berghmans, D.; Jiggins, P.; Mueller, D.

Space Weather JHelioviewer in a Heterogeneous World

COSPAR 42nd Assembly, Pasadena, California, USA, 14-22 July 2018 (invited talk)

213. West, M.; Palmerio, E.

Epoch Analysis of Post Flare Loop Systems

AGU Fall Meeting, Washington, D.C., USA, 10-14 December 2018

214. West, M.; Palmerio, E.; Seaton, D.

Post-Flare Loop Signatures

ESWW15, Leuven, Belgium, 5-9 November, 2018 (poster)

215. West, M.; Palmerio, E.; Seaton, D.; Savage, S.

X8.2 flare - 10 September 2017

SHINE, Cocoa Beach, Florida, USA, 30 July-3 August 2018

216. West, M.; Seaton, D.

Exploring the Middle Corona with a New Generation of Instruments

SDO Science Workshop, Ghent, Belgium, 29 October-2 November 2018 (invited talk)

217. West, M.; Seaton, D.; Dennis, B.; Savage, S.; Feng, L.; Palmerio, E.

RHESSI SWAP Post-Flare Giant Arch Signatures

COSPAR 42nd Assembly, Pasadena, California, USA, 14-22 July 2018

218. West, M.; Seaton, D.; Palmerio, E.

Post-Flare Loop Signatures

SHINE, Cocoa Beach, Florida, USA, 30 July-3 August 2018 (poster)

219. Wilken, V.; Kriegel, M.; Cesaroni, C.; Spogli, L.;

Bergeot, N.; Chevalier, J.-M.; Stanislawska, I.; Tomasik, L.;

van den Oord, B.

PECASUS - GNSS user domain

ESWW15, Leuven, Belgium, 5-9 November, 2018 (poster)

220. Yamauchi, M.; Dandouras, I.; De Keyser, J.; Marghitu, O.; Rème, H.; Yoshikawa, I.; Sakanoi, T.; and the ESCAPE Proposal Team

ESCAPE: A mission proposal for ESA-M5 to systematically study exosphere and atmospheric escape using European, Japanese, and US instruments

ISAS Future Missions Workshop, Japan, 9-10 January 2018

Public Outreach: Talks and publications for the general public

1. Andries, J.; Bergeot, N.; Berghmans, D.; Crosby, N.; De Donder, E.; Dehenaauw, D.; Dierckxsens, M.; Mailler, P.; Vanlommel, P.
PECASUS for ICAO
STCE Annual Meeting, Uccle, 7 June 2018 (invited talk)
2. Bergeot, N.
GNSS for Space Weather
Visit United Nations Ambassadors, Space Pole, Uccle, 23 January 2018
3. Bergeot, N.
Le GPS qui mène a la Base Princesse Elisabeth
Antarcticstories, [Maison des Arts d'Uccle](#), Uccle, 21 February 2018
4. Bergeot, N.
Life in Antarctica
Antarcticstories, [Maison des Arts d'Uccle](#), Uccle, 30 April 2018
5. Bergeot, N.; Chevalier, J.-M.; Defraigne, P.
L'imminence de frappes militaires américaines détectée à l'Observatoire royal de Belgique
[Daily Science](#), 9 July 2018
6. Berghmans, D.
Space Weather: Sunny days ahead
Switch to Space, Brussels, 8 October 2018
7. Calders, S.
Lopen er binnen tien jaar mensen rond op Mars?
Wooow Festival, Industriemuseum, Ghent, 25 November 2018
8. Calders, S.
Luisteren naar "vallende sterren" met het BRAMS network
Space Pole Open Doors, Uccle, 29-30 September 2018
9. Calders, S.
Wat zijn vallende sterren?
Space Pole Open Doors, Uccle, 28 September 2018
10. Calders, S.
Involving citizen scientists in radio meteor research
European Conference on Amateur Radio Astronomy, Bad Munstereifel, Germany, 15 September 2018
11. Calders, S.
Het BRAMS-netwerk en de detectie van radiometeoren
Volkssterrenwacht Beisbroek, Brugge, 21 February 2018
12. Calders, S.
Radio Meteor Zoo
Volkssterrenwacht Urania, Hove, 12 January 2018
13. Cessateur, G.
Les aurores: diagnostic de la météo spatiale
Space Pole Open Doors, Uccle, 29-30 September 2018
14. Chabanski, S.; De Donder, E.
The SSCC
Visit United Nations Ambassadors, Space Pole, Uccle, 23 January 2018
15. Dapieve, F.
Space radiation effects
STCE Annual Meeting, Uccle, 7 June 2018 (invited talk)
16. De Backer, H.; Bolsée, D.
Surface UV radiation
STCE Annual Meeting, Uccle, 7 June 2018 (invited talk)
17. Decraemer, B.
Golven in de corona van de zon
Space Pole Open Doors, Uccle, 29-30 September 2018
18. De Donder, E.
Radiation Expert Centre
SWIC, Uccle, 11-13 March 2018
19. De Donder, E.
Radiation Expert Centre
SWIC, Uccle, 26-28 November 2018
20. De Donder, E.
Space radiation environment specification with SPENVIS - Part 2
Four-day SPENVIS training for Airbus Defense and Space GmbH (WebEx), 8 March 2018
21. De Donder, E.
Solar cell degradation with SPENVIS
Four-day SPENVIS training for Airbus Defense and Space GmbH (WebEx), 15 March 2018
22. De Donder, E.; Messios, N.
Atomic oxygen erosion calculations with SPENVIS
Four-day SPENVIS training for Airbus Defense and Space GmbH (WebEx), 15 March 2018
23. Defraigne, P.
La mesure du temps avec les satellites GPS
Space Pole Open Doors, Uccle, 29-30 September 2018

24. De Keyser, J.
Poollicht: een thermometer voor het ruimteweer
Space Pole Open Doors, Uccle, 29-30 September 2018
25. De Keyser, J.
Public demonstration of the planeterrella
Space Pole Open Doors, Uccle, 29-30 September 2018
26. De Patoul, J.
La météo de l'espace et les prévisionnistes de l'Observatoire
Space Pole Open Doors, Uccle, 29-30 September 2018
27. De Patoul, J.; Janssens, J.
Space Weather Forecasters
Visit United Nations Ambassadors, ROB, 23 January 2018
28. D'Huys, E.
Ruimtevaart
Ingenium School, Tervuren, 2 March 2018
29. D'Huys, E.
De zon en ruimteweer
Ingenium School, Tervuren, 1 March 2018
30. D'Huys, E.
De Zon
Ingenium School, Tervuren, 27 February 2018
31. D'Huys, E.; Dominique, M.
SWAP and LYRA onboard PROBA2
Celebration 50 years ESA Redu station, Redu, 3 July 2018
32. Dierckxsens, M.
Oorzaak en Gevolgen van Energetische Zonnedeeltje
Volkssterrenwacht Urania, Hove, 27 February 2018
33. Dierckxsens, M.
The particle accelerator called the Sun
Pint of Science, Volkssterrenwacht Armand Pien, Ghent, 14 May 2018
34. Dolla, L.
Comment le champ magnétique structure l'atmosphère du Soleil
Space Pole Open Doors, Uccle, 29-30 September 2018
35. Dominique, M.
Ce que nous apprend la lumière du soleil
Space Pole Open Doors, Uccle, 29-30 September 2018
36. Janssens, J.; Marqué, C.
Sensors
SWIC, Uccle, 11-13 March 2018
37. Janssens, J.
Drivers of space weather
SWIC, Uccle, 11-13 March 2018
38. Janssens, J.
Earth environment - Magnetosphere
SWIC, Uccle, 11-13 March 2018
39. Janssens, J.
Earth environment - Ionosphere
SWIC, Uccle, 11-13 June 2018
40. Janssens, J.
Space weather impacts on the earth environment
SWIC, Uccle, 11-13 June 2018
41. Janssens, J.
SIDC/RWC and URSIgram + exercises
SWIC, Uccle, 11-13 June 2018
42. Janssens, J.; Bourgoignie, B.; Lemaitre, O.; Vanlommel, P.
Knowledge and Situations Quiz
SWIC, Uccle, 11-13 June 2018
43. Janssens, J.; Marqué, C.
Sensors
SWIC, Uccle, 26-28 November 2018
44. Janssens, J.
Drivers of space weather
SWIC, Uccle, 26-28 November 2018
45. Janssens, J.
Earth environment - Magnetosphere
SWIC, Uccle, 26-28 November 2018
46. Janssens, J.
Earth environment - Ionosphere
SWIC, Uccle, 26-28 November 2018
47. Janssens, J.
Space weather impacts on the earth environment
SWIC, Uccle, 26-28 November 2018
48. Janssens, J.
SIDC/RWC and URSIgram + exercises
SWIC, Uccle, 26-28 November 2018
49. Janssens, J.; Bourgoignie, B.; Lemaitre, O.; Vanlommel, P.
Knowledge and Situations Quiz
SWIC, Uccle, 26-28 November 2018
50. Janssens, J.
The SIDC - An Introduction
Presentation Visit FRAKAS TV, 19 April 2018
51. Janssens, J.
De Zon

- Lecture for Astronomy Course, MIRA Public Observatory, Grimbergen, 18 April 2018
52. Kraaikamp, E.
Foto's en video's gemaakt met de USET zonnetelescopen
Space Pole Open Doors, Uccle, 29-30 September 2018
53. Lamy, H.
A l'écoute des étoiles filantes avec le réseau BRAMS
Space Pole Open Doors, Uccle, 29-30 September 2018
54. Lefèvre, L.
4 siècles de variabilité solaire
Space Pole Open Doors, Uccle, 29-30 September 2018
55. Marqué, C.
Les observations solaires à la station de radioastronomie de Humain
Space Pole Open Doors, Uccle, 29-30 September 2018
56. Messios, N.
ESA's SPace ENVironment Information System (SPENVIS)
Four-day SPENVIS training for Airbus Defense and Space GmbH (WebEx), 22 February 2018
57. Messios, N.
SPENVIS mission definition & coordinate generators
Four-day SPENVIS training for Airbus Defense and Space GmbH (WebEx), 22 February 2018
58. Messios, N.
Space radiation environment specification with SPENVIS - Part 1
Four-day SPENVIS training for Airbus Defense and Space GmbH (WebEx), 1 March 2018
59. Messios, N.
SPENVIS Geant4 simulations
Four-day SPENVIS training for Airbus Defense and Space GmbH (WebEx), 1 March 2018
60. Messios, N.
Total ionising dose calculations with SPENVIS
Four-day SPENVIS training for Airbus Defense and Space GmbH (WebEx), 8 March 2018
61. Sapundjiev, D.; Verhulst, T.; Dierckxsens, M.; De Donder, E.; Crosby, N.; Stegen, K.; Stankov, S.
Cosmic Rays: Cooperation at the Space Pole
STCE Annual Meeting, Uccle, 7 June 2018 (invited talk)
62. SSCC team
ESA SSA SWE Portal 2.8.0 Release
Space Weather Euro News (SWEN), 22, 2, 10 April 2018
63. Vanlommel, P.; Janssens, J.
STCE Newsletters
Weekly newsletter, <http://www.stce.be/>, 2018
64. Vanlommel, P.
Introduction to Space Weather
SWIC, Uccle, 11-13 June 2018
65. Vanlommel, P.
Space Weather data exercise
SWIC, Uccle, 11-13 June 2018
66. Vanlommel, P.
Introduction to Space Weather
SWIC, Uccle, 26-28 November 2018
67. Vanlommel, P.
Space Weather data exercise
SWIC, Uccle, 26-28 November 2018
68. Vanlommel, P.
Het Noorderlicht: wetenschap en legende
Space Pole Open Doors, Uccle, 29-30 September 2018
69. Vanlommel, P.
Noorderlicht, de legende
Nacht van Wolvendael, Uccle, 19 August 2018
70. Vanlommel, P.
Zonnevlekken en de zonnecyclus
Nacht van Wolvendael, Uccle, 19 August 2018
71. Vanlommel, P.
Het noorderlicht: hoe zit het nu echt?
Festival Fabrik, Leuven, 31 October 2018
72. Vanlommel, P.
The atmosphere of our favourite study object, the Sun
Solar Eclipse Conference, Genk, 5 August 2018
73. Vanlommel, P.
Solar Data
Masterclass, Kunsthal Extra City^[1], Antwerpen–Berchem, 8 February 2018
74. Vanlommel, P.
Zonnesatellieten
Ingenium School, Tervuren, 1 March 2018
75. Vanlommel, P.
Ruimteweer
Ingenium School, Tervuren, 1 March 2018
76. Vanlommel, P.
De Zon
Ingenium School, Tervuren, 27 February 2018
77. Verbeeck, C.
Planetoïden, kometen en meteoren
Volkssterrenwacht Urania, Hove, 9 February 2018

78. Verbeeck, C.; Lamy, H.; Calders, S.; Martínez Picar, A.; Calegario, A.; Anciaux, M.; Ranvier, S.
The BRAMS network and the Radio Meteor Zoo
Meteor Workshop, Dunsink Observatory, Dublin, Ireland, 15 September 2018
79. Verbeeck, C.
Ruimteweer: de impact van zonnestormen op aarde
Space Pole Open Doors, Uccle, 29-30 September 2018
80. Verhasselt, K.
De geschiedenis van de tijd en de wisselwerking met de GNSS (GPS, Galileo...)
Space Pole Open Doors, Uccle, 29-30 September 2018
81. West, M.
The Sun in 2017
ESA - [Space In Images](#), 12 January 2018
82. West, M.
Partial solar eclipse from space
ESA - [Space In Images](#), 13 August 2018
83. West, M.
Live Space Weather Forecast (SIDC)
ESWW15, Leuven, Belgium, 5-9 November, 2018
84. Zychova, L.
Threats from the Universe
Asgard - Scientific balloons for space education, Space Pole, 26 April 2018
85. Zychova, L.
8 Ways the Universe Might Kill Us: Part 1 – Mass Extinctions
[Wtnschp.be](#), 28 March 2018
86. Zychova, L.
8 Ways the Universe Might Kill Us: Part 2 – Asteroids and Meteorites
[Wtnschp.be](#), 8 May 2018
87. Zychova, L.
8 Ways the Universe Might Kill Us: Part 3 – Solar Particle Radiation
[Wtnschp.be](#), 10 July 2018
88. Zychova, L.
Interstellar Bubbles
Pint of Science, UGent observatory, Ghent, Belgium, 16 May 2018
89. Zychova, L.
Space Weather and its Effects on Earth
Ostrava Planetarium, Ostrava, Czechia, 17 November 2018
90. Zychova, L.
Intriguing Space Weather Effects
Cosmo Tea, DTPA, Masaryk University, Brno, Czechia, 16 November 2018
91. Zychova, L.
Space Weather Workshop and Lecture
Astronomy Club, Brno, Czechia, 14 November 2018

List of abbreviations

~	About, proportional to		Investigation of the Corona of the Sun (PROBA-3)
1D	One dimensional	AT-RASC	Atlantic Radio Science meeting
2D	Two dimensional		
3D	Three dimensional	AU	Astronomical Unit; about 150 million km
α	Power-law slope		
Å	Ångstrom (0.1 nm)	AWDA	Automatic Whistler Detector and Analyzer
A	Article		
AAS	American Astronomical Society	B ₀	Heliographic latitude of the central point of the solar disk (The range of B ₀ is $\pm 7.23^\circ$)
ABL	Atmospheric Boundary Layer		
ACCESS-A	Australian Community Climate and Earth-System Simulator (version -A)	BAMC –UKMHD	British Applied Mathematics Colloquium UK Magnetohydrodynamics
ACE	Advanced Composition Explorer	BE	Belgium
ADA	Astronomical Data Analysis	BELSPO	Belgian Science Policy Office
ADF	Active Day Fraction	BeNELux	Belgium, The Netherlands, and Luxembourg
AFFECTS	Advanced Forecast For Ensuring Communications Through Space	BEZA-com	A networking project from BELSPO and its South African homologue NRF
AGU	American Geophysical Union	BIRA	Koninklijk Belgisch Instituut voor Ruimte-Aëronomie
AIA	Atmospheric Imaging Assembly (SDO)	BISA	Royal Belgian Institute for Space Aeronomy
ALADIN	Aire Limitée Adaptation Dynamique Développement International	BLH	Boundary Layer Height
ALARO	ALADIN and AROME combined model	BRAIN-be	Belgian Research Action through Interdisciplinary Networks (BELSPO)
ALC	Automatic LIDAR Ceilometer	BRAMS	Belgian Radio Meteor Stations
ALF	faint narrow-band radio bursts from sources propagating with velocities close to the local Alfvén velocity	BUKS	Belgium, UK, and Spain
		B.USOC	Belgian User Support and Operation Centre
A.NE.MO.S.	Athens Neutron Monitor Station	Bz	Component of the IMF perpendicular to the ecliptic (“north-south” component)
AR	Active Region	C-class flare	Common x-ray flare
ARCAS	Augmented Resolution Callisto Spectrometer	C/N ₀	Carrier-to-Noise density
AROME	Application de la Recherche à l'Opérationnel à Meso-Echelle	Ca II H	A blue line in the solar spectrum at 396.85 nm
ASGARD	An educational space programme for schools (no acronym)	Ca II K	A blue line in the solar spectrum at 393.37 nm
ASIC	Application Specific Integrated Circuit	CACTus	Computer Aided CME Tracking software
asl	above sea level	CaF ₂	Calcium fluoride
ASPIICS	Association of Spacecraft for Polarimetric and Imaging	CALLISTO	Compound Astronomical Low frequency Low cost Instrument for Spectroscopy and Transportable Observatory

CAMS	Copernicus Atmosphere Monitoring Service	dB-Hz	decibel-Hertz (bandwidth relative to 1 Hz)
CCMC	Community Coordinated Modeling Center	Digisonde	Digitally Integrating Goniometric IonoSONDE
CCSOM	Constraining CMEs and Shocks by Observations and Modelling	DIGISUN	A software application for digitization of scanned sunspot drawings
CESRA	Community of European Solar Radio Astronomers	DKIST	Daniel K. Inouye Solar Telescope
CH	Coronal Hole	DLR	German Aerospace Center
CHARM	Contemporary physical challenges in Heliospheric and AstRophysical Models	DOI	Digital Object Identifier
		DoY	Day of Year
		DPS4D	Digisonde-Portable-Sounder-4D
CIR	Co-rotating Interaction Region		
Cluster	ESA/NASA mission to study the Earth's magnetosphere (no acronym)	DSCOVR	Deep Space Climate Observatory
cm	centimeter	Dst	Disturbance Storm Time index (geomagnetic)
CME	Coronal Mass Ejection	DSW	Data Science Workshop
CMOS	Complementary Metal-Oxide-Semiconductor	E	East
CNES	Centre national d'études spatiales (France)	e-Callisto	extended Compact Astronomical Low-cost Low-frequency Instrument for Spectroscopy and Transportable Observatory
CNRS	Centre national de la recherche scientifique (France)	EC	European Commission
CO ₂	Carbon Dioxide	ECS	European CubeSat Symposium
COLAGE	Congreso Latinoamericano de Geofísica Espacial	ECSIM	Energy Conserving Semi-Implicit Method
COMESSEP	COronal Mass Ejections and Solar Energetic Particles	ECUVM	European conference on solar UV monitoring
COPUOS	COmmittee on the Peaceful Uses of Outer Space (UN)	Eds.	Editors
COR (1/2)	Coronagraph (Inner/Outer) onboard STEREO	EGU	European Geosciences Union
CORDEX	COordinated Regional Climate Downscaling Experiment	EISCAT	European Incoherent SCATter scientific association
CORS	Continuously Operating Reference Stations (GNSS)	EIT	Extreme ultraviolet Imaging Telescope (SOHO)
COSPAR	COmmittee on SPACE Research	EM	Electromagnetic
		EPN	EUREF Permanent Network
COST	(European) COoperation in Science & Technology	EPOS(-PL)	European Plate Observing System (- Poland)
COTS	Commercial off-the-shelf	EPSC	European Planetary Science Congress
CRRES	Combined Release and Radiation Effects Satellite	EPT	Energetic Particle Telescope (PROBA-V)
CSL	Centre Spatial de Liège	erg	10 ⁻⁷ Joule
CubeSat	A small satellite measuring 10cm x 10cm x 10cm	Es	Sporadic E-layer (ionosphere)
		ES	Earth System (Science and Environmental Management (COST))
Δ	Delta (difference)		
D2D	Digisonde-to-Digisonde	ESA	European Space Agency

ESAC	European Space Astronomy Centre	FMI	Finnish Meteorological Institute
ESC	Expert Service Centre	FNRS	Fonds National de la Recherche Scientifique
ESCAPE	European SpaceCraft for the study of Atmospheric Particle Escape	foF2	Critical frequency F2-layer
		FOV	Field-Of-View
ESERO	European Space Education Resource Office	FP7	Framework Programme 7 (EU)
ESLAB	European Space Research Organisation Laboratory	FRi3D	Model of a flux rope in 3D
		FRS	Fonds de la Recherche Scientifique
ESOC	European Space Operations Centre	FU	Frederick University
ESPM	European Solar Physics Meeting	FUV	Far Ultraviolet
		Galileo	European GNSS
ESTEC	European Space Research and Technology Centre	GB	Gigabyte (10 ⁹ bytes)
		GBO	Ground-Based Observatory
ESWW	European Space Weather Week	GCR	Galactic Cosmic Rays
		GeV	Giga electronvolt (10 ⁹ . 1.6 . 10 ⁻¹⁹ Joule)
EU	European Union	GFZ	Deutsches GeoForschungsZentrum (German Research Centre for Geosciences)
EUHFORIA	European Heliospheric Forecasting Information Asset		
EUI	Extreme-Ultraviolet Imager (Solar Orbiter)		
EUMETSAT	European Organisation for the Exploitation of Meteorological Satellites	GHz	Gigahertz (10 ⁹ Hz)
		GLASS	GNSS Linkage Advanced Software System
EUNADICS-AV	European Natural Airborne Disaster Information and Coordination System for Aviation	GLE	Ground Level Enhancement
		GLONASS	GLObal NAVigation Satellite System (Russia)
EUREF	EUropean Reference Frame	GmbH	Gesellschaft mit beschränkter Haftung (Company with limited liability)
EUV	Extreme Ultraviolet		
EUVI	Extreme Ultraviolet Imager (STEREO/SECCHI)	GNSS	Global Navigation Satellite System
EUVM	EUV Monitor (MAVEN)	GNSS4SWEC	Advanced GNSS tropospheric products for the monitoring of Severe Weather Events and Climate
EVE	Extreme ultraviolet Variability Experiment (SDO)		
ExoMars	Exobiology on Mars (ESA, Roscosmos)	GOES	Geostationary Operational Environmental Satellite
f-number	the ratio of the system's focal length to the diameter of the entrance pupil	GOME	Global Ozone Monitoring experiment (SCIAMACHY)
F _{10.7 cm}	Solar radio flux at 10.7 cm wavelength	GOMESCIA	GOME/SCIAMACHY/GOME-2
F10.7P	Proxy for F _{10.7 cm} solar radio flux	GONG	Global Oscillation Network Group
F ₂	Main ionospheric layer	GPS	Global Positioning System (USA)
FAS	Frequency-Angular-Sounding	GSFC	Goddard Space Flight Center
FHNW	Fachhochschule Nordwestschweiz (University of Applied Sciences and Arts Northwestern Switzerland)	GUI	Graphical user interface
		GUVI	Global Ultraviolet Imager (TIMED)

h	(1) hour ; (2) Planck's constant ($6.62607004 \times 10^{-34} \text{ m}^2 \text{ kg / s}$)	INSPIRE	International Satellite Program in Research and Education
H	(1) Hydrogen ; (2) Heat flux	IPAG	Institut de Planétologie et d'Astrophysique de Grenoble
H-alpha ($H\alpha$)	A red visible spectral line at 656.28 nm created by Hydrogen	IR	Infrared
HAC	Hvar Astrophysical Colloquium	IRI	International Reference Ionosphere
HEK	Heliophysics Events Knowledgebase	IRM	Institut Royal Météorologique
HESPERIA	High Energy Solar Particle Events forecasting and Analysis project	ISAS	Institute of Space and Astronautical Science
HF	High Frequency	ISC	(1) International Science Council ; (2) International Steering Committee
HI	Heliospheric Imager (STEREO)	ISEST	International Study of Earth-Affecting Solar Transients
$h_m F_2$	peak density height of F_2 -layer	ISS	International Space Station
HMI	Heliospheric and Magnetic Imager (SDO)	ISSI	International Space Science Institute
HSRS	Humain Solar Radio Spectrograph	ISSS	(1) International School of Space Science ; (2) International School/Symposium for Space Simulations
HSS	High Speed Stream	IT	Information Technology
HuRAS	Humain Radio Astronomy Station	jHV	jHelioViewer
HXR	Hard x-rays	JPEG	Joint Photographic Experts Group
Hz	Hertz (per second)	JSWSC	Journal of Space Weather and Space Climate
I/Ps	Ionosphere-Plasmasphere system	JUICE	JUper ICy moons Explorer
IAG	International Association of Geodesy	K	(1) Local K-index: A 3-hour geomagnetic index, ranging from 0 (quiet) to 9 (extremely severe storm) ; (2) degrees Kelvin
IAGA	International Association of Geomagnetism and Aeronomy	K*	Local 1-minute resolution K index
IAS(B)	Institut royal d'Aéronomie Spatiale de Belgique	KAW	Kinetic Alfvén Waves
IASC	International Arctic Science Committee	keV	kilo electronvolt ($10^3 \cdot 1.6 \cdot 10^{-19}$ Joule)
IAU	International Astronomical Union	kHz	kilo Hertz (10^3 /second)
ICAO	International Civil Aviation Organization	km	kilometer
ICME	Interplanetary CME	km/s	kilometers per second
ICT	Information and Communication Technologies	KMI	Koninklijk Meteorologisch Instituut
IEEE	Institute of Electrical and Electronics Engineers	KNMI	Koninklijk Nederlands Meteorologisch Instituut
IGS	International GNSS Service	K_p	A geomagnetic index, ranging from 0 (quiet) to 9 (extremely severe storm)
IMC	International Meteor Conference		
IMF	Interplanetary Magnetic Field		
INGV	Istituto nazionale di geofisica e vulcanologia		

KSB	Koninklijke Sterrenwacht van België	MAGION-5	A Czech subsatellite
KUL	Katholieke Universiteit Leuven	MAJIS	Moons And Jupiter Imaging Spectrometer
kV	kiloVolt (10^3 Volt)	MAVEN	Mars Atmosphere and Volatile Evolution (NASA)
λ	wavelength	MB	Megabyte (10^6 bytes)
l/m^2	Liter per square meter	mbar	millibar
L-class	Large class satellite (ESA)	MeV	Mega electronvolt ($10^6 \cdot 1.6 \cdot 10^{-19}$ Joule)
L	Letter (manuscript)	MHD	Magnetohydrodynamics
L*	Set of Earth's magnetic field lines which cross the Earth's magnetic equator at * earth radii from the centre of the Earth (e.g. L = 2)	MHz	Megahertz ($10^6/s$)
L_0	Heliographic longitude of the central point of the solar disk	MIT	Massachusetts Institute of Technology
L1	First Lagrangian point	MJD	Modified Julian Day
L1, L2	GPS frequencies: L1 = 1575.42 MHz, L2 = 1227.60 MHz	MLE	Maximum Likelihood Estimator
LASCO	Large Angle Spectrometric Coronagraph (SOHO); small (C2) and wide (C3) field of view	MLT	Magnetic Local Time
LATMOS	Laboratoire ATmosphères, Milieux, Observations Spatiales (France)	MPS	Max Planck Institute for Solar System Research
LDE	Long Duration Event	ms	millisecond (10^{-3} second)
LEO	Low Earth Orbit	MUV	Mid Ultraviolet
LIDAR	Light Detection And Radar	v	Frequency
LIEDR	Local Ionospheric Electron Density profile Reconstruction	N	North
LMSAL	Lockheed Martin Solar and Astrophysics Laboratory	N-S	North-South
LOC	Local Organising Committee	N_2	Nitrogen
LOFAR	Low-Frequency Array	NASA	National Aeronautics and Space Administration
LT	Local Time	NASU	National Academy of Sciences of Ukraine
LVF	Linear Variable Filter	NATO	North Atlantic Treaty Organization
Ly- α	Lyman-alpha, a spectral line in the VUV at 121.6 nm	NeQuick	Electron density Quick calculation model (ionospheric model)
LYRA	Large Yield Radiometer, formerly called Lyman Alpha Radiometer (PROBA2)	Net-TIDE	Pilot Network for Identification of Travelling Ionospheric Disturbances in Europe
LWS	Living With a Star	NIR	Near IR
μm	micrometer (10^{-6} meter)	NL	The Netherlands
M-class	Medium class satellite (ESA)	NM	Neutron Monitor
M-class flare	Medium x-ray flare	No.	Number of
M ³ G	Metadata Management and distribution system for Multiple GNSS Networks	nm	nanometer (10^{-9} meter)
MADAWG	Modelling and Data analysis Working Group (Solar Orbiter)	NMDB	Neutron Monitor DataBase
		$N_m F_2$	peak density of F ₂ -layer
		NOAA	National Oceanic and Atmospheric Administration
		NOMAD	Nadir and Occultation for Mars Discovery (ExoMars)
		NRF	National Research Foundation (South-Africa)
		ns	nanosecond (10^{-9} second)

NSO	National Solar Observatory	R-ESC	Space Radiation ESC
nT	nano-Tesla (10^{-9} Tesla)	RAS	Royal Astronomical Society
NUV	Near Ultraviolet	ReSource	Radio Sciences Research on Antarctic Atmosphere
NWP	Numerical Weather Prediction		
O	Oxygen	RF	Radio Frequency
O ₃	Ozone	RHESSI	Reuven Ramaty High Energy Solar Spectroscopic Imager
OGSE	Optics Ground Support Equipment	RMI(B)	Royal Meteorological Institute (of Belgium)
OIC	Organization of Islamic Cooperation	RMS	Root Mean Square
OMI	Ozone Monitoring Instrument	ROB	Royal Observatory of Belgium
OpenGGCM	Open Geospace General Circulation Model	RSSB	Royal Statistical Society of Belgium
ORB	Observatoire Royal de Belgique	R _{sun}	Solar radius (~ 696.000 km)
ORFEES	Observation Radio Fréquences pour l'Etude des Eruptions Solaires	RTIM	Real Time Ionosphere Monitoring
P	The position angle between the geocentric north pole and the solar rotational north pole measured eastward from geocentric north. The range in P is $\pm 26.3^\circ$	RWC	Regional Warning Center
		σ	sigma (confidence level)
		s	second
		S	South
		S-class	Small class satellite (ESA)
		SAMP	Simple Application Messaging Protocol
P2SC	PROBA2 Science Center	SANSA	South African National Space Agency
PB	Petabyte (10^{15} bytes)	SASFF	Self-Adjusted Solar Flux Forecasting tool
PEA	Princess Elisabeth Antarctic	SC24, SC25	Solar Cycle 24, Solar Cycle 25
PECASUS	Pan-European Consortium for Aviation Space weather User Services	SCAR	Scientific Committee on Antarctic Research
PFSS	Potential Field Source Surface particle (proton) flux unit: the number of particles registered per second, per square cm, and per steradian	SCIAMACHY	SCanning Imaging Absorption spectrometer for Atmospheric CHartography (ENVISAT)
pfu		SCK-CEN	Studiecentrum voor Kernenergie – Centre d'Etude de l'Energie Nucléaire
PhD	Doctor of Philosophy	SDO	Solar Dynamics Observatory
PI	Principal Investigator	SECCHI	Sun Earth Connection Coronal and Heliospheric Investigation (STEREO)
PLIP	Polar Lights Imaging Polarimeter	SEP	Solar Energetic Particle
POSKEN	Positioning Knowledge Exchange Network	SEPPEM	Solar Energetic Particle Environment Modelling
PROBA	PROject for OnBoard Autonomy	SFU, sfu	Solar Flux Unit (10^{-22} W m ⁻² Hz ⁻¹)
PRODEX	PROgramme for the Development of scientific Experiments	SHINE	Solar Heliospheric & Interplanetary Environment
ps	picosecond (10^{-12} second)	SIDC	Solar Influences Data analysis Center
PTB	Physikalisch-Technische Bundesanstalt (Germany)	SILSO	Sunspot Index and Long-term Solar Observations
Q&A	Questions and Answers		
QPP	Quasi-periodic pulsation		
R&D	Research and Development		

SIMBA	Sun-earth IMBalance radiometer	STEREO	Solar-Terrestrial Relations Observatory
SLP	Sweeping / Segmented / Single/ Split / Spherical Langmuir Probe	SUMER	Solar Ultraviolet Measurements of Emitted Radiation (SOHO)
SLT	Solar Local Time	SUVI	Solar Ultraviolet Imager (GOES)
SMOS	Soil Moisture and Ocean Salinity (ESA)	SWAP	Sun Watcher using APS detector and image Processing (PROBA2)
sms	short message service	SWAVES	STEREO WAVES
SN	Sunspot Number	SWE	Space Weather
SN	Space weather and Near-earth objects	SWEK	Space Weather Event Knowledgebase
SOC	Science Operations Centre	SWIC	Space Weather Introductory Course
SOHO	SOLar & Heliospheric Observatory	SWPC	Space Weather Prediction Center (USA)
SOLAR-ISS	Name of the new Solar Reference Spectrum	SWSC	Space Weather and Space Climate journal
SOLIS	Synoptic Optical Long-term Investigations of the Sun (NSO)	SWT	Science Working Team
Solo	Solar Orbiter	SWx	Space weather
SOLSPEC	SOLar SPECtrum	SXR	Soft x-rays
SOOPs	Solar Orbiter Operation Plans	SXT	Soft X-Ray Telescope (Yohkoh)
SORCE	Solar Radiation and Climate Experiment	TB	Terabyte (10 ¹² bytes)
SPADE	Small Phased Array DEMonstrator	TCS	Thematic Core Services
SPD	Solar Physics Division (AAS)	TEC	Total Electron Content
SPENVIS (-NG)	SPace ENVIRONMENT Information System (- Next Generation)	Tech-TIDE	Warning and Mitigation Technologies for TIDs Effects
SPS	Science for Peace and Security (NATO)	TECu	TEC unit (10 ¹⁶ e·m ⁻²)
sr	steradian	TESS	Triennial Earth-Sun Summit
SRB	Solar Radio Burst	THEMIS	Time History of Events and Macroscale Interactions during Substorms (NASA mission)
SRC	Space Research Center of the Polish Academy of Sciences	TID	Travelling Ionospheric Disturbance
SREM	Standard Radiation Environment Monitor (Integral, Rosetta)	TIMED	Thermosphere Ionosphere Mesosphere Energetics and Dynamics (satellite)
SSA	Space Situational Awareness	TRACE	Transition Region and Coronal Explorer
SSCC	SSA Space Weather Coordination Centre	TSI	Total Solar Irradiance
SSI	Solar Spectral Irradiance	UCL	Université Catholique de Louvain
SSN	SunSpot Number	UFO	Unidentified Flying Object
STAFF	Solar Timelines viewer for AFFECTS	UHF	Ultra High Frequency
STCE	Solar-Terrestrial Centre of Excellence	UK	United Kingdom
STCL	Space Technology & Calibration Laboratories	ULB	Université libre de Bruxelles

UNCOPUOS	United Nations Committee on the Peaceful Use of Outer Space	VKI	Von Karman Institute
		VLF	Very Low Frequency
URAN	Ukrainian Radio Interferometer of NASU	VSWMC	Virtual Space Weather Modelling Centre
URSI	International Union of Radio Science – Union Radio-Scientifique Internationale	VUB	Vrije Universiteit Brussel
		VUV	Vacuum Ultraviolet
US(A)	United States (of America)	VVS	Vereniging Voor Sterrenkunde
USET	Uccle Solar Equatorial Table	W	(1) Watt; (2) West
UT(C)	(Coordinated) Universal Time	W/m ²	Watt per square meter
UV	Ultraviolet	WAVES	Radio and plasma wave investigation (WIND, STEREO)
v	Velocity (speed)	WDC	World Data Center
V	Volt	WG	Working Group
VarSITI	Variability of the Sun and Its Terrestrial Impact	WMO	World Meteorological Organization
VBI	Visible Broadband Imager (DKIST)	WP	Work Package
VHF	Very High Frequency	WRC	World Radiation Center
VIP	Very Important Person	WS	Workshop
VIS	Visible	X-class flare	Extreme x-ray flare
		XRT	X-Ray Telescope (Hinode)